MOLECULAR BIOLOGICAL CHANGES IN A RABBIT MODEL OF VOCAL FOLD DEHYDRATION

by

Taylor W. Bailey

A Dissertation

Submitted to the Faculty of Purdue University

In Partial Fulfillment of the Requirements for the degree of

Doctor of Philosophy

Department of Comparative Pathobiology

West Lafayette, Indiana

May 2022

THE PURDUE UNIVERSITY GRADUATE SCHOOL
STATEMENT OF COMMITTEE APPROVAL

Dr. Andrea Pires dos Santos, Chair

Department of Comparative Pathobiology

Dr. Abigail Cox

Department of Comparative Pathobiology

Dr. M. Preeti Sivasankar

Department of Speech, Language, and Hearing Sciences

Dr. Sanjeev Narayanan

Department of Comparative Pathobiology

Approved by:

Dr. Sanjeev Narayanan

To my mom, who could not be here to see this,

and to my dad.

ACKNOWLEDGMENTS

My journey through higher education has been tortuous, and it is not without the effort of the village that I have arrived here. I am eternally grateful for so many who have contributed to my progress in science, professionally, and as a person. I am especially grateful for the members of my committee who have shared with me the most challenging events of my life and could not have been more patient and supportive throughout.

I thank Drs. Andrea Pires dos Santos and Naíla Cannes do Nascimento for their years of friendship and continued guidance in my pursuit of science.

I thank Drs. Abigail Cox and Preeti Sivasankar for affording me this opportunity and creating a home for me in their research group with no experience in the field. I am fortunate to have been a part of this team.

I thank Dr. Sanjeev Narayanan for always facilitating my opportunities for progress in the face of multiple obstacles overtime.

I thank Julie Lewellen for being such a wonderful friend and constant source of support and encouragement.

This research would not have been possible without the invaluable support of my fellow lab members Anumitha Venkatraman and Chenwei Duan, or without Jessica Engen for her assistance and training for working with the rabbits. I am grateful for Christa Crain and Robyn McCain of the Purdue Center for Comparative Translational Research for their support throughout this project, and I would like to recognize Stephanie Griswold and laboratory animal care team for always readily accommodating the unique circumstances of my experiments.

TABLE OF CONTENTS

LIST OF TABLES

LIST OF FIGURES

ABSTRACT

There is a considerable body of evidence suggestive that dehydration can negatively impact voice production. However, our understanding of the underlying biology and physiological changes, particularly at the molecular level, that contribute to this dysphonia are limited. Further, our ability to assess underlying changes in humans is restricted largely to post-mortem tissue or tissue resected during interventional vocal fold surgery, both of which are subject to bias in age and disease state. Here we have utilized a New Zealand white rabbit model of vocal fold dehydration to probe the *in vivo* molecular response to dehydration, focusing on differential gene and protein regulation. In the first study, a single 8-hour exposure to low humidity was used to induce airway surface dehydration. RNA Sequencing was used to obtain a global snapshot of differential transcriptional regulation. This informed a second study wherein 8-hour exposures to low humidity over 15 consecutive days were used and followed by LC-MS/MS proteomic analysis to interrogate potential functional changes. In the third study, systemic dehydration was induced with a 5-day water restriction protocol. A third rehydrated group was included that returned to *ad libitum* consumption for 3 days. LC-MS/MS proteomic analysis was used. We have found evidence for transcriptional and protein expression changes under both dehydration paradigms. Our findings serve to inform our molecular biological understanding of dehydration of the vocal folds with implications to prophylaxis against and clinical intervention thereof.

CHAPTER 1. INTRODUCTION

1.1 Mammalian Larynx and Vocal Folds

1.1.1 Larynx

The larynx is an important multifunctional and evolutionarily conserved organ with a common high-level organization across mammalian species. It serves as a rigid protective body to the entry of the lower airway, houses the functional components of phonation, and participates in maintaining normal respiration. The gross anatomy and histology of the larynx are well described [1]. The larynx comprises multiple cartilages, including the thyroid, the cricoid, and the bilateral arytenoids. The epiglottis, a flexible cartilaginous fold, marks the entry of the larynx, which extends anteriorly from the distal pharynx at the level of the hyoid bone. The laryngeal cartilages are connected to each other by planar sheets of connective tissues referred to as "ligaments" or "membranes". Inferiorly, the larynx transitions into the trachea. Although the peripheral cartilaginous frame of the larynx is largely static, internal laryngeal dynamics, especially those related to phonation, are controlled by a set of intrinsic laryngeal muscles, including the thyroarytenoid (TA), cricothyroid (CT), and posterior cricoarytenoid (PCA). As a distal extension of the vagus nerve, the superior and recurrent laryngeal nerves mediate sensory and mechanical function within the larynx. Afferent blood flow is supplied through the superior and inferior laryngeal arteries.

The lumen of the larynx is a mucosal surface in contact with inspired and expired air. Two sets of bilateral mucosal folds are present along the lateral walls of the lumen: the ventricular folds, commonly referred to as the "false vocal cords" as they do not participate in routine phonation, and the true vocal folds, which comprise a portion of the glottis. Ventricular folds are not appreciated in all species [2-4]. The interior laryngeal space can thus be divided into three compartments: the vestibule, the space between the epiglottis and the ventricular folds; the ventricle, the space between the ventricular folds and the true vocal folds; and the subglottic space between the true vocal folds and the laryngotracheal transition below the cricoid cartilage. The epithelial layer of the larynx is predominately consistent with respiratory epithelium elsewhere in the airways, comprised of ciliated pseudostratified columnar cells, except for the epiglottis and the vocal folds, which exhibit a stratified squamous epithelial layer with adjacent

transitional epithelium [1]. While the vocal folds (and at a secondary extent, the false vocal folds) are unique to the generation of phonation, broad physiology with the larynx should be considered due to its airspace, luminal lubrication maintained by secretions throughout, and roles in immunological response, all of which may affect the normal function of the vocal folds.

1.1.2 Vocal Folds

The glottis is a crucial multifunctional internal structure of the larynx. The vocal folds are the fundamental structures of phonation and comprise the "membranous" sections of the anterior glottis, while the posterior cartilaginous sections participate in respiration [1]. The anterior and posterior glottis can be spatially differentiated relative to the arytenoid cartilages; the vocal folds extend from the anterior tips of the vocal processes of the arytenoids and converge at the anterior commissure at the thyroid cartilage. Internally, the vocal folds are supported by the thyroarytenoid muscles. Overlaying the deep skeletal muscle layer is a thick, variably composed lamina propria. Composition and spatial differences within the lamina propria exist between mammalian species, but generally, collagen, elastin, fibronectin (Fbn), and hyaluronic acid (HA) are prominent features [5-7]. In histology, the lamina propria in mammals is generally differentiated into two or three distinct layers with differences between species [3,8-10]. Recently, high-resolution optical tomography demonstrated that a discrete stratification often used to describe the lamina propria depth is more accurately considered a continuous network of fibers of various sizes and orientations anchored to collagen between layers with elastic fibers enriched in the intermediate layer [5]. Seromucinous submucosal glands (SMG) are sometimes identified [10], but evidence for their presence in different species in the literature is inconsistent [11,12]. The epithelium of the mid-membranous vocal folds is generally non-keratinized stratified squamous in contrast to the respiratory epithelium of the posterior glottis.

1.1.3 Phonation

Phonation refers to the production of sound through the vibration of the vocal folds, a phenomenon in humans typically appreciated as "voice". Contemporary understanding of the underlying physiology of phonation is recently reviewed [13]. Phonation is a complex process that may naïvely be reduced to airflow, prototypically expiratory from the lungs, through a pressure-

sensitive, viscoelastic value (the glottis). With the appropriate pressure, sustained oscillations of the vocal folds are induced. The long-standing anatomical model for phonation considers the vocal folds in two primary layers: the body (TA muscle and deep lamina propria) and the cover (the superficial lamina propria and the epithelium) [14]. The body controls internal stability and mediates certain dynamic control, and the cover participates in the sound-producing oscillations. Oscillations of the vocal fold cover occur from the lower margin traveling upward in a mucosal wave, and in many instances of phonation, the vocal folds collide directly along the sagittal midline. The forces with which the vocal folds collide are substantial, with recent computational modeling suggesting they are sufficient to displace interstitial water within the local tissue [15]. A minimal air pressure and air flux (phonation threshold pressure, PTP; phonation threshold flow, PTF) are required to initiate oscillations, but the intrinsic laryngeal musculature can reposition the vocal folds relative to each other in 3-dimensions as well and lengthen or shorten them along the anteroposterior axis [16] influencing the PTP/PTF as well as the resulting fundamental frequency of oscillations. Sustained oscillations are dependent on the viscoelastic nature of the lamina propria, and further, as the vocal folds directly contact each other, the entire process may be influenced by the surface conditions of the laryngeal lumen. Taken together, one must appreciate the breadth of phonatory mastery achieved by the human species given such a complicated phonatory system.

1.1.4 Human Specialization

Humans have developed the capacity for complex phonatory control beyond a fundamental need for basic communication. While the voice qualities relate only partially to the vocal folds themselves, this phonatory potential suggests a unique or differentially advantageous structure of adaptations of the human larynx or vocal folds. One such characteristic is well-defined macula flavae (MF). The MFs are dense, round structures that can be appreciated at the anterior and posterior poles of the vocal folds. They contain stellate cells that are thought to contribute to the lamina propria [17,18] and are perhaps more critical to producing new extracellular matrix components (ECM) within the vocal folds, whereas vocal folds fibroblasts (VFF) contribute more to the remodeling of the existing ECM [18]. MFs are not appreciated in all mammalian species. A study of human, rat, rabbit, canine, and porcine vocal folds specifically sought to identify MF and vocal fold stellate cells (VFSC). Neither porcine, canine, nor rabbit

samples demonstrated defined MF or VFSC population; rat samples exhibited both [10]. A second consideration is a well-defined, 3-zone lamina propria in the context of regular, complex phonation. It is known that vibratory stress is a mediating factor for normal vocal fold development through the activation of EM-producing cells. Thus, the pervasive nature of vocalization in humans compared to other mammalian species provides a unique potential for structural adaptation. The collagen-elastin composition of vocal folds is shared among mammalian species, but the well-differentiated superficial, intermediate, and deep layers of the lamina propria are not appreciated across species. It is difficult to test experimentally given the great disparity in phonatory potential in non-human models, but it is intriguing to consider what unique properties the superficial lamina propria (also called "Reinke's space") imparts to human vocalization.

1.2 Challenges of Biological Vocal Fold Studies

Molecular study of the vocal folds in humans presents a considerable challenge. Relatively non-invasive methods of visualization are available for the diagnosis of gross structural or function pathology. Imaging techniques including ultrasound, computer tomography, and magnetic resonance imaging have been used for various anatomical and physiological measurements. However, molecular-level studies are largely restricted to samples collected post-mortem or resected during a surgical intervention. Thus, primary logistical challenges are the availability of tissue, bias of tissue related to patient demographics such as advanced age, and risk of confounding from pathology at the time of collection. Ethical considerations preclude tissue-based analysis of *in vivo* human models for the risk of causing permanent dysphonia in subjects. The need for surrogate models is apparent, but these too present logistical and translational challenges. A variety of systems have been used to study vocal folds biology and the current state of systems used for vocal fold tissue engineering are recently comprehensively reviewed [19]. A summary of approaches illustrating various logistical considerations is provided here.

VFF plated on a polyurethane scaffold subjected to complex vibratory and directional stress exhibited enhanced cell proliferation and a statistically non-significant transcriptional upregulation of collagen, fibronectin (Fbn), and TGFβ1 [20]. Use of a collagen-gelatin sponge extended-release of basic fibroblast growth factors in culture and accelerated rat-isolated

fibroblast cell growth [21]. An autograft was constructed *ex vivo* using epithelial and fibroblast cells isolated from the oral mucosa of canine patients co-cultured on top of a collagen gel. Implantation onto vocal folds from which the membranous section has been resected resulted in reconstitution of the epithelial and mucosal compartments with only mild changes to lamina propria elastin and mucosal wave propagation [22]. Human vocal fold fibroblasts (hVFF) cultured on a flexible plate coated with collagen I were subjected to extended vibratory stress resulting in transcriptional downregulation of fibronectin and hyaluronic acid synthase (HAS) and a statistically non-significant upregulation of collagen [23]. Primary vocal fold epithelial cells extracted from rabbits grown on collagen-coated inserts above 3T3 feeder cells successfully propagated and stratified for at least two passages; however, the epithelial layers appear marginally thinner than a true vocal folds control with a mildly altered cell appearance [24]. Co-culture of upper airway epithelial cells on top of VFF without a scaffold exhibited cell viability and VFF differentiation response to TGFβ1 [25]. MF stellate cells and VFF both respond to vibratory stress. Stellate cells transcriptionally upregulated collagen, Timp1, and Fbn, and upregulated TGFβ in response; VFF upregulated matrix metalloprotease 1 (MMP1) and downregulated collagen and Fbn [18]. VFF plated on a polyurethane scaffold transcriptionally upregulated various adhesion factors in response to vibration [26]. VFF plated on flexible plates coated in a synthetic Fbn analog, pronectin, transcriptionally upregulated collagen, HA synthetase, and TGFβ [27]. An immortalized aneuploid keratinocyte line transcriptionally upregulated EFG and EFGR and exhibited increased f-actin bundling in response to vibration [28]. Overall, these different approaches demonstrate important experimental considerations of *in vitro* models: co-culture of epithelial cells and fibroblasts, vibration as a cell-differentiating factor, and providing physiologically relevant substrate.

Many organoid models exist for the respiratory system, but evidence for organoid models of the larynx is limited. A synthetic 3-dimensional silicone model was used to assess physical characteristics of vocal folds vibration but does not address biology [29,30]. An organoid model of trachea and larynx was created with postnatal mouse and human tissues, but while they differentiated into appropriate tissue types, the reported model is foundational with limited translational value to vocal fold research [31].

A common challenge identified when using primary cell lines is limited passage viability limiting experimental parameters and duration. A porcine primary cell culture model highlights

this challenge [32], with another recent protocol describing an efficient cell extract from mucosal samples with four-generation passage viability [33]. Two recent studies show promising advancements in addressing this limitation. A first study took a unique approach to generate their model using commercially available human induced pluripotent stem cells and step-wise differentiated them into vocal folds basal progenitors [34]. Under appropriate culturing conditions, these cells developed into a vocal fold approximating layer, though with identified molecular differences. The same group later designed an immortalized vocal fold epithelial cell line by a stable retroviral transformation of post-mortem obtained primary vocal fold epithelia [35]. While this addresses an immediate problem of cell viability, the translational potential is bounded by the absence of 3-dimensional structure and vibration to match the normal *in vivo* environment.

1.2.1 Animal Models

Aspects of the larynx or vocal folds have been characterized in many mammalians species including baboon [36], cat [36], cow [2], dog [10,37-39], lion [8], monkey [39], mouse [40], pig [9,10,39,41], rat [42,43], rabbit [10,11,36,44-46], sheep[47,48], and tiger [8]. Much of the laryngeal structure identified between species for vocal folds is common, though there are obviously considerable variations in size, and other anatomical and histological differences are appreciated. Taken together, this heterogeneity requires careful evaluation of animal models when translating molecular-level findings across species and especially to humans. Nevertheless, the positive implications of the *in vivo* conditions are likely to outweigh the negative limitations of *in vitro* models. The state of the use of excised animal larynx models is recently reviewed [49].

1.2.2 Rabbits

The rabbit larynx is well described. It has been measured by CT scan to be 8.6×5.3mm (anterior-posterior, transverse) and 8.2×5.5mm at the level of the arytenoids and the cricoid, respectively [46]; the latter is larger than was measured by caliper as 5.8×5.4mm [44]. This size is consistent with human children leading to serving as a model of pediatric laryngeal surgery. Various proteins in the vocal folds were recently shown similar localization to humans, including aquaporins and the sodium-potassium ATPase [50]. A study comparing the baboon, cat, and rabbit [36] identified the extraocular isoform of the myosin heavy chain uniquely in the TA and PCA of

the rabbit. The intrinsic muscles of the rabbit larynx, except for the CT, are innervated by the recurrent laryngeal nerve [45], as in humans. An important fundamental difference with critical physiological implications is an inconsistently reported absence of submucosal glands in the rabbit larynx or trachea in contrast to the hamster, guinea pig, mouse, and rat [11]. Authors in one study did appreciate with electron microscopy mucosal pits that they surmise might represent collections of goblet cells [11]. Such a fundamental physiological discrepancy is important when considering normal lubricative homeostatic maintenance of the rabbit larynx, particularly in the context of hydration of the mucosal surface.

The rabbit is an attractive model for vocal folds research for multiple reasons. The relatively small size of the animals while exhibiting human-relevant anatomy serve translational research more effectively than smaller species. The relatively low cost compared to larger animals improves the feasibility of running adequately powered studies. Notably, the rabbit larynx model has been well validated. Rabbits have been used in studies characterizing vocal fold injury and its sequelae [51,52]. The absence of routine vocalization is a limitation of the model, as described above; however, models of *in situ* [53,54] and *ex vivo* [55,56] phonation have been developed.

1.3 Dehydration

Dehydration describes a suboptimal content of water. Concerning the larynx, we consider two distinct presentations of dehydration: on the luminal surface due to evaporation or systemically with water drawn from the tissue into the systemic circulation. A substantial body of literature suggests that dehydration from either perspective has implications to vocal folds state and phonation, but there is a gap in our understanding of the specific mechanisms and biological bases for changes described. Further, it is unclear whether surface and systemic dehydration would present similar underlying pathology. The immediate assumptions are that surface dehydration is likely to affect the hydration state of the vocal folds cover and inter-vocal folds contact dynamics, while systemic dehydration is likely to affect the viscoelastic properties of the vocal folds body, perhaps extending into the cover. Changes in measures of voice associated with dysphonic pathology are considered negative.

1.3.1 Dehydration as a Vocal Insult

A considerable body of early work describing the potential impacts of surface dehydration on phonation has used *ex vivo* animal models. Microdissected ovine vocal folds subjected to dry airflow exhibited increased viscosity and stiffness [57]. Application of viscous fluid to the surface of excised porcine larynges increased contact time and fundamental frequency in artificial phonation [58]. An *ex vivo* canine model demonstrated that desiccated air increases PTP, PTF, and diminished sound intensity [59], eventually precluding phonation altogether [60]. Mucosal wave and frequency both decreased [61]. Taken together, these data provide objective evidence for surface dehydration to manifest as a vocal insult. Vocal folds studies in animal models provide the benefit of allowing tissue modulation and the ability to gain molecular insights from an *in vivo* context unavailable in humans. However, they are inherently limited in the assessment of functional phonation within the context of an intact, *in vivo* homeostatically driven system.

Voice studies in humans provide the benefit of functional measures in the context of natural phonation but are limited in the inability to offer molecular insights from the *in vivo* context, leaving voice to represent vocal folds status indirectly. Thus, measurements in humans are typically reserved to acoustic (e.g., jitter, shimmer, fundamental frequency), aerodynamic (e.g., PTP, PTF), physical (e.g., direct visual observation, electroglottalgraphy), but also subjective measures such as perceived phonatory effort (PPE) and the GRBAS scale. Dehydration impact on voice studies in humans have been previously systemically reviewed. An earlier review focused specifically on PTP as a measure of phonatory effort. The meta-study concluded that PTP may be an insufficiently sensitive measure to draw conclusions on the related effects of dehydration and that among the large body of literature available at the time, relatively few studies (9 out of 34) met rigorous quality criteria. The latter highlights a logistical challenge to studies of voice [62]. A later review considering literature specifically from 2007-2017 related to both surface and systemic dehydration concluded that when considered together, evidence (20 studies meeting inclusion criteria out of 48) suggests both surface and systemic dehydration negatively impact voice [63]. An important limitation commonly appreciated in human voice studies is the inherently large variances in measures of voice; thus, statistical power is low, and it is difficult to assert biologically meaningful changes.

1.3.2 Biology of Surface Dehydration of the Vocal Folds

Laryngeal Mucosa

The laryngeal mucosa largely serves the role of a canonical ciliated pseudostratified columnar respiratory epithelium with the vocal folds as a notable exception, which are instead covered by a stratified squamous epithelium. The respiratory epithelium is covered by a thin, stratified hydration layer. The deeper layer is a non-viscous periciliary fluid layer, measured to approximately 7 microns, sometimes referred to as the "sol" layer. The superficial layer is thicker, more viscous, and composed of a variety of substances, notably mucin glycoproteins affording the name the "mucus" layer. This airway surface fluid serves as a protective barrier from various insults, including pathogens and abrasive environmental conditions. Further, the viscosity of this fluid has direct implications for the function of the vocal folds through changes to the dynamic properties of the mucosal wave during phonation.

Airway Surface Fluid

The airway surface fluid (ASF) of a variety of mammals in the healthy state has been characterized, including cat[64], dog [65,66], ferret [67], human [68-70], mouse [69,71,72], rat [73], and cell culture models of cow [69,72]. Various methods have been used to quantify molecular components, including atomic absorption spectrophotometry [67], atomic emission spectrophotometry [64,70], capillary electrophoresis [71,73], dispersive x-ray analysis [68], fluorophore encapsulating liposomes [69], and indirect potentiometry [70]. Osmolality, when reported explicitly, has been calculated [67], measured by vapor pressure osmometer [64,65], or with fluorophore encapsulating liposomes [72]. Reported ASF varies between 282 and 290mOsm in dogs [65,74] to 370mOsm in cat [64]. The character of the ASF relative to plasma is also inconsistent between species: hyperosmolar in cat [64], dog [65] and ferret [67] and hyposmolar in mouse [71], rat [73]. For mice, there is a considerable difference between the *in vitro* capillary electrophoresis analysis demonstrating 87.2mM and 57.0 mM sodium and chloride ion concentration in the ASF [71], respectively, and *in situ*

fluorescence analysis demonstrating 115mM and 140mM [69]. It is therefore important to validate measures against both collection and analytical methods when assessing the ASF. Further, relative few studies using vocal fold specific tissue are available while lower respiratory models predomindate. In either circumstance, direct analysis of the ASF is challenging, with certain assays requiring invasive and time intensive sample collection. Thus, in voice studies ASF is not directly measured, and it is reasonable to assume with *in situ* or *ex vivo* models that the mechanisms of the lower airway extend to the mucosa of the larynx, including the vocal folds.

Mechanisms of fluid regulation in the airways are well characterized and diverse with common themes. (See Webster and Tarran 2018 for a comprehensive review [75].) At the apical surface, volume is generally regulated with the absorption of sodium ions by the epithelial sodium channel (ENaC encoded by the *SCNNA* set of genes) and the secretion of chloride ions by a variety of chloride channels (e.g., Cystic Fibrosis Transmembrane Conductance Regulator (CFTR) and Solute Carrier Family Member 26 A9). Aquaporins have documented expression in the vocal folds of sheep [47], mice [76], and recently humans and rabbits [50]. Despite their contribution of overall water permeability, it does not appear that the aquaporins are requisite for functional water flux in the airways [77]. Importantly, the shared molecular foundation for airway fluid homeostasis, despite the species specificity in ASF composition, suggests similarities of mechanism across species robust to those differences.

Physiological Response to Osmotic Perturbations in the Airway

The homeostatic composition of the ASF is important. Airway surface dehydration is defined as the loss of water from the ASF and so represents an intangible phenomenon that is sensed indirectly. The concentration of ASF solutes results in increased osmolality, and osmotic perturbations have been demonstrated to elicit a variety of physiological responses. Thus, we may conceptualize surface dehydration of the airway function of ASF osmolality. Unfortunately, there is limited literature relating specifically to the vocal folds epithelium response to osmotic perturbations. Physiological responses to perturbations in ASF osmolality elsewhere within the conducting airway, have been studied in a variety of models, including dog [66,78], guinea pig [79], human [80-82], rat [83-86], and sheep [48]. Physiological responses have included changes to blood flow [83-85,87], the epithelial function [48,66,78,81,82], muscle tone [79,80], and neurogenic inflammation [86].

The epithelium covers the mucosal surface and logically should respond to changes in the luminal environment of the airway. Experiments with primary human nasal epithelial cell culture demonstrated a response to 150mOsm mannitol of altered electrolyte transport, increased transepithelial electrical resistance (TEER), and reduced cell layer thickness [82]. Interestingly, and with important anatomical significance, it was found that serosal exposure of the same hyperosmotic solution elicited none of the same response. A study of primary human bronchial cell culture showed an increased transepithelial osmotic permeability in response to 150mM raffinose luminally, from 168.6 to 220µm/s, accompanied by a rapid reduction in the height of the superficial layer of the epithelial [81]. Serosal exposure was again found not to elicit the same response, although the size of basal cells of the epithelium was mildly affected. Using primary canine bronchial and tracheal cell culture, it was shown that both cells types exhibit a basal level of fluid absorption, but only tracheal cells exhibited a shift to secretion in response to cAMP enrichment [78]. Blockade of sodium transport with amiloride diminished but did not abolish absorption, importantly demonstrating that not all fluid flux is coupled to electrolyte transport. This conclusion was reinforced in an *in vivo* canine trachea model using aerosolized mannitol. It was demonstrated that the epithelium responds to decreased ASF electrolyte concentration by secretion of sodium and chloride ions with a concomitant increase is respiratory fluid output collected at the posterior commissure; however, while this occurred with both 250 and 950mOsm aerosols, the latter resulted in a larger fluid output without a proportional increase in electrolyte secretion [66]. An *ex vivo* study of ovine vocal folds treated with 150mOsm luminally demonstrated a trend of mildly increased luminally directed transepithelial secretion that did not quite reach statistical significance [48]. In contrast to what was found with human nasal epithelial cell culture, there was no related impact on bioelectric properties. This supports the proposed electrolyte-uncoupled secretion observed elsewhere [66,78]. Taken together, these data clearly demonstrate the capacity of the respiratory epithelium to respond to increased luminal osmolality (assumed as the result of surface dehydration).

Osmotic perturbations of the airway lumen also affect extraepithelial physiology. The stimulation of vagal nerve C fibers is associated with neurogenic inflammation and increased negative interstitial fluid pressure in an *in situ* post-mortem rat trachea model [86], a change mitigated by pre-treatment with corticotropic releasing hormone [88]. Intactness of the superior laryngeal nerve was shown to be influential in FOS expression in the brain in response to water

deprivation such that the diminishing impact of post-deprivation water intake was blunted when the nerve was sectioned, suggesting the potential for the superior laryngeal nerve to serve as a homeostatic sensor of surface hydration within the larynx [89]. Locally, aerosolized hypertonic saline resulted in increased vascular permeability attributed to neurogenic inflammation in the rat trachea [85] while application of hypertonic solutions induced vasodilation and hypotonic solutions induced vasoconstriction [83,84]. Luminal application of hyperosmolar solution in an *ex vivo* guinea pig trachea model induced smooth muscle relaxation that was dependent on intactness of the epithelium and was not induced with serosal exposure [79], suggesting the epithelium itself can serve a sensory role. The nature of this epithelial signaling has been further characterized with "epithelium-derived relaxing factor(s)" being differentiated from nitric oxide (NO) associated with vascular endothelium-mediated relaxation [90] Recent works suggest proteins Bactericidal/Permeability-Increasing Protein Fold–Containing Family Member A1 [91] and Stanniocalcin-1 [92] as examples of EDRFs. Further, evidence suggests the EDRF response is uncoupled from the stress of cell shrinkage resulting from hyperosmotic exposure [93]. Directly translating the findings from respiratory epithelium and smooth muscle to the stratified squamous epithelium and skeletal muscle of the vocal folds is limiting. However, these data strongly support a potential mechanism for surface dehydration to influence deeper tissue distinct from tissue changes related directly to homeostatic water flux.

1.3.3 Biology of Systemic Dehydration in the Vocal Folds

Systemic dehydration within vocal folds describes a loss of intracellular and/or interstitial water directed inward into the systemic circulation. Unfortunately, with shared limitations but even more so restrictive than surface dehydration, systemic dehydration presents considerable challenges to study *in vivo* systems due principally to its non-localized nature and inability to assess vocal folds biomechanics. Thus, our understanding of the implications of systemic dehydration to vocal folds function is extrapolated predominately from *ex vivo* and computational models. The vocal folds lamina propria provide an internal structure that is both resilient to mechanical stress but sufficiently pliable for physiologically relevant forces to induce dynamic changes. Compositional changes may directly impart biomechanical changes (See Kumai (2019) for a comprehensive review of vocal folds fibrosis [94].) However, cell volume, cell-ECM interactions, fibrillar superstructure and organization, and overall tissue volume may all be

influenced by dehydration also with net biomechanical effects. It is not yet clear if dysphonic changes of systemic dehydration are simply biomechanical perturbations or manifestations of underlying biological changes.

Recent work supports a connection between tissue hydration status and biomechanical properties of the vocal folds and provides evidence of biomolecular changes. *Ex vivo* porcine larynges submerged in hypertonic solution [95] and *ex vivo* canine larynges dried in an oven [96] both exhibited increased stiffness. Porcine vocal folds treated with hyaluronidase exhibited increased stiffness, also seen with dehydration in hypertonic solution [97]. Such experimental systems exhibit inherently limited translation to a homeostatically driven *in vivo* system, so importantly potential for systemic dehydration to manifest measurable changes in the vocal folds was specifically validated with MRI of larynges of live rats following systemic dehydration from water withholding [98,99] and subsequent rehydration [98]. An *in vivo* study of rabbits subject to water restriction demonstrated downregulation of various epithelial and cell adhesion-related genes [100]. Water-restricted rats exhibited increased hyaluronidase-2 gene expression with histological evidence of diminished HA in the lamina propria [101]. This change is particularly interesting given that the optimal concentration of HA is associated with sustained vocal folds oscillations [102] and localized hydration and tissue viscosity [6]. Further studies are necessary to fully characterize the systemically dehydrated *in vivo* vocal folds and elucidate the underlying mechanisms for the biological changes observed.

1.3.4 Is Rehydration Effective?

With evidence that vocal fold dehydration negatively affects phonation, the immediate assumption is that rehydration should improve the related parameters. It has long been established that the amount of water vapor lost through respiration is influenced by the humidity of the inspired air [103], and so aerosolized hydration is a naturally suggested therapeutic. Earlier work fails to conclusively establish the benefits of surface hydration as either a therapeutic or a prophylactic to dysphonia due in part to limitations previously discussed; recent work is more promising. A mixed sex study of non-dysphonic hospital staff showed desiccated air induced negative acoustic changes, all of which improved with aerosolized water, iso- and hypertonic saline with isotonic saline providing the greatest resolution [104]. A study of pre-professional female singers with control and systemically “hypohydrated” groups demonstrates improvement

of subjective voice assessment but the inconsistent impact on acoustic measures [105] following nebulized saline. A mixed-sex study with euhydrated control and dysphonic groups suggests improvements with nebulized saline that are diminished with underlying dysphonia and exhibit different magnitudes between sexes [106]. Non-professional voice users without a history of dysphonia exhibited improved voice measures while nasally breathing through water moistened gauze during vocal exercises [107]. A mixed-sex study of amateur singers concluded that nebulization of normal saline did not improve but may preserve vocal quality [108]. Thus, recent data support inclusion of surface hydration as a neutral to positive component in a general vocal hygiene regimen but still fail to conclusively validate its clinical efficacy in the context of dysphonia.

While there is abundant study of the effects of systemic dehydration on voice (See Hartley and Tibeault (2014) and Alves et al (2019) for comprehensive review.), there is a relative dearth of literature on the effects of systemic rehydration as a restorative therapeutic within the context of the vocal folds or dehydration-induced dysphonia. An early study of females with laryngeal nodules or polyps demonstrated that a hydration protocol including oral hydration and high humidity exposure improved the outcome of treatments by multiple measures [109]. Study of water 10-hour water deprivation followed by a 2 hour oral rehydration protocol demonstrated partial resolution of changes in fundamental frequency, jitter, shimmer, and harmonic-to-noise ratio, that notably except for the latter did not return to baseline measures [110]. A later study using a 14-hour water deprivation followed by a 20-minute, large magnitude oral rehydration protocol also identified positive effects on jitter and shimmer but note marked inconsistences between individual participants and different target phonations [111]. While these studies support the potential utility of oral rehydration, they are limited in explaining the underlying physiological mechanisms contributing to dysphonia or its resolution. Additional study at more granular levels of time and biology are warranted to improve our understanding.

1.4 Conclusion and Hypotheses

Taken together, evidence largely suggests that dehydration, whether surface or systemic, creates pathological changes in phonation. However, while the obvious assumption then is that adequate hydration should stave off the deleterious effects, the adequacy of hydration as either a treatment or prophylactic is inconsistently substantiated in the literature. Further, the biology

underlying the observed changes is unclear. Here we seek to describe a molecular basis for changes in the vocal folds resulting from dehydration. We have utilized the rabbit as an economically and logistically feasible, and validated model of vocal fold biology. We first considered the acute changes of a single low humidity exposure to induce airway surface dehydration with a high throughput transcriptional analysis. Secondly, we considered changes related to recurring daily exposure to low humidity to more accurately reflect the occupational circumstances of professional voice users subjected to low humidity environments. Lastly, we considered the impact of dehydration with subsequent oral rehydration in a water-restriction model of systemic dehydration.

CHAPTER 2. RNA SEQUENCING IDENTIFIES TRANSCRIPTIONAL CHANGES IN THE RABBIT LARYNX IN RESPONSE TO LOW HUMIDITY CHALLENGE

This chapter represents original work previously published.
Bailey, Taylor W., et al. "RNA Sequencing Identifies Transcriptional Changes in the Rabbit Larynx in Response to Low Humidity Challenge." *BMC Genomics*, vol. 21, no. 1, BioMed Central Ltd, 2020, doi:10.1186/s12864-020-07301-7.

2.1 Abstract

Voice disorders are a worldwide problem impacting human health, particularly for occupational voice users. Avoidance of surface dehydration is commonly prescribed as a protective factor against the development of dysphonia. The available literature inconclusively supports this practice and a biological mechanism for how surface dehydration of the laryngeal tissue affects voice has not been described. In this study, we used an *in vivo* male New Zealand white rabbit model to elucidate biological changes based on gene expression within the vocal folds from surface dehydration. Surface dehydration was induced by exposure to low humidity air (18.6% $\pm$ 4.3%) for 8 hours. Exposure to moderate humidity (43.0% $\pm$ 4.3%) served as the control condition. Ilumina-based RNA sequencing was performed and used for transcriptome analysis with validation by RT-qPCR. There were 103 genes identified through Cuffdiff with 64 genes meeting significance by both false discovery rate and fold change. Functional annotation enrichment and predicted protein interaction mapping showed enrichment of various loci, including cellular stress and inflammatory response, ciliary function, and keratinocyte development. Eight genes were selected for RT-qPCR validation. Matrix metalloproteinase 12 (*MMP12*) and macrophage cationic peptide 1 (*MCP1*) were significantly upregulated and an epithelial chloride channel protein (*ECCP)* was significantly downregulated after surface dehydration by RNA-Seq and RT-qPCR. Suprabasin (*SPBN*) and zinc activated cationic channel (*ZACN*) were marginally, but non-significantly down- and upregulated by RT-qPCR, respectively. The data together support the notion that surface dehydration induces physiological changes in the vocal folds and justifies targeted analysis to further explore the underlying

biology of compensatory fluid/ion flux and inflammatory mediators in response to airway surface dehydration.

2.2 Introduction

Voice disorders are a prevalent communication disorder affecting human health worldwide [112-117]. In the United States general population, the prevalence of voice disorders has been estimated at 6.2% [118], and more recently, at 7.6% [119]. Data from the National Longitudinal Study of Adolescent to Adult Health shows the same 6% estimate among the adolescent population [120]. The development of voice disorders is identified as an occupational hazard, particularly among speakers who depend on a healthy voice for their livelihood. School teachers, entertainers, legal professionals are all at greater risk of dysphonia from voice disorders [114,118,121-124]. The economic impact of voice disorders is substantial. The average associated health care costs in the United States have been estimated at almost 200 million dollars [125], and a study of Brazilian teachers having to take time away from work due to dysphonia illustrates the potential impact of a loss of productivity in the workforce [126]. Taken together, the impact of voice disorders on society supports the need for a more comprehensive understanding of the development of voice disorders and therapies to address them.

Interventions for voice disorders exist along a continuum of non-invasive behavioral modifications to phonosurgery. The focus of this study is on the molecular biological responses to laryngeal surface dehydration as a means of substantiating the commonly prescribed prophylactic and therapeutic practice among speech-language pathologists [63,115,127-129].

Dehydration, as it relates to voice, occurs under two paradigms: systemic dehydration and airway surface dehydration. Systemic dehydration, decreased total body water, has been shown to negatively impact phonatory effort in humans and acoustic measures in humans and *ex vivo* animal models [59,130-132]. Surface dehydration as related to voice is defined as loss of water from the luminal surface of the larynx and vocal folds. In everyday life, this may be caused by exposure to air of low humidity or increased respiratory rate from exercise. While there is evidence suggesting that surface dehydration within the larynx negatively impacts phonation with similar outcomes as systemic dehydration, recent studies in humans [133-136] do not always find a significant correlation between the two.

Unfortunately, rigorous *in vivo* analysis of the physiology of laryngeal surface dehydration is precluded by the invasive nature of data collection and the ethical implications of causing vocal injury in human subjects. Human studies are, therefore, generally limited to acoustic and aerodynamic measures or post-mortem evaluation. Conversely, animal models have largely allowed for *ex vivo* studies, which provide ample evidence that surface dehydration impacts vocal fold biomechanics and function [58,61,137], but the molecular pathobiology and resulting homeostatic compensatory mechanisms remain unclear. An attractive surrogate to the vocal folds is the airway distal to the larynx, which has been studied in the context of airway surface fluid homeostasis and response to luminal perturbations [83,87,138]. It has long been established that the humidity of inspired air can affect the magnitude of water lost to respiration [103] and that the resulting concentration of luminal electrolytes can cause dramatic physiological responses in the trachea, upper and lower airways [82,139]. The vocal folds are covered by nonkeratinized stratified squamous epithelium, and the laryngeal lumen is predominately covered by respiratory epithelium. Therefore, the larynx may respond to perturbations similarly to the tracheal epithelium. This potential is supported in studies assessing vocal fold ion flux to altered composition of luminal surface fluid [48,140,141]. However, these were *in vitro* studies limiting the generalization of the data. Further studies are required to address questions of the specific underlying biology.

To probe for potential physiological responses to surface dehydration, we used an *in vivo* rabbit model. Anatomically, the rabbit larynx is grossly similar to the human larynx. Its size has been approximated to 8.6×5.5mm at the level of the arytenoids [44,46], consistent with the dimensions of the human newborn larynx [142]. Additionally, the literature demonstrates that rabbit larynges exhibit sufficient biological similarity to humans and have been used in molecular and histological studies of the vocal folds [52,143-146]. The rabbit larynx has also been used to characterize the physiological response to injury secondary to phonation [52,146] or laryngeal and vocal fold surgery [147-149]. The common use of rabbits for laryngeal studies and the relatively small size for handling and housing makes this animal a suitable model for this study.

In this study, we sought to identify transcriptional-level changes in response to low humidity exposure that suggest a response to surface dehydration within the membranous vocal folds or the vocal fold lamina propria. We successfully addressed the following aims: [1] construction and evaluation of an environmental chamber capable of exposing rabbits to a

consistent, physiologically-realistic low relative humidity environment and [2] investigation of the effects of 8 hours of low humidity exposure on rabbit larynx by way of RNA sequencing (RNA-Seq). An 8-hour exposure was selected as representative of a typical working day for human subjects. We used low humidity rather than desiccated air as the surface dehydration challenge to increase the ecological validity of the study. Rabbits exposed to moderate humidity served as the control condition.

2.3 Materials and Methods

2.3.1 Animals

All experiments were conducted in accordance with the guidelines and after approval of the Purdue Animal Care and Use Committee (Protocol # 1606001428). Animals were obtained from Envigo Global (Indianapolis, IN) and acclimatized for at least one week. Male New Zealand White rabbits, six to eight months of age, and approximately 3 Kg were used for all experiments. Each experiment was run with two rabbits at a time randomly assigned to either the low (n=8) or moderate (n=6) humidity group. Samples sizes were selected based on recommendation from the Purdue Bioinformatics Core to ensure ideal minimum samples for statistical validity of RNA-Seq (n=6 from each group). Changes to PCV were examined for all rabbits. RT-qPCR validation was conducted with 13 rabbits (low n=7, moderate n=6); one rabbit was excluded due to poor quality of RNA obtained after repeat extraction. Food and water were withheld during experiments under both humidity conditions. To encourage consistent, baseline hydration, all animals were pre-hydrated with 0.1 M sucrose in water *ad libitum* for the two days preceding the experiment. Euthanasia was completed by a single 1.0 mL IV dose of Beuthanasia-D Special (Schering Plough Animal Health Corp., Union, NJ).

2.3.2 Humidity Challenge Protocol

Eight hour low humidity and moderate humidity exposure were conducted in a specially fabricated environmental chamber. The chamber interior was segmented into three similar compartments, each with dimensions approximately 61cm × 61cm × 46cm (Fig. 1a, b). Two compartments were sealed to limit the influx of room air and were intended for low humidity exposure, whereas the third compartment was left open to room air and was intended for a

moderate humidity control. Gated duct caps were included within the wall of the low humidity compartment to allow for titration of room air as necessary.

Low humidity was achieved with a 70-pint commercial dehumidifier (Hisense DH70K1G: Qingdao, China) set to High Continuous attached to the chamber via 4-inch ducting. Moderate humidity exposure was achieved by opening the chamber airspace to room air without conditioning from the dehumidifier. Internal relative humidity and temperature were tracked using a HOBO Data Logger with a 12-bit Temperature/Relative Humidity Smart Sensor (U14-002, S-THB-M002: ONSET, Bourne, MA) at one-minute intervals.

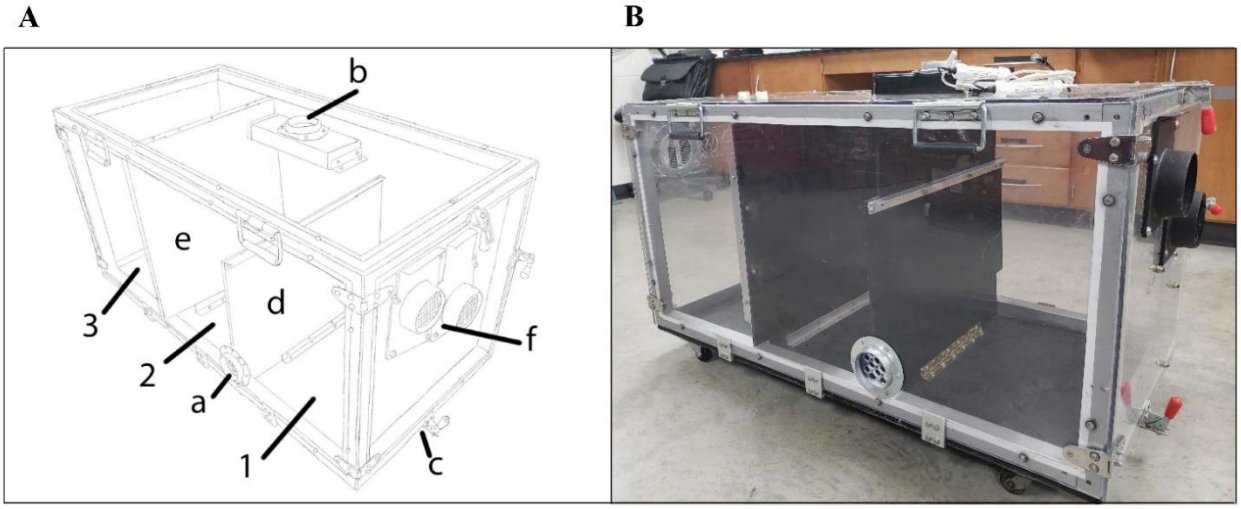

Figure 2.1. Environmental chamber used in this experiment. **A.** Schematic design of the environmental chamber. Air output toward dehumidifier (a), air intake plenum from dehumidifier (b), latches for chamber doors that open longitudinally (c), mobile divider for separating challenge compartment into two sections (d, 1, 2), permanent divider separating challenge from control compartment (e, 3), and gated vent caps for titration of room air (f). **B.** Picture of chamber

2.3.3 Blood Collection and Analysis

Blood was collected in heparinized tubes at the beginning of the 8-hour experiment and immediately prior to euthanasia via venipuncture of the lateral ear vein to minimize trauma and distress of collection. Packed cell volume (PCV) was measured manually by visual assessment using a microhematocrit reader card following centrifugation.

2.3.4 Sample Collection and RNA Extraction

The larynx and proximal trachea were excised from each animal immediately following euthanasia. The larynx was bisected posteriorly along the sagittal midline and pinned onto wax to expose the laryngeal lumen. Full-thickness soft tissue was microdissected bilaterally at the level of the glottis under magnification with microdissection scissors. Sections approximately 2-3mm in any dimension collectively representing the vocal fold and surrounding tissue were immediately stored in RNAlater® Stabilization Solution (Invitrogen, Waltham, MA), stored at 4°C overnight, and at -80°C until processing. Total RNA was extracted with the RNeasy Fibrous Tissue Mini Kit following the manufacturer protocol (QIAGEN®, Hilden, Germany).

2.3.5 RNA Sequencing (RNA-Seq)

RNA quality was assessed by RNA Eukaryotic Pico Chip (Agilent Technologies Inc., Santa Clara, CA) and used to construct poly-A derived cDNA libraries with the Universal Plus mRNA-Seq kit (NuGEN Technologies, Inc., Redwood City, CA). High throughput sequencing was completed with an Illumina® NovaSeq™ 6000 Sequencing System (Illumina Inc., San Diego, CA) by 100 million reads, paired, of 150 bases per sample. Differential gene expression analysis was conducted by the Purdue Bioinformatics Core using Cuffdiff with default parameters [150]. Data were submitted to the NCBI GEO database under accession number GSE148588.

2.3.6 Quality Control and Read Mapping

Sequence quality was assessed using FastQC (v0.11.7) (https://www.bioinformatics.babraham.ac.uk/projects/fastqc/) for all samples, and quality trimming was done using FASTX-Toolkit (v 0.0.14) (http://hannonlab.cshl.edu/fastx_toolkit/) to remove bases with Phred33 score of less than 30, while retaining the resulting reads of at least 50 bases in length. The quality trimmed reads were mapped against the reference genome of *Oryctolagus cuniculus* using STAR (v 2.5.4b) [151].

2.3.7 Differential Gene Expression Analysis and Annotation

Differential gene expression analysis between low and moderate-humidity groups was carried out using 'R' (v 3.5.1; http://www.r-project.org/). STAR mapping (bam) files were used

for analysis by the Cuffdiff from Cufflinks (v 2.2.1) [150] suite of programs that perform differential expression analysis based on FPKM values. Cuffdiff uses bam files to calculate Fragments per Kilobase of exon per Million fragments mapped (FPKM) values, from which differential gene expression between the pairwise comparisons can be ascertained. FPKM obtained were used for principal component analysis comparing individual rabbits; low expression genes were not removed. The gene annotations were retrieved from BioMart databases using biomartr package in 'R'.

2.3.8 Functional Enrichment Analysis and Predicted Protein Interactions

Differential gene expression data were filtered for a false discovery rate (FDR) of less than or equal to 0.05. Log2 FC positive values imply upregulation, while negative values imply downregulation of genes in the vocal folds exposed to low humidity versus moderate humidity challenge. The set of differentially expressed genes provided by Cufflinks meeting the FDR criterion (n=103) was used as input by Ensembl gene ID for DAVID (v6.8) [152] to obtain functional annotation analysis with 86 being found within the database. The same set of genes was used as input for STRING (Search Tool for the Retrieval of Interacting Genes/Proteins) v.11.0 (https://string-db.org) for prediction of protein interaction analysis, providing a full, supplemented network of 100 nodes. In parallel, genes were ranked in descending order based on -log10 P-value multiplied by the sign of log2 transformed FC as input for GSEAPreranked (versions 7.2.0) that was used to perform gene set enrichment analysis using GO gene sets.

GO and KEGG enrichments were obtained from DAVID with default settings. STRING analysis parameters were set with line thickness representing the strength of the data to support interaction including text mining, experimental, database, co-expression, neighborhood, gene fusion, and co-occurrence sources, the minimum required interaction score set to 0.4, shell parameters set to "None", and disconnected nodes to be hidden. Clusters were generated based on the Markov Cluster Algorithm with the inflation parameter set to 2.

2.3.9 Quantitative Reverse Transcription PCR (RT-qPCR)

Total RNA was used to generate cDNA with SuperScript™ IV VILO™ Master Mix (Invitrogen) using 374 ng of RNA as the template. RT-qPCR was performed in triplicate using

SYBR Green 2x PCR Master Mix (Applied Biosystems, Waltham, MA) with 0.1M of each primer and 2.5 µL of template cDNA in a 25 µL reaction volume using a QuantStudio 3 System (Applied Biosystems) thermocycler. Data was collected over 40 cycles by QuantStudio Design & Analysis Software v1.5.1. Primers used in this study are listed in Table 2.1. Relative expression quantification of each gene was calculated using the $2^{(-\Delta\Delta Ct)}$ method [153].

Table 2.1. qPCR primers used in this study.

GENE	RT-qPCR Primers (5' to 3')
ECCP	F: TATGCACGAGTCAGCCAAGG R: TCAGCACCTGCCCCATTATC
CDHR4	F: GGTGACACCCGTCAATGAGT R: GAACCTCTCCTGAGACGTAGT
CDSN	F: TCTCCTCCTGCCAGGAACCT R: CTAGAGCTGCTGGAGCCACT
MCP1	F: GCACGTTTCAGTGAGCATCG R: ACCACACCTGCCTTTACACC
MMP12	F: AGGCCATAATGTTTCCCACCT R: CTGCTCTGGGCCTCCATAAAG
MUC21	F: TTCTGTGTGAGAAAGTGCCTGT R: GTGCCCCATCCATCTCCAAG
SPBN	F: GCTGAATGGTGGTCAAGGCG R: ATGTTGGCGACGTTCCTCCA
ZACN	F: AACTGCGACTTTGAGCTCCT R: TGACCACGTATTCCCGCTTG

2.3.10 Statistical Analysis

Statistical analysis was completed and visualized using RStudio™ Version 1.2.1335 (RStudio Inc., Boston, MA) with libraries *Tidyverse* [154] and *outliers* [155]. Changes in PCV were evaluated with Mann-Whitney nonparametric test. Relative gene expressions from RT-qPCR were tested with Welch two-sample t-test following removal of outlier values as determined by Grubb's test. A p-value < 0.05 was considered statistically significant for all analyses.

2.4 Results

2.4.1 Humidity Challenge and Gross Physical Assessment

A total of eight rabbits were challenged with low humidity, and six rabbits were exposed to moderate humidity (control condition) in a specially fabricated environmental chamber (Fig. 1; see Methods section for details). Low humidity was 18.6 ± 4.3% (mean ± standard deviation) over the 8 hours. The moderate humidity exposure was 43.0 ± 4.3% over the 8 hours (Fig. 2). There was no observable behavioral differences or evidence of respiratory distress following exposure in either group. No gross evidence of inflammation or damage to the laryngeal mucosa was observed during visual examination under a dissecting microscope.

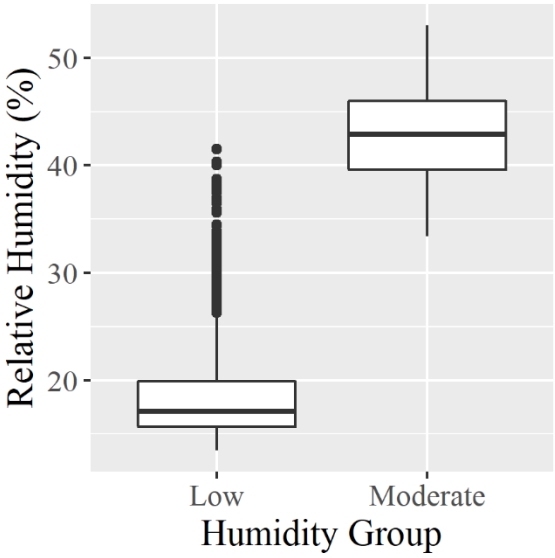

Figure 2.2. Relative humidity measured during experimental exposures of 8 hours. Aggregate data for relative humidity measured across all experiments for each group. Box plots represent the quartiles of the population distribution.

2.4.2 Packed Cell Volume (PCV)

The pre-experiment PCV (%) across all 14 rabbits was 46.7 ± 2.8 (mean ± SD). The % change in PCV from baseline to after the experiment did not differ significantly between the low and moderate humidity groups ($p = 0.1692$).

2.4.3 Sequence Read Mapping and RNA-Seq

Approximately 69 to 112 million paired reads were obtained by RNA-Seq with an average of 70% quality reads mapping to genes in the rabbit genome in each sample. In total, 23,669 annotations were obtained. Differential gene expression by Cuffdiff revealed 103 genes reaching an FDR < 0.05 with 61 meeting the additional fold change ($|\log2\ FC| \geq 1$) filtering criterion. Of these, 48 genes were considered significantly downregulated and 13 genes were significantly upregulated. The 10 genes with the greatest up- and downregulated fold changes from this list of 61 are shown in Table 2.2. A complete list of all genes identified is provided within the Additional file 1: Table S1 (available here: https://doi.org/10.1186/s12864-020-07301-7).

Rabbits were compared using principal component analysis based on FPKM obtained from Cuffdiff without low expression genes being removed (Fig 3). The first two principal components explain 44% of the total variability. Although neither PC1 nor PC2 were able to distinguish low humidity rabbits from control rabbits, rabbits tended to cluster according to their treatment information based on PC1 and PC2 together. The rabbits with the most prominent deviations, LH26 and CH35, were not found to be consistent outliers within the qRT-PCR analyses discussed below.

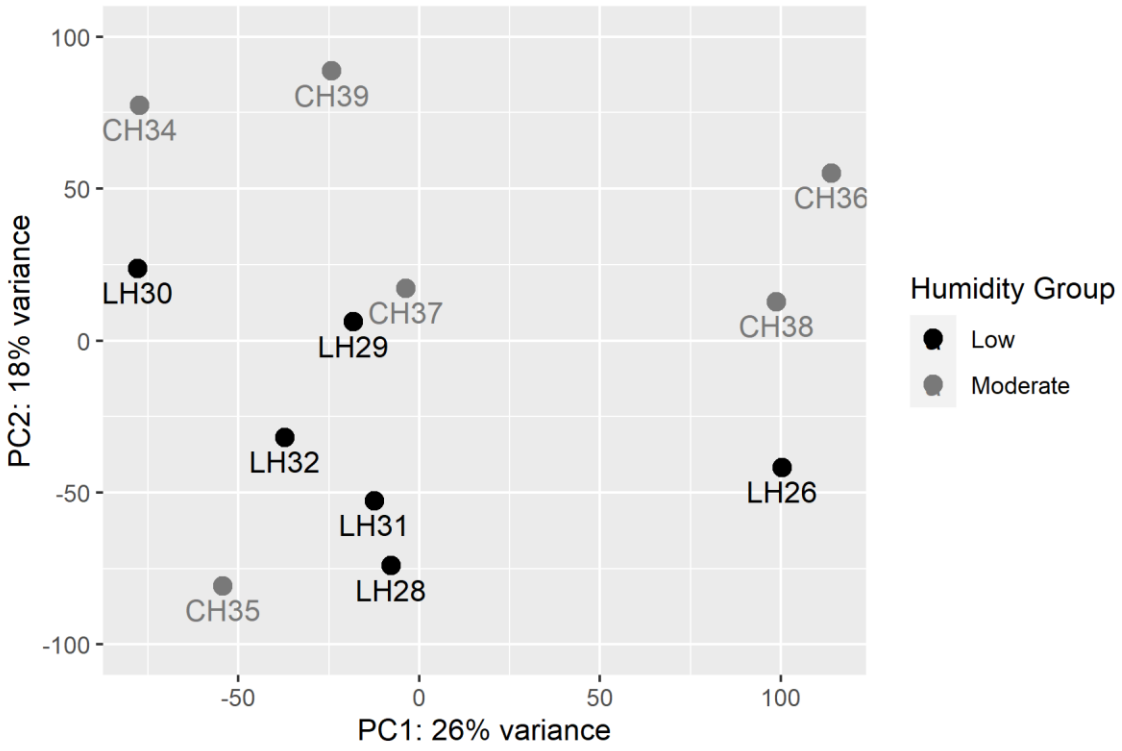

Figure 2.3. Principal component analysis of rabbits across groups based on FPKM obtained by Cuffdiff.

Table 2.2. List of the ten most significantly upregulated and downregulated genes as identified by RNA-Seq.

ENSEMBL ID	Gene symbol	log2 FC	FDR	Biomart Annotation
ENSOCUG00000003548	*ECCP* [a]	-2.574	0.0121	epithelial chloride channel protein[b]
ENSOCUG00000024036	*COL6A5*	-2.550	0.0121	collagen type VI alpha 5 chain
ENSOCUG00000013994	*PLA2G4D*	-2.529	0.0121	phospholipase A2 group IVD
ENSOCUG00000010912	*KRTDAP*	-2.505	0.0121	keratinocyte differentiation associated protein
ENSOCUG00000011842	*CRNN*	-2.197	0.0121	cornulin
ENSOCUG00000029191	-	-2.072	0.0121	immunoglobulin lambda variable precursor[c]
ENSOCUG00000011037	*MYH7*	-2.030	0.0121	myosin heavy chain 7
ENSOCUG00000014187	*MINAR1*	-2.009	0.0212	membrane integral NOTCH2 associated receptor 1
ENSOCUG00000008772	*FANK1*	-1.905	0.0121	fibronectin type III and ankyrin repeat domains 1
ENSOCUG00000011472	*FOXJ1*	-1.854	0.0121	forkhead box J1
ENSOCUG00000013331	-	1.469	0.0121	glutathione peroxidase**
ENSOCUG00000027549	-	1.497	0.0212	immunoglobulin heavy constant IG chain C[c]
ENSOCUG00000016426	*AGER*	1.516	0.0300	advanced glycosylation end-product specific receptor
ENSOCUG00000006499	*MGARP*	1.566	0.0121	mitochondria localized glutamic acid-rich protein
ENSOCUG00000007106	*RAE2*	1.689	0.0121	ribonuclease 8
ENSOCUG00000027406	*LDHA*	1.747	0.0120	lactate dehydrogenase A chain[c]
ENSOCUG00000024691	*ATPB*	1.856	0.0121	ATP synthase subunit B[c]
ENSOCUG00000024788		1.941	0.0121	L-lactate dehydrogenase A chain-like
ENSOCUG00000003229	*MCP-1*	2.226	0.0121	macrophage cationic peptide 1[b]
ENSOCUG00000008303	*MMP12*	2.277	0.0364	matrix metallopeptidase 12[b]

The twenty genes listed meet both filtering criteria of FDR < 0.05 and |log2 FC| ≥ 1. Annotations were obtained with Biomart from references to NCBI database information

[a]*ECCP* is not a formal gene symbol and is used for the purpose of this study

[b]Genes selected for validation by RT-qPCR

[c]Annotation not available through Biomart and was obtained by a search of ENSEMBL database by ID. Negative and positive values of log2 FC denote down- and upregulated genes, respectively

2.4.4 Functional Enrichment Analysis

Functional enrichment analysis by DAVID and STRING provided similar but distinct sets with FDR < 0.05. DAVID identified 4 GO terms for biological process, 6 GO terms for cellular component, 2 GO terms for molecular function, and 7 processes by KEGG with FDR < 0.05. GO terms and KEGG processes included cardiac muscle function, calcium binding, chemical carcinogenesis, and ECM-receptor interaction. STRING provided a richer set with 7, 15, and 19 GO terms for biological process, cellular component, and molecular function, respectively, and 2 KEGG processes. GO terms included stress and inflammatory response, cytoskeleton, and ion binding.

For GSEA, 16 genes sets were significantly enriched in the low humidity group with an FDR < 0.25. There were 5, 6, 5 terms for biological process, cellular compartment, and molecular function, respectively. These include collagen, basement and plasma membrane, epidermis development, and epithelial cell differentiation. In the moderate humidity group 6 gene sets were significantly enriched with FDR <0.25. There were 3, 1, and 2 terms for biological process, cellular compartment, and molecular function, respectively. These include olfactory receptor activity and cellular response to calcium. The full lists of terms, functions, associated genes, and statistics for the aforementioned DAVID and STRING analyses, and the subset of data with FDR < 0.05 from GSEA are provided in Additional file 2: Table S2 (available here: https://doi.org/10.1186/s12864-020-07301-7).

The predicted protein-interacting network generated by STRING is shown in Fig. 4. There were 8 clusters identified with between 2 to 10 gene products. Larger clusters contain members that are associated with cellular response to external stimuli and immune response (dark green, lavender), muscle function (red), keratinocyte development (light green), and ciliary function (aqua).

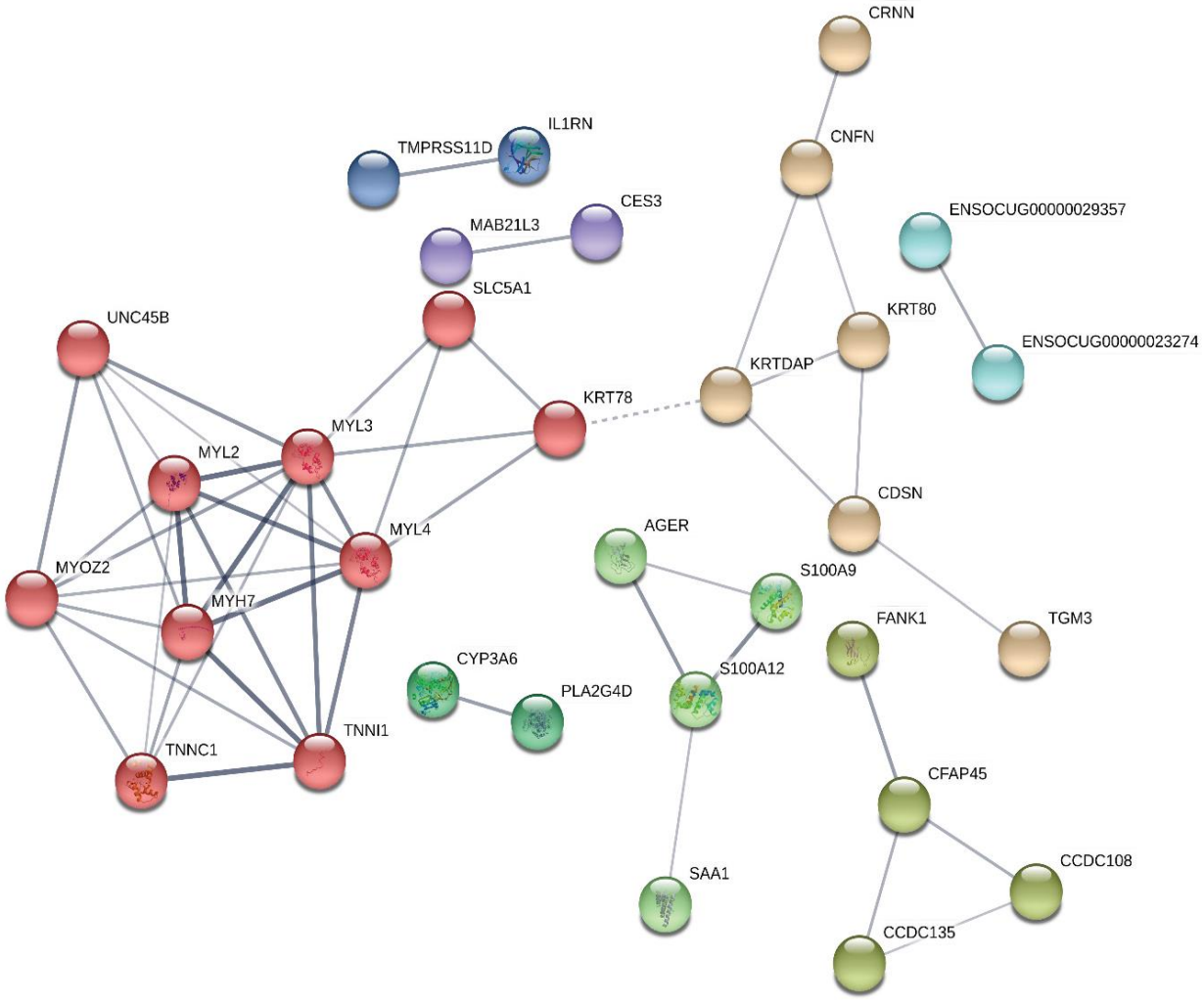

Figure 2.4 Protein interaction network was created using STRING. A 100 node network was obtained from an input set of 103 differentially expressed genes identified by Cuffdiff with an FDR < 0.05. The line thickness represents the strength of the data to support the interaction, including text mining, experimental, database, co-expression, neighborhood, gene fusion, and co-occurrence sources. The minimum required interaction score was set to 0.4. Shell parameters were set to "None". Disconnected nodes are not shown. Cluster colors are based on the Markov Cluster Algorithm with the inflation parameter set to 2.

2.4.5 RT-qPCR Validation

Eight genes were selected for subsequent data validation by RT-qPCR based on their predicted functions and assumption of relevance to vocal fold or laryngeal physiology; they consist of ENSOCUG00000003548, annotated as an epithelial chloride channel protein which will be referred to as "*ECCP*", cadherin related family member 4 (*CDHR4*), corneodesmosin (*CDSN*), macrophage cationic peptide 1 (*MCP1*), matrix metallopeptidase 12 (*MMP12*), suprabasin (*SPBN*), zinc activated cationic channel (*ZACN*), and mucin 21 (*MUC21*), although the absolute value of log2 FC for *MUC21* by RNA-Seq was only 0.79.

Of the eight genes tested, significant differences in relative expression were validated for *ECCP* ($p = 0.028$), *MCP1* ($p = 0.030$), and *MMP12* ($p = 0.045$) and were marginally non-significant for SPBN ($p = 0.067$) and *ZACN* ($p = 0.066$). The most prominent fold changes between the low and moderate humidity groups was observed for *MMP12* (FC = 6.8), *MCP1* (FC = 5.2), and *ZACN* (FC = 2.76). *ECCP* exhibited the largest downregulation (FC = 3.74). The remaining genes exhibited non-significant changes despite differential expression by RNA-Seq analysis (Fig. 5). Comparison of data from RNA-Seq and RT-qPCR are provided in Table 2.3.

2.4.6 *In silico* analysis of ENSOCUG00000003548 gene (*ECCP*)

ENSOCUG00000003548 maps to NCBI gene accession number 100352679, annotated as epithelial chloride channel protein. This gene lies downstream of LOC100338755 (calcium-activated chloride channel regulator 4-like), calcium-activated chloride channels 4, 2, and 1 (*CLCA4, CLCA2, CACL1*).

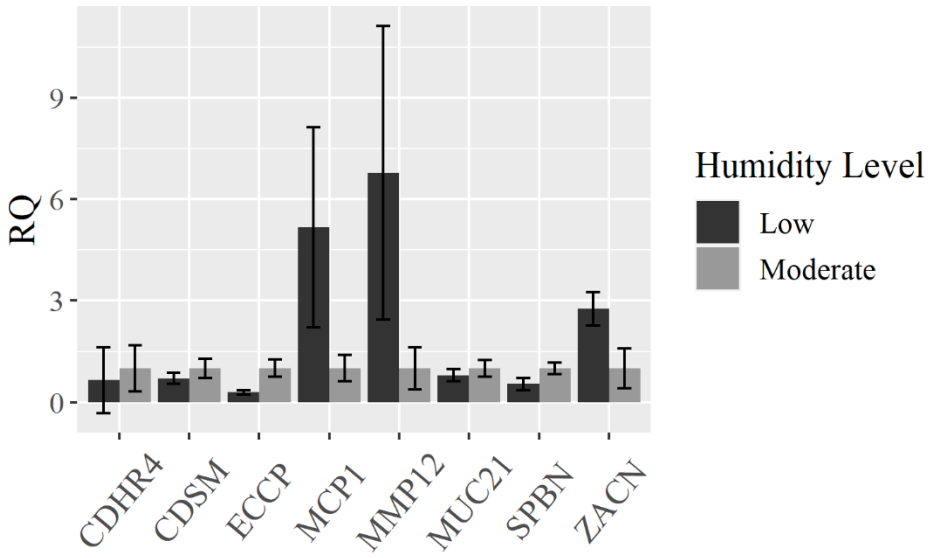

Figure 2.5. RT-qPCR validation. Relative quantification for each gene was determined by the ΔΔCt method. All reactions were run in triplicate. The level of expression of each tested gene was standardized to the housekeeping gene HPRT1, and ΔΔCt was calculated using the average of the ΔCts from the control group for the respective gene. ECCP, MCP1 and MMP12 were significantly different ($p < 0.05$) and SPBN and ZACN marginally non-significant ($p = 0.06$). Differences between groups as determined by the Welch t-test. Results represent 5–7 samples/group for each gene after the removal of outlier values as determined by the iterative application of a two-tailed Grubb's test. Error bars represent the SEM for relative quantification within the respective humidity group.

Table 2.3. Summary of genes selected for follow up analysis by RT-qPCR.

Ensembl ID (NCBI Gene ID)	Gene	log2 FC (RNA-Seq)	FDR RNA-Seq	log2 FC (qPCR)	P-value qPCR
ENSOCUG00000003548(100352679)	*ECCP**	-2.57	0.01	-1.796	0.028
ENSOCUG00000009174(100358424)	*CDHR4*	-1.80	0.01	-0.618	0.363
ENSOCUG00000006280(100338321)	*CDSN*	-1.32	0.01	-0.513	0.186
ENSOCUG00000003229(100009115)	*MCP1*	2.23	0.01	2.371	0.030
ENSOCUG00000008303(100009559)	*MMP12*	2.28	0.04	2.764	0.045
ENSOCUG00000001869(108177417)	*MUC21*	-0.79	0.01	-0.329	0.228
ENSOCUG00000010917(100346157)	*SPBN*	-1.15	0.01	-0.905	0.067
ENSOCUG00000000422(100358831)	*ZACN*	1.27	0.01	1.466	0.066

**ECCP* is not a formal gene symbol and is used for the purpose of this study

2.5 Discussion

The transcriptional changes observed in this study indicate that just 8 hour exposure to a low humidity environment can adversely affect vocal fold biology. To the best of our knowledge, this is the first study to demonstrate the effects of surface dehydration on vocal fold tissue *in vivo*. Important to our methodology, evaluation of the change in PCV following experimental challenge ruled out systemic dehydration as an unintended confounding factor in our analysis. There is considerable evidence that systemic dehydration negatively impacts phonation [59,130-132]. Surface dehydration represents a loss of water from the mucosal surface of the larynx, and while some level of local tissue water loss may be experienced through compensatory rehydration of the epithelial surface, we would not expect systemic dehydration to result. We hypothesize that the homeostatic responses to surface and systemic dehydration are governed by different cellular mechanisms, thus we used % PCV change to control for unintended systemic consequences of low humidity exposure with the concomitant withholding of food and water.

We developed a method to efficiently challenge rabbits to low humidity. We achieved average low relative humidity of approximately 20%, representing physiologically-realistic and substandard occupational conditions per Occupational Safety and Health Administration (OSHA) recommendations [156]. Moderate humidity control exposures were conducted in the same chamber with all compartments open to room air of variable temperature within housing guidelines for rabbits. Low humidity challenge and moderate humidity exposure could not be conducted at the same time because preliminary tests demonstrated that a fully closed air circuit that is needed to lower humidity in the chamber measurably increased the interior temperature of the compartments. By separating them, we successfully maintained appropriate ambient temperatures for the low humidity exposures [157] and maintained a 2-fold increase in moderate humidity exposures.

It is noteworthy that exposure to low relative humidity below the Occupational Health and Safety Administration (OHSA) recommended limit of 20% induced transcriptional changes within functional gene categories including inflammation, ion transport, and keratinocyte development. The most robust functional enrichments identified by STRING were stress, defense, and inflammatory responses. Additionally, outside of the STRING analysis, various genes for immunoglobulin chains were identified, three of which were downregulated and one

that was upregulated. Interestingly, this cluster presents two opposing interpretations of innate immune dampening and possible macrophage activation.

While none of these genes or corresponding proteins are described within the larynx, the downregulated cluster can be interpreted as a dampening of acute inflammatory response. ORM1 and SAA1 are both acute phase proteins. ORM1 is an acute phase protein that has been shown to polarize M2 macrophage differentiation [158] and to enhance epithelial integrity in a culture model of the blood-brain barrier [159]. While ORM1 exhibits anti-inflammatory activity and its downregulation may allow for the development of a more robust inflammatory process, it may also be interpreted as indicative of surface dehydration not contributing to an activating inflammatory event. SAA1 is also an acute phase protein and is associated with a variety of pathological conditions, but it has also been shown to positively influence keratinocyte activity [160]. The S100 proteins are diverse with involvement in several cellular processes, but both S100A9 [161] and S100A12 [162] have been described as damage associated molecular patterns in the literature. Taken together, these results suggest that either surface dehydration is not inducing inflammatory pathways or that there is active repression of pro-inflammatory mediators. The latter is substantiated by the increase of *IL1RN* which encodes the IL-1 receptor antagonist (IL1RA). *IL1RN* was upregulated in the posterior cricoarytenoid muscle one week following transection of the recurrent laryngeal nerve in a rat model [163], and IL1RA was significantly increased following 8 hours of industrial exposure to respirable and inhalable dust in humans [164]. Together this substantiates a role for the increased *IL1RN* we observed and of a possible active innate immunity repression in response to the low humidity challenge.

Conversely, the upregulation of *MMP12* and *MCP1* genes may suggest the activation of inflammatory macrophages. *MMP12* was the most significantly upregulated gene in this study by RNA-Seq and RT-qPCR. MMP12 exhibits proteolytic activity on multiple ECM components including elastin, fibronectin, entactin, and type IV collagen [165], all of which are expressed within the vocal folds. Although called “macrophage elastase”, it is also expressed in human vocal fold fibroblasts [166] and bronchial epithelial cells *in vitro* [167], and in both superficial and deep epidermal layers of the skin in response to ultraviolet radiation [168]. MMP12 has a potential role in the development of dysphonia following low humidity exposure since type IV collagen and elastin play an important role in the viscoelasticity and phonatory function of the vocal folds [169,170]. MMP12 may contribute directly to inflammation though epidermal growth factor receptor

(EGFR) dependent induction of IL-8 from the respiratory epithelium [171]. Interestingly, MMP12 has been shown to positively influence wound healing following epithelial injury to the cornea [172], so it is unclear if the upregulated response to low humidity would be deleterious or influence a reparative response in the vocal folds. *MCP1* is an α-defensin expressed in the lungs of fetal and adult rabbits [173]; it is secreted from neutrophils and rabbit lung macrophages and exhibits broad antimicrobial activity In our study, the expression of *MCP1* was novelly detected in the rabbit larynx, and its upregulation in repsose to low humidity warrants further investiation including targeted anaylsis of differential expression between inflammatory cells and the larygeal tissue.

It is not surprising to find evidence of a pro-inflammatory response with surface dehydration as other environmental stressors such as simulated acidic reflux [174], hypertonic challenge [141], and phonotrauma [52,175] can perturb the epithelial tight junctions of the vocal folds—indicative of the activation of proinflammatory pathways. As we did not investigate for cell-specific gene expression in this study, we are limited to conclude if the upregulation of these genes reflects activation of macrophages or activity of the epithelium or lamina propria fibroblasts, and further study is warranted. An intriguing hypothesis for a case of macrophage activation would be altered response to local microbiome or pathogens resulting from changes to the laryngeal microenvironment following dehydration.

The perturbation of ion transport or other lubrication mechanisms is anticipated as a response to the altered hydration state of the laryngeal surface [65]. Although no gene or protein interaction enrichment cluster was identified within the 103 DEGs analyzed, presumably due to the diversity of substrate and transporter type, a considerable set of ion and solute transporter related genes were identified by RNA-Seq, including *ECCP*, *SLC5A1*, *SLC13A5*, *SLC23*A1, *SLC27A2*, and *ZACN*. All SLC family members were downregulated. This set represents predominantly ion transport, with SLC13A5 and SLC27A2 being involved in glucose transport and fatty acid ligation. In *vitro* studies of human nasal epithelial cells [82] and human bronchial cell culture [81] demonstrated that apical osmotic pressure can result in altered epithelial electrolyte transport; however, studies with canine tracheal and bronchial cell culture [78] and an *in vivo* canine model [66] concluded that not all epithelial fluid flux is coupled to electrolyte transport. This evidence suggests that the epithelium may respond to either aberrant electrolyte concentrations or non-ionic osmotic pressure. It is not surprising to find evidence of altered

chloride secretion specifically, as balanced sodium and chloride ion secretion is attributed to volume regulation of the airway surface fluid, but the contribution of transport of other ionic and non-ionic species is not well described for airway surface fluid regulation. Our results suggest the pertinence of future targeted study of noncanonical secretion products in the respiratory tract.

Although the *ECCP* is annotated as an epithelial chloride channel protein, the translation product for *ECCP* is neither well characterized nor has a direct ortholog in humans. It may belong to the calcium-activated chloride channel proteins (CLCA) family as identified by conserved functional domains, although it exhibits limited homology to the rabbit CLCA proteins. The genes for *CLCA1, CLCA2,* and *CLCA4* lie within the same genetic neighborhood as *ECCP* but were identified by RNA-Seq with FDR > 0.99, indicating they are not differentially expressed in our model of surface dehydration. This suggests a distinct role for *ECCP* and its downregulation that warrant further investigation as an ion channel protein newly described in the context laryngeal surface dehydration. In contrast to *ECCP,* ZACN was upregulated in low humidity compared to moderate humidity but failed to reach statistical significance by RT-qPCR. ZACN is a cation channel expressed in the human trachea and other tissues and demonstrates permeability to potassium ions but not to chloride ions [176]; there is no discussion of its expression in the vocal folds in the literature, and it is unclear if it may also be sodium ion permeable. Taken together with the SLC family members identified, these results support a potential role for solute flux as a homeostatic response to surface dehydration. Interestingly, however, the downregulation of chloride transportation would be a counterintuitive response to surface dehydration at the apical membrane as chloride is generally directed out of the cell and aberrant chloride transport can be detrimental in the airways as seen in cystic fibrosis. There is a distinction between the respiratory epithelium of the airways and the nonkeratinized stratified squamous epithelium of the vocal folds, so care must be taken with direct translations of actions between the two.

The mucins are equally important to maintain satisfactory hydration of the laryngeal surface as ion and fluid flux. *MUC12*, *MUC21*, and *TFF1* were identified as downregulated by RNA-Seq. Both mucins are members of the cell-surface associated mucin family, and as such, should originate directly from the epithelial cells. The first exon of *MUC12* exhibited increased expression in laryngeal epithelium from laryngeal reflux patients compared to reflux negative patients [177]. Exogenous surface expression of MUC21 in *in vitro* cell culture reduced intercellular

adhesion and adhesion to extracellular components [178]. It is interesting then to observe all three to be downregulated. However, in addition to roles as epithelial protectants, mucins and related proteins also serve roles in cell signaling with physiological consequences. This is recently shown for MUC21 overexpression as influencing the development of lung adenocarcinoma [179] and TFF1 influencing epithelial-mesenchymal transition. Together, this may be a contributing factor to the STRING cluster of keratinocyte differentiation factors discussed below, but further study is warranted to determine which cell types are expressing these genes and which cell signaling may be impacted.

Although there was no gross inflammation observed, some level of epithelial cellular response to surface dehydration is expected. The vocal folds are covered by a non-keratinized stratified squamous epithelium for which some aspects of development are well understood, such as embryological developmental factors and differentially expressed structural components [34,180], but a comprehensive molecular description is not available as for other epithelia like the epidermis. It is interesting that several keratinocyte developmental and epithelial structural factors were identified with RNA-Seq, enriched in the low humidity group by GSEA, and as a protein interaction cluster in the STRING analysis: CDSN, CNFN, CRNN, KRT80, KRTDAP, and TGM3. Also identified by RNA-Seq were *SPBN*, another keratinocyte factor, and *CDHR4*, a cell interaction mediator. All of these were downregulated. *SPBN*, *CDHR4*, and *CDSN* were selected for RT-qPCR validation. All three gene products may be involved in maintaining the integrity of the stratified squamous epithelium, though none have been described specifically within the vocal folds until this study. SPBN is expressed in the suprabasal layers of tongue, stomach, and epidermis [181]. It is required for keratinocyte differentiation in an *in vitro* skin model [182] and skin development in murine embryos [183]. The specific activity of CDHR4 is not described in the literature, but family member CDHR2 is expressed in gastrointestinal epithelial cells and is associated with microvillus development [184], while family member CHDR3 is expressed in ciliated respiratory epithelial cells and is associated with ciliary development and intercellular interactions [185]. CDSN is expressed in the stratum granulosum of human skin and appears to participate in cellular cohesion at this level, with its loss associated with desquamation [186,187]. That the entire cluster was downregulated substantiates surface dehydration as capable to influence vocal fold epithelial maintenance. Further study is required to elucidate the specific roles of these proteins within the vocal folds, as this epithelium is distinct from the epidermis.

2.5.1 Limitations

A limitation of designing an environmental chamber as described here was that it precluded the provision of relative humidity lower than 15%. While environmental rooms and chambers are commercially available, they are cost prohibitive and their small size precludes the use of certain animal models, such as rabbits. Another limitation of the study is that we only observed a single time point after low humidity exposure. It has been shown that local response to vocal fold injury is transient and time-dependent [143,148,188]. Further studies specifically observing for inflammatory response at multiple times points within a single challenge or within repeated or chronic challenges would be helpful in further characterization of vocal fold biology. Finally, the dissected vocal fold tissue included striated muscle and small amounts of respiratory epithelium immediately above and below the region of the vocal folds. Therefore, genes associated with muscle or respiratory epithelium were not selected for the discussion.

2.6 Acknowledgements

We acknowledge Jessica Engen and Chenwei Duan for invaluable support to animal husbandry and sample collection, Dr. Mara Varvil for assistance with physical assessment of animals and technical support, Norvin Bruns from the Purdue Biomedical Engineering Machine Shop for assistance in the construction of the environmental chamber, Alison Sorg formally from the Purdue Genomics Core, and Kenneth Price for the schematic illustration of the environmental chamber.

CHAPTER 3. RECURRING EXPOSURE TO LOW HUMIDITY INDUCES TRANSCRIPTIONAL AND PROTEIN LEVEL CHANGES IN THE VOCAL FOLDS OF RABBITS

The chapter represents original research previously published.
Bailey, Taylor W., et al. "Recurring exposure to low humidity induces transcriptional and protein level changes in the vocal folds of rabbits". Scientific Reports, vol. 11(1), https://doi.org/10.1038/s41598-021-03489-0

3.1 Abstract

Voice disorders are an important human health condition. Hydration is a commonly recommended preventive measure for voice disorders though it is unclear how vocal fold dehydration is harmful at the cellular level. Airway surface dehydration can result from exposure to low humidity air. Here we have induced airway surface dehydration in New Zealand White rabbits exposed to a recurring 8-hour low humidity environment over 15 days. This model mimics an occupational exposure to a low humidity environment. Exposure to moderate humidity was the control condition. Full thickness soft-tissue samples, including the vocal folds and surrounding laryngeal tissue, were collected for molecular analysis. RT-qPCR demonstrated a significant upregulation of *MUC4* (mucin 4) and *SCL26A9* (chloride channel) and a large fold-change though statistically non-significant upregulation of *SCNNA1* (epithelial sodium channel). Proteomic analysis demonstrated differential regulation of proteins clustering into prospective functional groups of muscle structure and function, oxidative stress response, and protein chaperonin stress response. Together, the data demonstrate that recurring exposure to low humidity is sufficient to induce both transcriptional and translational level changes in laryngeal tissue and suggest that low humidity exposure induces cellular stress at the level of the vocal folds.

3.2 Introduction

Voice disorders are an important health problem affecting people worldwide, particularly individuals whose profession requires the use of voice [116,123,189]. Maintaining proper hydration is recommended to avoid developing voice problems and to alleviate the symptoms of voice

disorders. Research pertaining to the homeostatic mechanisms regulating the airway surface hydration is abundant the literature [75,138,190,191]; however, data specific to vocal fold tissue is not available. Studies of vocal perturbations in response to surface dehydrating activities such as breathing desiccated air demonstrate increases in acoustic, aerodynamic, and subjective measures of phonation [63]. However, there is a gap in our knowledge of the biological processes that underlie these changes. The effect of dehydration in the vocal fold under ecologically valid environments is still uncertain. Furthermore, dehydration may occur through two distinct physiological modalities: systemic dehydration where the body draws water centrally from tissues or surface dehydration involving the evaporative water loss from the laryngeal surface. It is unclear if systemic and surface dehydration would share similar molecular pathology.

We have begun to characterize the biological changes in vocal fold tissue after systemic dehydration. Acute dehydration by drug-induced diuresis in rabbits was associated with downregulation of various genes related to epithelial development and junctional integrity identified by RNA Sequencing and validated by RT-qPCR [100,101]. Vocal folds from rats subjected to water restriction exhibited decreased transcriptional expression of *interleukin-1α* and *desmogelin-1* with histologically observed decreases in hyaluronan attributed to an increased transcription of *hyaluronidase-2* [101]. Our most recent study showed that a single eight hour exposure to low humidity induced gene expression of *matrix metalloprotease 12* and *macrophage cationic peptide 1* while decreasing expression of an uncharacterized epithelial chloride channel [192]. To further explore the molecular effects to the vocal folds of low humidity exposure in realistic environments, here we have used repeated low humidity exposure (8 hours over 15 days). This is a model that allows us greater insight into the implications of low humidity exposure as they relate to occupationally relevant contexts, as professional voice users subject to suboptimal environmental conditions are among those at greatest risk for developing voice disorders. The present study seeks to enhance the translational value of our understanding through novel description of the biological response at the gene expression and proteome level.

Detailed study of human laryngeal physiology is precluded predominantly by ethical considerations of intentionally damaging the larynx of individuals, given its critical roles in airway protection and voice production. Thus *in vivo* human studies are limited to non-invasive measures of acoustic, aerodynamic, and functional parameters, while *ex vivo* studies are limited to interventionally-resected or post-mortem tissues. Many animal models have been used to

study the larynx, including dogs [60], pigs [58], rabbits [24], and sheep [137]. Adult rabbit larynges approximate juvenile human larynges and share the same basic cellular and histological composition [143-145]. The primary structural difference is that rabbits lack the pair of vestibular folds ("false vocal folds") present in humans and other animals. While this may impact functional studies of the larynx, molecular analysis of vocal folds themselves is facilitated by the absence of a secondary complex structure. The rabbit is also validated as a model for vocal fold injury [52,146] and recently as a training model for laryngotracheal surgery [149].

Here we have used a New Zealand White rabbit model of exposure to a low humidity environment. Three experiments were conducted: 1) a gene expression experiment; 2) a pilot proteomics experiment; and 3) a comprehensive proteomics experiment. In each experiment, a recurring exposure of 15 days was selected to mimic a two-week occupational exposure to a low humidity environment. The controlled exposure was moderate relative humidity (at least a 2-fold higher percentage than low humidity). Packed cell volume (PCV) was measured during the experiment to rule out the development of systemic dehydration as a confounding factor [193], as a published study by our group demonstrated that systemic dehydration resulted in transcriptional changes in the rabbit vocal fold tissue [100]. We hypothesized that recurring exposure to low humidity environments would produce observable molecular effects. To investigate this hypothesis, we analyzed a targeted set of genes with known expression in the larynx by RT-qPCR. Additionally, a high throughput proteomic approach was applied to compare the effects to the proteomic profile in low humidity, using moderate humidity as the control.

3.3 Materials and Methods

3.3.1 Rabbit Care

All experiments were conducted in accordance with the guidelines and after approval of the Purdue Animal Care and Use Committee (Protocol # 1606001428) and following ARRIVE guidelines. Male New Zealand White rabbits, six months of age, were obtained from Envigo Global (Indianapolis, IN) and acclimatized for at least one week before experimentation. For this study, a total of 30 rabbits were used in 3 experiments: 1) gene expression experiment; 2) pilot proteomics experiment; and 3) comprehensive proteomics experiment. Due to the technical limitation that our humidity exposure system could support only six rabbits at a time, multiple

cohorts were necessary. The cohorts are designated as A, B, C, D, and E. Experiment 1 involved cohorts A (rabbits M1-3 and L1-3) and B (rabbits M4-6 and L4-6) and resulted in RT-qPCR data. Experiment 2 involved cohort C (rabbits M7-9 and L7-9) and resulted in pilot proteomics data. Experiment 3 involved cohorts D (rabbits M20-22 and L20-22) and E (rabbits M23-25 and L23-25) and resulted in comprehensive proteomics data.

Rabbits were randomly assigned to two humidity groups in each cohort: three rabbits with moderate humidity (control) and three rabbits with low humidity. No rabbits were excluded from the analysis. Sample sizes for experiments were determined following consultation with the Purdue Bioinformatics Core and the Purdue Proteomics Core. Food and water were withheld during experimental exposures and provided *ad libitum* between exposures. Blood was collected via venipuncture of the lateral ear vein at the start (day 1) and the midpoint (day 8) of the experiment and immediately preceding euthanasia (day 15) in order to measure packed cell volume (PCV). Euthanasia was completed with a single IV dose (1 mL) of Beuthanasia-D Special (Schering Plough Animal Health Corp., Union, NJ, USA) through the lateral ear vein.

3.3.2 Humidity Challenge Protocol

Low humidity exposure was conducted in a specially fabricated environmental chamber (Figure 3.1). Rabbits were housed three at a time in individual compartments with shared airspace. A 70-pint commercial dehumidifier (Hisense, DH70KG: Qingdao, China) was set to high continuous and attached to the chamber in a semi-closed air circuit with 4-inch ducting. Dehumidified air entered the center of the chamber lid through a plenum designed to minimize the force of airflow and exited through three ports near the bottom of each rabbit compartment. Room air was titrated as necessary through wall ports of the rabbit compartments and at the outflow from the dehumidifier. Moderate humidity exposures were conducted simultaneously in an environmental chamber in a different room left open to room air. Internal relative humidity for both chambers was tracked using a HOBO Data Logger with a 12-bit Temperature/Relative Humidity Smart Senor (U14-002, S-THD-M002: ONSET, Bourne, MA, USA) at one-minute intervals.

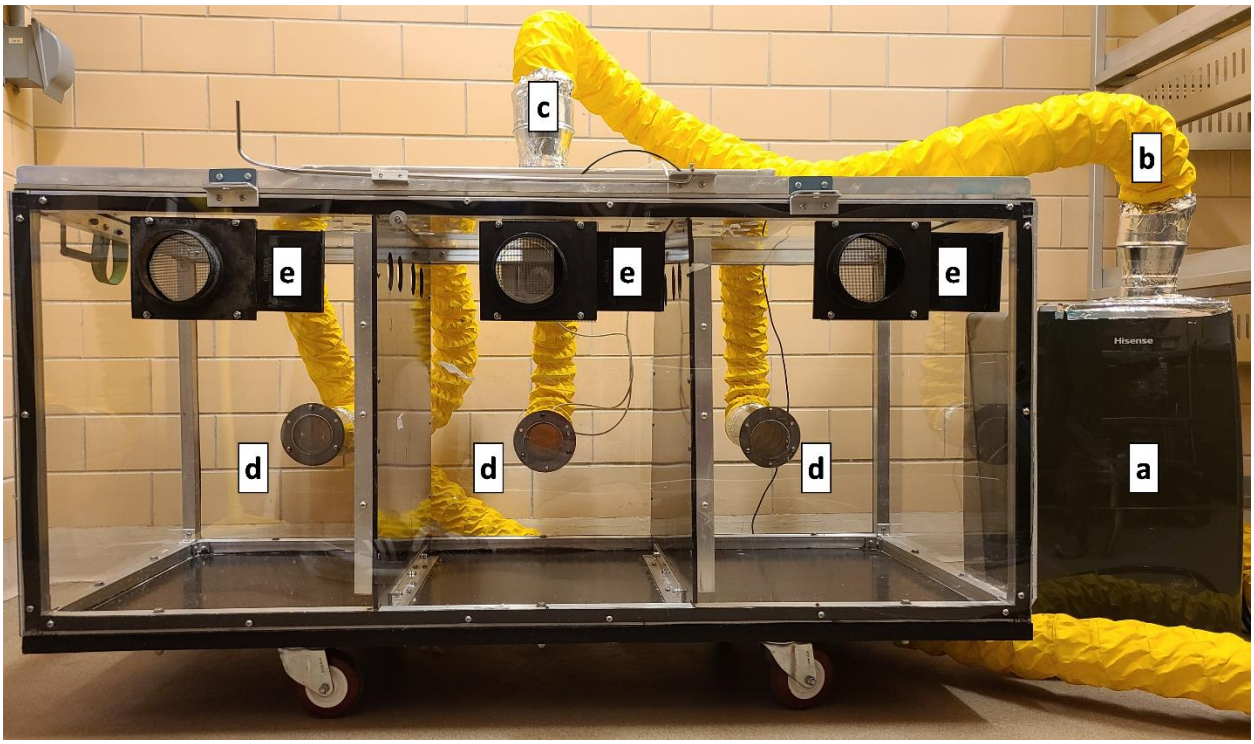

Figure 3.1. Environmental chamber. (a) 70-pint dehumidifier with vertical outflow captured by a plenum into 4-inch ducting (b) to an intake plenum on the roof of the environmental chamber (c). Air flowed out of the chamber through three ports (d) in the rear wall, which fed back into the dehumidifier through 4-inch ducting. Room air was titrated through closable ports (e) on the front wall of the chamber.

3.3.3 Sample Collection

The larynx and proximal trachea were excised from each animal immediately following euthanasia. The larynx was bisected posteriorly along the sagittal midline and pinned onto wax to expose the laryngeal lumen. Full-thickness soft tissue, 2-3 mm each, was microdissected bilaterally at the level of the glottis under magnification with microdissection scissors. Samples for RNA analysis were immediately placed in RNAlater® Stabilization Solution (Invitrogen, Waltham, MA, USA), stored at 4 °C overnight, and -80 °C until processing. Samples for proteomic analysis were immediately frozen in liquid nitrogen and stored at -80 °C until processing.

3.3.4 RNA Extraction and Reverse Transcription-Quantitative Polymerase Chain Reaction (RT-qPCR)

Total RNA from vocal fold tissue was extracted with the RNeasy Fibrous Tissue Mini Kit following the manufacturer protocol (QIAGEN®, Hilden, Germany). Total RNA (400 µg) was used to generate cDNA with SuperScript™ IV VILO™ Master Mix (Invitrogen). RT-qPCR was performed using SYBR Green 2x PCR Master Mix (Applied Biosystems, Waltham, MA, USA) with 0.1 M of each primer and 2.5 µL of template cDNA in a 25 µL reaction volume using a QuantStudio 3 System (Applied Biosystems) thermocycler. Data was collected over 40 cycles by QuantStudio Design & Analysis Software v1.5.1. Relative expression quantification of each gene was calculated using the $2^{(-\Delta\Delta Ct)}$ method [153] and is reported as fold change compared to standardized expression from animals in the moderate humidity group. *HPRT1* gene was used as endogenous control to normalize the relative quantification of target genes. This gene showed consistent expression across vocal fold samples from both humidity groups and was used as normalizer in previous rabbit studies of our group [100,192].

Twelve target genes were selected for analysis based on either previous results from our group (Matrix metalloproteases 1 and 12: *MMP1*, *MMP12*, and a Zinc activated cation channel *ZACN*) [192] or with anticipated relation to vocal fold hydration given documented laryngeal expression. These include aquaporins (*AQP1*, *AQP4*, *AQP5*) [76], bradykinin receptor 2B (*BDKR2B*) [194], chloride channels (*CFTR*, *SLC26A9*) [75], matrix metalloproteinases, mucins (*MUC4*, *MUC5AC*) [195] and sodium channel (*SCNNA1*) [75], and a zinc activated cation channel () [192]. The sequences of primers used are provided in Table 3.1.

Table 3.1**. q**PCR primers used in this study

Gene Symbol	**Direction 5' - 3'**	**Sequence**
AQP1	F	CCTTGCCATCGGCTTTTCTG
	R	AAGTCGTAGATGAGCACGGC
AQP4	F	AGCAAGGCGGTGGGGTAAG
	R	TGTTCCACCCCAGTTGATGG
AQP5	F	CAACGCGCTCAACAACAAC
	R	CGTGAGTCGGTGGAAGAGAAA
BDKRB2	F	GTTCCTGACAGTCTATGACGACC
	R	CCTGGATGACGTTGAGCCAG
CFTR	F	TGCAGATGAGGTTGGACTCAG
	R	ACTGGGTTCATCAAGCAGCA
SCNNA1	F	GGTGCACGGACAGGATGAG
	R	CCGGGCCGCAAGTTAAA
MMP1	F	TTGGGGCTTTGATGTACCCC
	R	CCCGCATGTAGAACCTGTCTT
MMP12	F	AGGCCATAATGTTTCCCACCT
	R	CTGCTCTGGGCCTCCATAAAG
MUC4	F	AGGGACGATGGGACTTACGA
	R	CATCCAACCAAAGTGCCAAGG
MUC5AC	F	ACTCGAAGACCTCGCTGAG
	R	GCACCTGCACCAATGACAAGA
SCL26A9	F	GCAACGCCTTCAGATGTTCC
	R	CACCAGGATGCTGATGACGG
ZACN	F	AACTGCGACTTTGAGCTCCT
	R	TGACCACGTATTCCCGCTTG

3.3.5 In-solution Digestion of Soluble and Insoluble Protein Fractions

Tissues were transferred to 2 mL vials lysed with ceramic beads in 100 mM ammonium bicarbonate (ABC, 350 uL) using a Precellys24 tissue homogenizer (Bertin Technologies, Rockville, MD, USA). The lysate was transferred to a new vial and centrifuged at 14,000 rpm for 15 minutes. The protein content was initially measured by Bicinchoninic Acid (BCA) assay, and 50 µg (equivalent volume) was aliquoted and ultra-centrifuged at 55k rpm for 40 minutes in an Optima MAX-XP ultracentrifuge (Beckman Coulter, Indianapolis, IN) to fractionate the soluble

and insoluble proteins. The supernatant containing the soluble fraction was collected and mixed with four volumes of cold 100% acetone, mixed thoroughly, and stored at -20 °C overnight to precipitate the proteins. The pellet from the soluble fraction after protein precipitation and the insoluble pellet fraction were reduced with 10 mM dithiothreitol, 8 M urea in 25 mM ABC (10 uL), and alkylated with 4% iodoethanol, 1% triethylphosphine in acetonitrile (10 uL). Both fractions were mixed with mass spectrometry grade trypsin and Lys-C mix (Promega, Madison, WI, USA) at a minimum 1:25 enzyme to substrate ratio and digested on a barocycler NEP2320 (Pressure Biosciences, South Easton, MA, USA) run at 50 °C for 60 cycles of 50 seconds at 20 kpsi and 10 seconds at atmospheric pressure. Peptides were desalted using Mini spin C18 spin columns (The Nest Group, Southborough, MA, USA), eluted with 80% acetonitrile (ACN), and 0.1% formic acid (FA), and dried at room temperature in a vacuum concentrator. Clean, dry peptides were resuspended in 3% ACN, 0.1% FA in water at a final concentration of 1 µg/µL, and 1 µL was used for LC-MS/MS analysis.

3.3.6 Mass Spectrometry Analysis

Samples were analyzed by reverse-phase LC-ESI-MS/MS system using the Dionex UltiMate 3000 RSLC nano System coupled to the Orbitrap Fusion Lumos Mass Spectrometer (Thermo Fisher Scientific, Waltham, MA, USA). Reverse phase peptide separation was accomplished using a trap column (300 µm ID × 5 mm) packed with 5 µm 100 Å PepMap C18 medium, and then separated on a reverse-phase column (50-cm long × 75 µm ID) packed with 2 µm 100 Å PepMap C18 silica (Thermo Fisher Scientific). The column temperature was maintained at 50 °C. The mass spectrometer was calibrated prior to starting the queue and at every 72 hours. The mass accuracy during calibration was maintained at <2 ppm to ensure high mass accuracy data collection.

Mobile phase solvent A was 0.1% formic acid (FA) in water, and solvent B was 0.1% FA in 80% acetonitrile (ACN). The loading buffer was 2% ACN,0.1% FA in water. Peptides were separated by reverse-phase by loading into the trap column in a loading buffer for 5 min at 5 µL/min flow rate and eluted from the analytical column with a linear 82 min linear gradient of 6.5-27% of buffer B, then changing to 40% of B at 90 min, 100% of B at 97 min at which point the gradient was held for 7 min before reverting to 2% of B at 104 min. Peptides were separated from the analytical column at a flow rate of 300 nL/min. The mass spectrometer was operated in

positive ion and standard data-dependent acquisition mode with the Advanced Peak Detection function activated. The fragmentation of precursor ion was accomplished by higher energy collision dissociation at a normalized collision energy setting of 30%. The resolution of Orbitrap mass analyzer was set to 120,000 and 15,000 at 200 m/z for MS1 and MS2, respectively, with maximum injection time of 50 ms for MS1 and 20 ms for MS2. The dynamic exclusion was set at 60 seconds to avoid repeated scanning of identical peptides, and charge state was set at 2-7 with 2 as a default charge and mass tolerance of 10 ppm for both high and low masses. The full scan MS1 spectra were collected in the mass range of 375-1,500 m/z and MS2 in 300-1,250 m/z. The spray voltage was set at 2, and the Automatic Gain Control (AGC) target of 4e5 for MS1 and 5e4 for MS2, respectively.

3.3.7 Bioinformatics and Data Analysis

The raw MS/MS data were processed using MaxQuant (v1.6.3.3) [196] with the spectra matched against the rabbit (*Oryctolagus cuniculus*) protein database downloaded from Uniprot (http://www.uniprot.org) on 03/13/2020. Data were searched using trypsin/P and LysC enzyme digestion, allowing for up to two missed cleavages. MaxQuant search was set to 1% FDR (False Discovery Rate) both at the peptide and protein levels. The minimum peptide length required for database search was set to seven amino acids. Precursor mass tolerance of ± 10 ppm, MS/MS fragment ions tolerance of ± 20 ppm, alkylation of cysteine, and oxidation of methionine were set as fixed and variable modifications, respectively. MaxQuant results were filtered for all contaminants. All proteins without any quantifiable peaks and those with <2 MS/MS counts were removed from downstream analysis. The “unique plus razor peptides” were used for peptide quantitation. Razor peptides are the non-redundant, non-unique peptides assigned to the protein group with most other peptides. Label-free quantification intensity values (LFQ) were used for relative protein abundance measurement. Proteins detected with at least one unique peptide and at least two MS/MS counts were included for the final analysis.

Due to the limitations of mass spectrometry-based proteomics related to sample complexity-- lysates from vocal tissues contain thousands of proteins and hundreds of thousands of peptides upon digestion with Trypsin and LysC-- sample complexity was reduced to maximize protein identification by dividing the lysate into soluble and insoluble fractions by differential centrifugation. The experience of the Purdue Proteomics Core is that this improves

protein identification by about 20-25% under our experimental condition. Importantly, the goal of our fractionation was not to determine sub-cellular localization of proteins but rather to increase proteome coverage. Data were merged during database searches, although they were run separately during LC-MS acquisition.

The resulting data were used to analyze differential protein expression. Two parallel analyses were conducted as outlined in Figure 3.2. The Analysis 1 set was obtained with combined LC-MS/MS data from both pilot and comprehensive proteomic experiments (cohorts C-E; n= 18; 9 per humidity group), and the Analysis 2 set included data only from the comprehensive proteomics experiment (cohorts D and E; n= 12; 6 per humidity group). Analysis 2 was conducted due to the disproportionate number of missing values within the Analysis 1 dataset belonging to the pilot experiment subset (i.e., proteins not identified in the pilot but identified in the comprehensive experiment) based on the assumption that the discrepancy resulted from the smaller sample size. Valid values were defined as LFQ greater than 0. Analysis 1 was more conservatively restricted to proteins with at least five valid LFQ values in at least one humidity group with at least two valid values in either humidity group from the pilot experiment subset; i.e., proteins identified in at least 5 of 9 rabbits with at least 2 identifications necessarily in either humidity group of the pilot rabbits subset. Analysis 2 was restricted to proteins with at least three valid values in either humidity group; i.e., proteins identified in at least 50% of samples (3 of 6 rabbits) in either humidity group. Proteins identified as potential contaminants were validated by peptides sequences obtained during mass spectrometry and are not reported. Further details of statistical analysis are described under the section Statistical Analysis.

Analysis 2 UniProt IDs were converted to gene names using the "UniProt Retrieve/ID mapping" tool (https://www.uniprot.org/uploadlists). Available gene names were supplied for enrichment analysis conducted with Metascape (https://metascape.org) [197], including the options for GO Molecular Functions, GO Biological Processes [198,199], WikiPathways [200], and KEGG Pathway [201-203], with default settings for "Pathway & Process Enrichment" and "Protein-protein Interaction Enrichment". Enrichment clusters defined by Metascape are considered. Specific details of the enrichment analysis are available from the Metascape website. Cytoscape [204] was used to visualize relationships of enrichment term clusters. To facilitate the identification of protein subsets that may differentiate between experimental groups, the enrichment hits

(enrichment term associated genes) were collapsed into their largest unique sets. Entries of interest with similar functional descriptions were subjectively combined into seven subgroups for principal component analysis. Briefly, individual enrichment terms were merged based on their associated genes, and analysis subgroups were created from these merged terms based on descriptions that shared similar functions.

Figure 3.2. Workflow for proteomics data analysis. (a) Number of proteins identified by unique FASTA identifier. Proteins with LFQ= 0 for all related samples were filtered out before downstream analysis. (b) Analysis 1 included proteins with LC-MS/MS data from Experiment 2 (Pilot) and Experiment 3 (Comprehensive) combined and was more conservatively filtered due to the overrepresentation of proteins with no valid values in the Experiment 2 subset. Analysis 2 used only proteins identified from Experiment 3. Missing values (LFQ= 0) were imputed from a downshifted normal distribution and protein expression between humidity groups was analyzed by Welch's t-Test. Distribution of the log10(p) and group mean difference (log2 scale) are shown below: black vertical lines represent a mean difference of 0.58 (1.5 fold-change), the red and blue horizontal lines represent p= 0.1 and p= 0.05, respectively. This data was arranged by ascending p-value and assessed by principal component analysis. Separation between humidity groups was observed for the top 95 and 515 proteins for Analysis 1 and Analysis 2, respectively, and these points are indicated on the graphs. Analysis 1 concluded due to the low number of significantly differentially expressed proteins identified. Analysis 2 separated the 515 proteins into those positively (red) and negatively (blue) correlated with the first principal component, and these lists were filtered by p< 0.1. These lists were mapped to available gene names by the UniProt Retrieve ID/Mapping tool and supplied to Metascape for gene enrichment analysis.

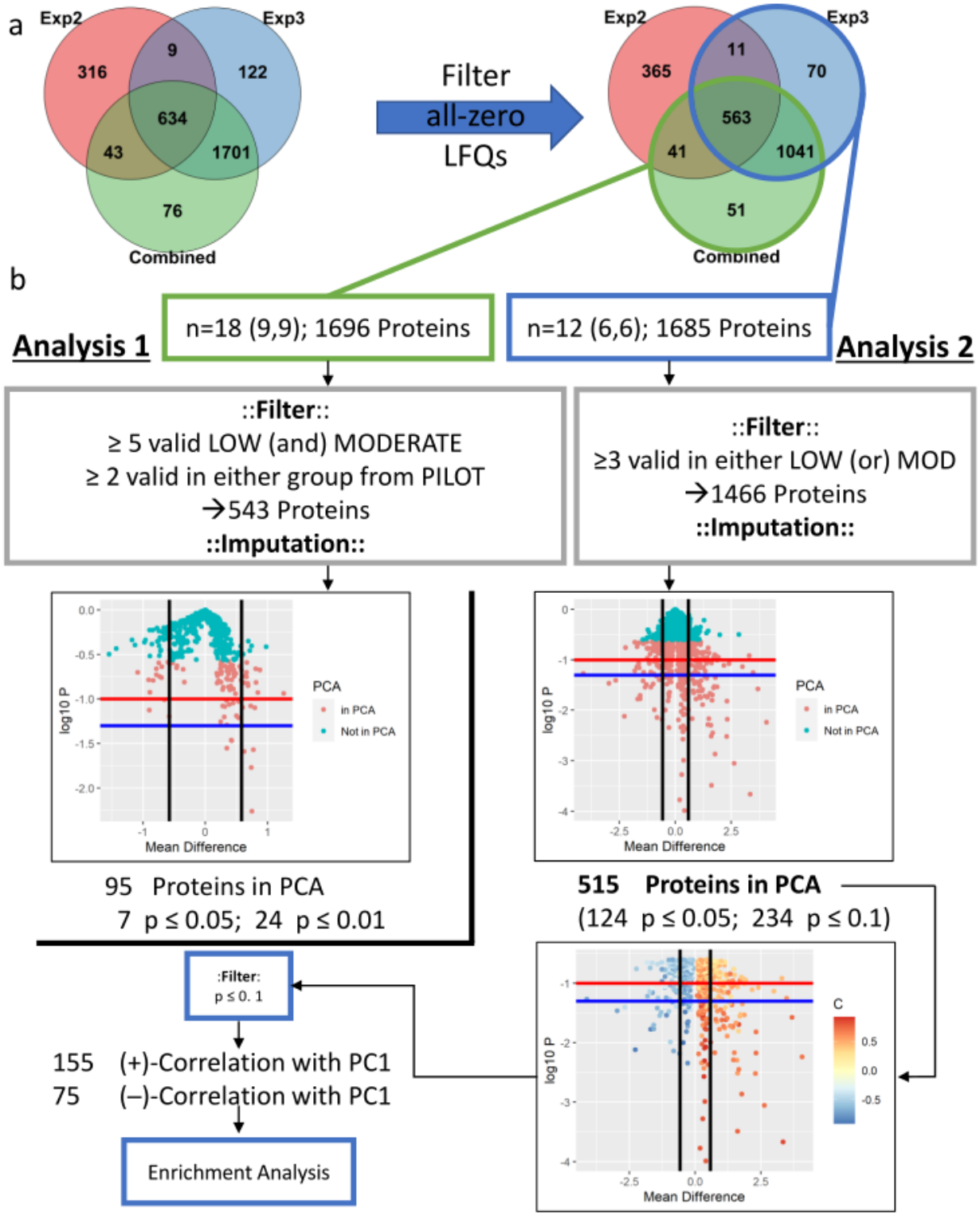
a
Exp2
Exp3
316
9
122
634
43
1701
76
Combined
Filter
all-zero
LFQs
Exp2
Exp3
365
11
70
563
41
1041
51
Combined
b
Analysis 1
n=18 (9,9); 1696 Proteins
n=12 (6,6); 1685 Proteins
Analysis 2
::Filter::
≥ 5 valid LOW (and) MODERATE
≥ 2 valid in either group from PILOT
→543 Proteins
::Imputation::
::Filter::
≥3 valid in either LOW (or) MOD
→1466 Proteins
::Imputation::
log10 P
Mean Difference
PCA
in PCA
Not in PCA
95 Proteins in PCA
7 p ≤ 0.05; 24 p ≤ 0.01
515 Proteins in PCA
(124 p ≤ 0.05; 234 p ≤ 0.1)
:Filter:
p ≤ 0. 1
155 (+)-Correlation with PC1
75 (–)-Correlation with PC1
Enrichment Analysis
C
0.5
0.0
-0.5

3.3.8 Statistical Analysis

All data were analyzed using R (v 4.0.4; http://www.r-project.org) with RStudio™ Version 1.4.1717 (RStudio Inc., Boston, MA, USA) including packages (ggpubr [205], ggsignif [206], lme4 [207], outliers [208], plotrix [209], stringr [210], tidyverse [154]). PCV was evaluated with a linear mixed effects model to validate assumptions of a pooled analysis of cohorts. The percent change in PCV was calculated between days 1 and 15, and mean difference between humidity groups was compared with Welch's t-Test. Relative gene expression for RT-qPCR was tested with Wilcoxon Rank-Sums tests following removal of outlier values, as determined by two-tailed Grubb's test. Differential protein expression data were filtered differently for Analysis 1 (at least five valid values in either humidity group with at least two valid values in either humidity group specifically from the pilot experiment subset) and Analysis 2 (at least three valid values in either humidity group). LFQ values were log-2 transformed and median centered, and missing values were then imputed sample-wise by a downshifted normal distribution. Group means were compared with Welch's t-Tests. Data were arranged by ascending p-value, and principal component analysis was performed on subsets of varying lengths to determine protein subsets of maximum size allowing for discrimination between humidity groups; clustering was validated by the method of k-means (k= 2). Forward analysis considered subsets of proteins based on both p-values and correlation with relevant principal components. Statistical significance was defined with α set to 0.05; however, 95% confidence intervals are provided alongside notable mean effects with non-significant p-values where explicitly discussed.

3.4 Results

3.4.1 Humidity Conditions

The low humidity aggregated across all exposures was 21.9% ± 3.8% (mean ± standard deviation). The moderate humidity aggregated across all exposures was 61.5% ± 11.2%, representing an average fold-change of 2.9 between humidity groups. The relative humidity distribution is shown by the experimental cohort in Fig 3.3, with associated summary statistics provided in Table 3.2. Distributions of relative humidity measures for each 8-hour exposure are provided in Figure 3.4.

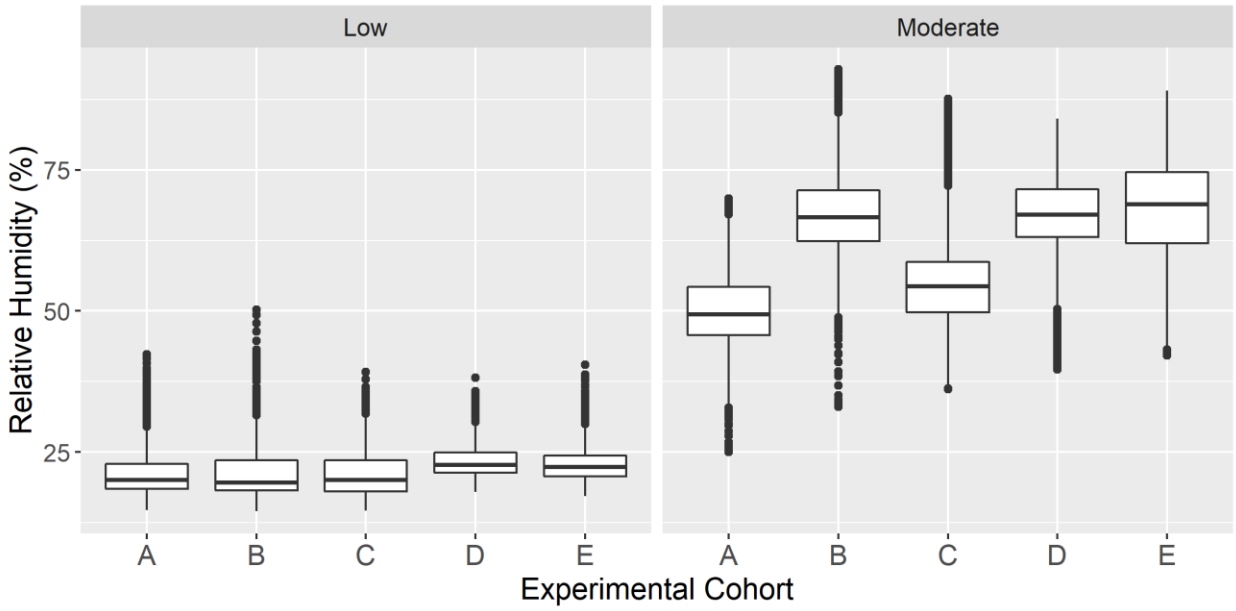

Figure 3.3. Relative humidity measures for low and moderate humidity groups by experimental cohort. Aggregate data for the 15-day humidity exposures are shown by humidity group and cohort. Box boundaries represent the first and third quartiles; the interior bar represents the median. Dots represent values greater than 1.5 times the interquartile range from the box boundary. Summary statistics are provided in Table 3.2.

Table 3.2. Summary statistics for relative humidity exposures by experimental cohort.

Cohort	Group	Mean	StdDev	Q3
A	Moderate	49.8	7.2	54.3
	Low	21.1	3.9	22.9
B	Moderate	67	8.1	71.4
	Low	21	4.1	23.5
C	Moderate	55	8.7	58.7
	Low	21.1	3.9	23.5
D	Moderate	67	7.7	71.6
	Low	23.3	2.8	24.9
E	Moderate	68.6	8.8	74.6
	Low	23	3.3	24.4

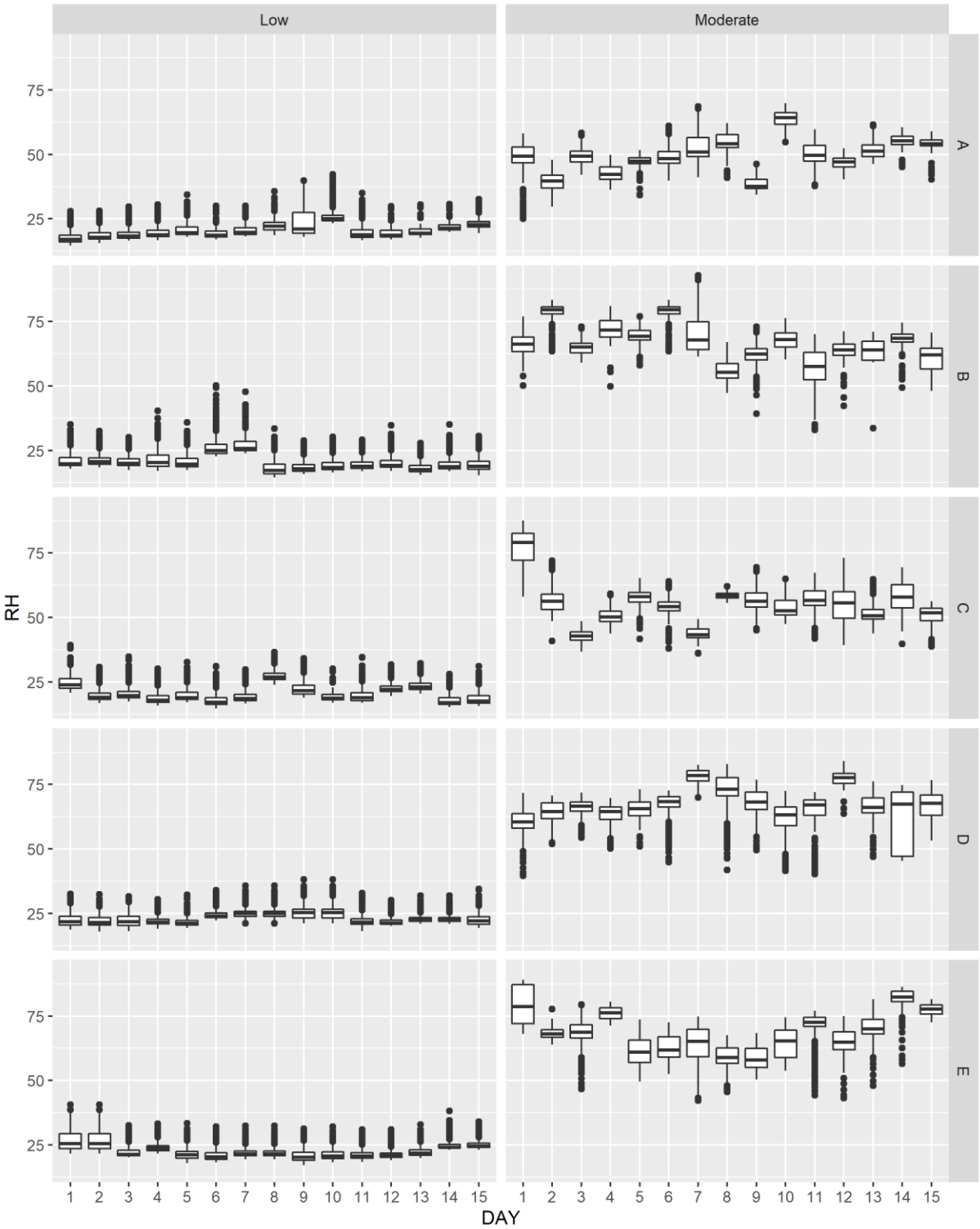

Figure 3.4. Daily relative humidity measures for low and moderate humidity groups by experimental cohort. Cohorts A and B: RT-qPCR experiment; Cohort C: pilot proteomics experiment; Cohorts D and E: comprehensive proteomics experiment. Box boundaries represent the first and third quartiles; the interior bar represents the median. Dots represent values greater than 1.5 times the interquartile range from the box boundary.

3.4.2 Packed Cell Volume (PCV)

PCV for each rabbit was measured prior to the experimental exposure on day 1, on day 8 of experimental exposure, and after the experimental exposure immediately before euthanasia on day 15. A linear model was used to test for main effects and first-order interactions of measurement day, humidity group, and experimental cohort. This informed a linear mixed model testing for fixed main and interaction effects of humidity group and experimental cohort with random intercept and slope effects among rabbits nested within experimental cohorts. All fixed effects were found to be non-significant, justifying aggregation of groups between experimental cohorts. Missing data for cohort B on day 15 resulted from centrifuge failure. The percent change in PCV from day 1 to day 15 was calculated for each rabbit, and means of the humidity groups were compared by Welch's t-Test. No significant difference was found (p= 0.39) by a two-tailed test, nor was the mean of the low humidity group greater than the moderate humidity group (p= 0.19). Data are shown in Figure 3.5.

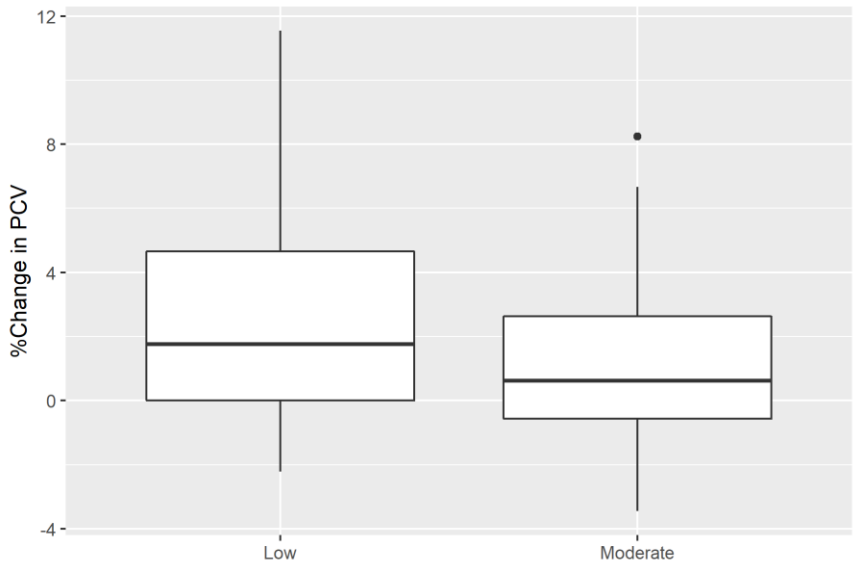

Figure 3.5. Percent change in PCV from day 1 to day 15 between groups. There is no significant difference between means of the two humidity groups (p= 0.39). Box boundaries represent the first and third quartiles; the interior bar represents the median. Dots represent values greater than 1.5 times the interquartile range from the box boundary.

3.4.3 Differential Gene Expression

Significant up-regulation was observed for *MUC4* (FC= 6.1, p= 0.019) and *SLC26A9* (FC= 3.6, p= 0.009) in the low humidity compared to the moderate humidity group. A notable mean increase was observed for *SCNNA1* in the low humidity group despite the large variability seen in both humidity groups (FC= 3.8, p= 0.095). Although a notable decrease in the mean relative expression of *MUC5AC* (FC= -1.8, p= 0.329) and a marked downregulation of *MMP1* (FC= -33, p= 0.167) observed in the low humidity group, considerable variability was observed for the moderate and low humidity groups, respectively, suggesting these genes need further investigation with a larger sample size. The remainder of the genes analyzed did not reach significance. Three outlying values were removed prior to group mean comparisons: *MMP1* for rabbit M5, *MUC4* for rabbit M3, and *ZACN* for rabbit L1. Data are shown in Fig 3.6, and a numerical summary is provided in Table 3.3.

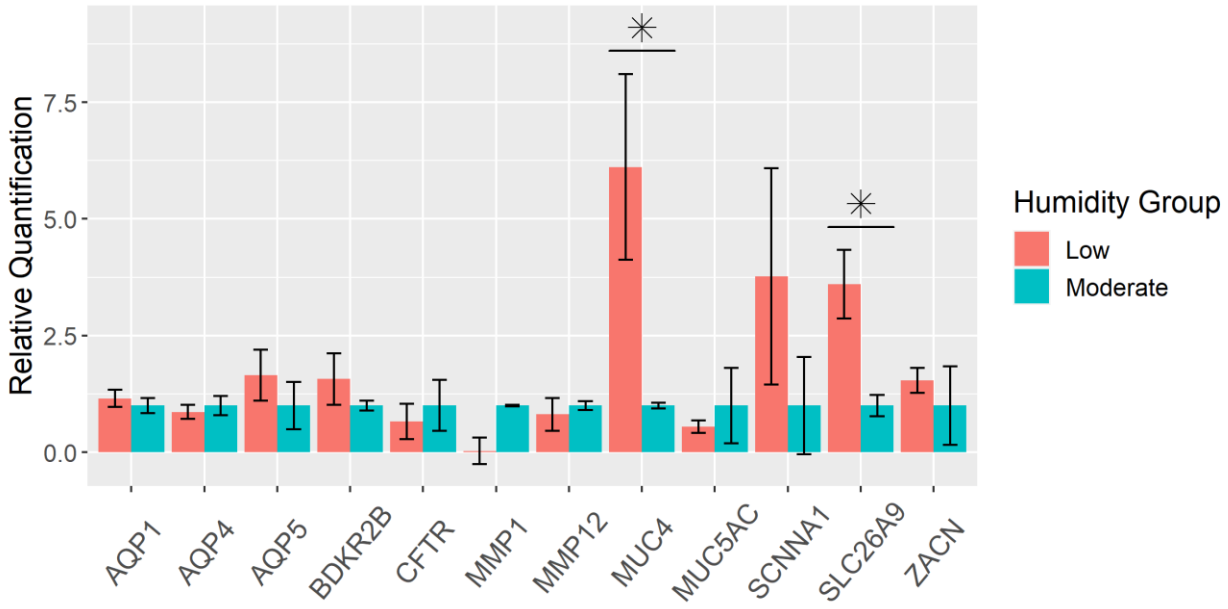

Figure 3.6. RT-qPCR for differential gene expression. Relative quantification for each gene was determined by the $2^{(-\Delta\Delta Ct)}$ method (n= 6 per humidity group except for three outlying values removed). *HPRT1* was used as an endogenous control. Individual ΔΔCt was calculated for each sample using the average ΔCts from the moderate humidity group for the respective gene. Data are reported as aggregated means of $2^{-\Delta\Delta Ct}$ with standardized values for the moderate humidity group. Standard errors of the mean are represented by the error bars and were calculated from individual sample values. *MUC4* (p= 0.019) and *SLC26A9* (p= 0.009) exhibited significantly different expression between humidity groups. *SCNNA1* exhibited a substantial fold change of expression but failed to reach statistical significance (p= 0.095).

Table 3.3**.** Summary statistics for low humidity group RT-qPCR results

Gene Symbol	Fold Change	SEM	P-value
AQP1	1.2	0.18	1
AQP4	-1.2	0.15	0.662
AQP5	1.6	0.55	0.247
BDKR2B	1.6	0.55	0.792
CFTR	-1.5	0.38	0.429
MMP1	-33	0.28	0.167
MMP12	-1.2	0.35	1
MUC4	6.1	2.0	0.019
MUC5AC	-1.8	0.13	0.329
SCNNA1	3.8	2.3	0.095
SLC26A9	3.6	0.73	0.009
ZACN	1.5	0.27	0.841

3.4.4 Proteomics

Three protein datasets were obtained filtering out LC-MS/MS results with all-zero LFQ values: 1) data from only the pilot experiment (cohort C; n= 6; 3 per group) demonstrating 980 unique proteins by FASTA header, 2) data from only the comprehensive experiment (cohorts D and E; n= 12; 6 per group) demonstrating 1,685 unique proteins, and 3) data combined from both experiments before searching MaxQuant (cohorts C-E; n= 18; 9 per group) demonstrating 1,696 proteins. The follow-up comprehensive experiment and combined sets shared 1604 proteins, while 81 were uniquely identified in the comprehensive experimental set (n= 12), and 92 proteins were identified uniquely in the combined set (n= 18).

Analysis 1 filtered the combined dataset resulting in a list of 543 proteins. The conservative compound filter described in the Bioinformatics and Data Analysis subsection was used to account for the overrepresentation of missing values within the pilot experiment subset of the combined data. The top 95 proteins arranged by ascending p-value provide linear separation between humidity groups with PC1 and PC2 explaining 37.9% and 15.1% of the variance, respectively (Figure 3.7a). Within each cohort, separation is observed between humidity groups. Differences across cohorts are also evident. No correct clustering into cohort, humidity group, or humidity group within cohort was achieved by the k-means algorithm. Seven proteins were

significantly differentially expressed ($p \leq 0.05$), all representing increased expression in the low humidity group, NAD(P)H quinone dehydrogenase 1 (p= 0.005, mean difference (d)= 0.75), Isoleucyl-tRNA synthetase (mitochondrial) (p= 0.017, d= 0.74), NDRG family member 2 (p= 0.026, d= 0.63), an uncharacterized proteins with Hsp70 homology (p= 0.027, d= 0.77), Glutathione S-transferase (p= 0.028, d= 0.35), Damage specific DNA binding protein 1 (p= 0.034, d= 0.43), and Fructose-bisphosphate aldolase (p= 0.034, d= 0.42). Enrichment analysis was not performed due to the small number of significant differences, even when relaxing the criterion to $p < 0.1$.

Analysis 2 filtered the comprehensive experiment dataset resulting in a list of 1,466 proteins. The less conservative filter was chosen to allow for the capture of proteins validly not expressed in one of the humidity groups. Principal component analysis with the top 515 proteins arranged by ascending p-values provided clear linear separation with 33.3% and 14.4% of the overall variance explained by PC1 and PC2, respectively (Figure 3.7b). A full list of these proteins is provided in Supplementary Table 1 (available here: https://doi.org/10.1038/s41598-021-03489-0). Samples are correctly classified by k-means into humidity group when using both PC1 and PC2, and 11 of the 12 samples are classified correctly when using only PC1 (sample L20 is misclassified as moderate). Given the ability of PC1 to sufficiently discriminate between humidity groups, an expanded set of proteins with $p \leq 0.1$ was considered for further evaluation. This included 234 proteins: 155 with increased ("positive group") and 79 with decreased expression ("negative group") in the low humidity group. Of these, 124 were significantly differentially expressed ($p \leq 0.05$), 91 with increased expression and 33 with decreased expression in the low humidity group. Expression levels for the top 50 proteins by absolute mean difference from both the full filtered set (a) and the subset with $p \leq 0.1$ (b) are shown in Figure 3.8.

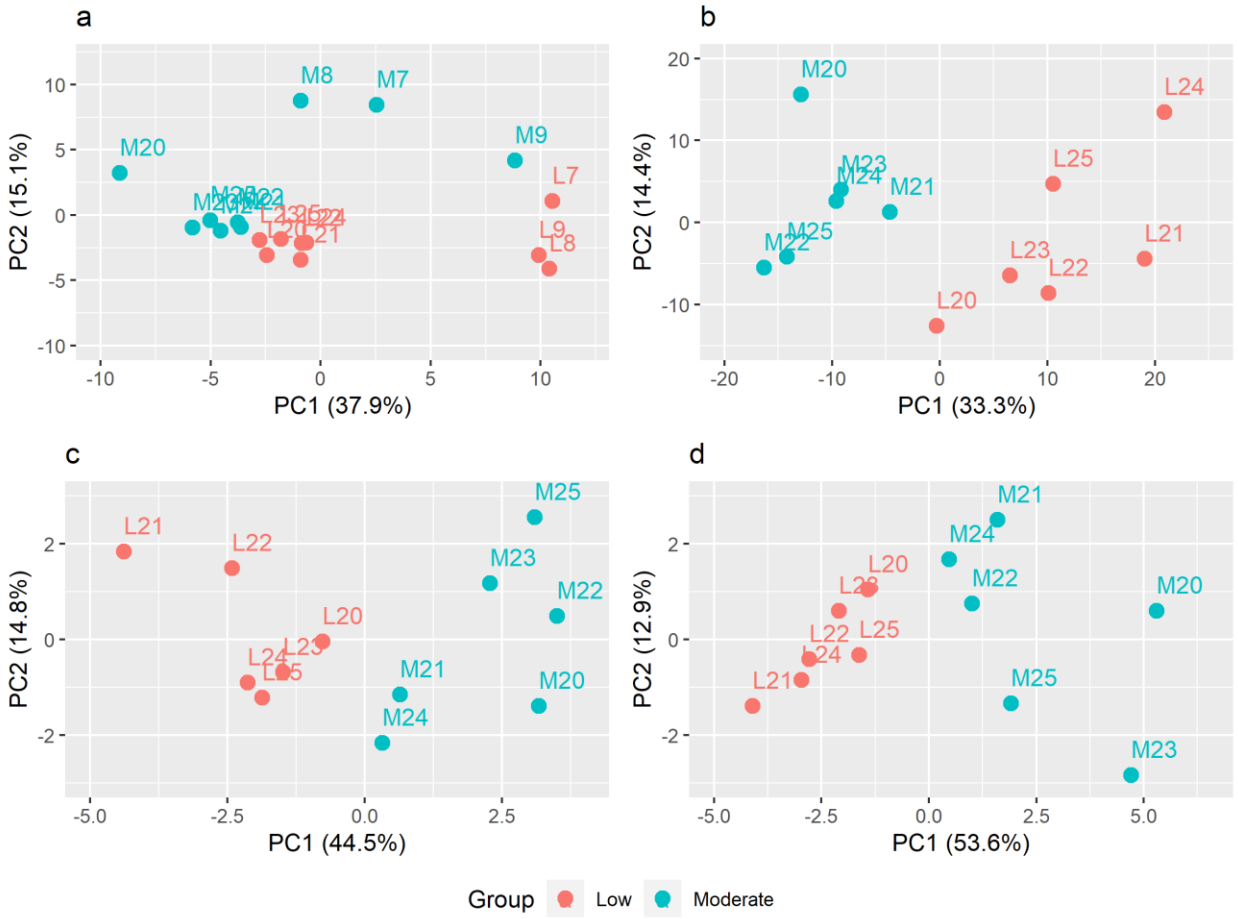

Figure 3.7. Principal component analysis. (a) PCA for the top 95 proteins arranged by ascending p-value from Analysis 1. (b) PCA for the top 515 proteins arranged by ascending p-value from Analysis 2. (c-d) Similar separation between humidity groups is observed by PCA for proteins corresponding to the aggregated functional clusters chaperone response and glutathione-related, respectively. M7-9 and M20-25 indicate the samples from control rabbits exposed to moderate humidity, and L7-9 and L20-25, samples from rabbits exposed to low humidity.

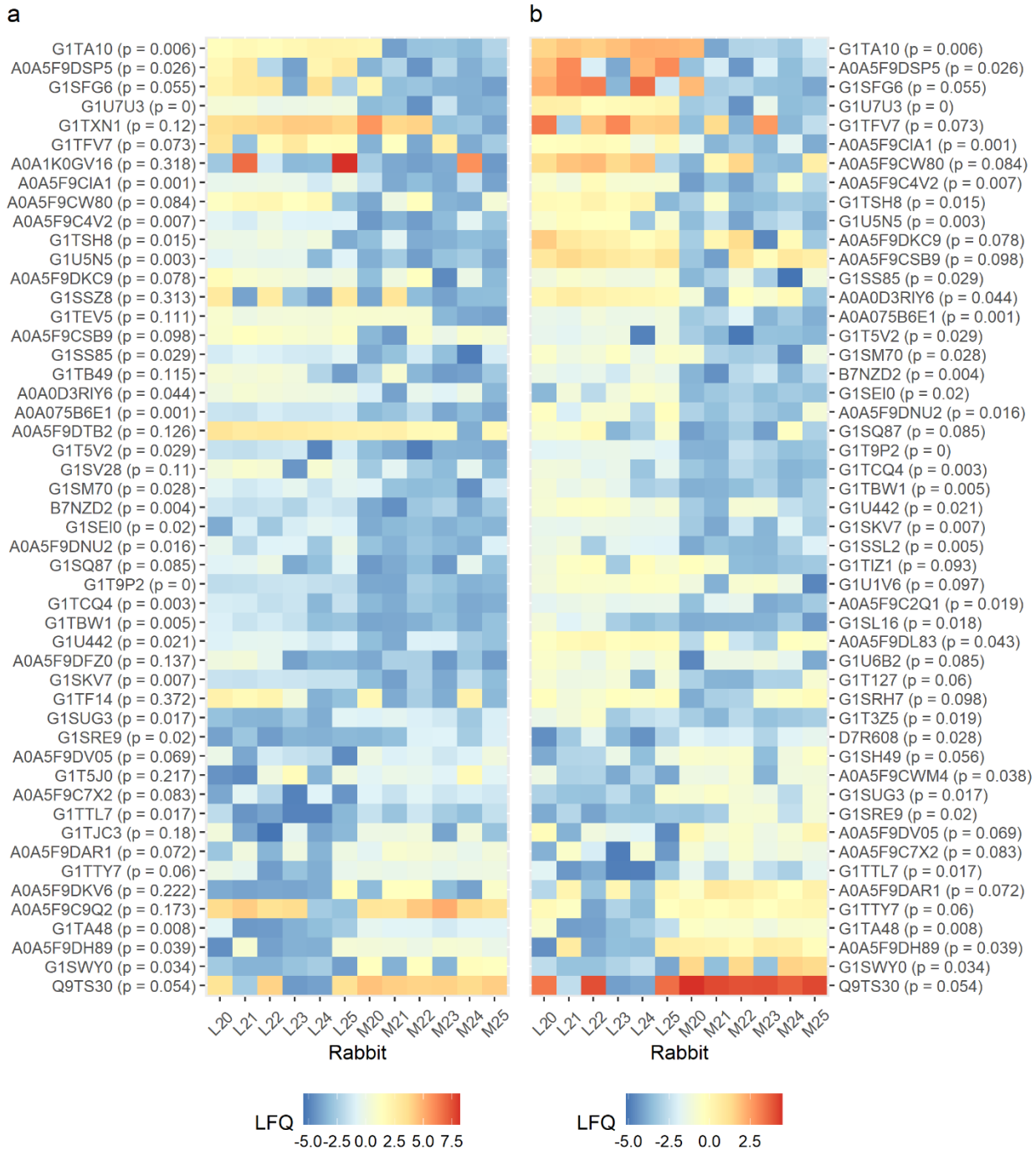

Figure 3.8. Heatmaps for differential protein expression in Analysis 2. (a) The top 50 proteins by absolute mean difference (log2 scale) from the full set of proteins (n= 1466). (b) The top 50 proteins by absolute mean difference (log2 scale) from the contracted set of proteins with $p \leq 0.1$ (n= 234) were considered for gene enrichment principal component analysis. C20-25 indicate the control rabbits exposed to moderate humidity, and L20-25 the rabbits exposed to low humidity.

Of the 155 and 79 proteins noted, 109 and 60, respectively, mapped to gene names with the Uniprot "Retrieve/ID mapping" tool and were provided to Metascape independently for enrichment analysis. The positive group demonstrated 401 unique enrichment terms from the Gene Ontology database classified by Metascape into 49 functional clusters. The negative group demonstrated 226 unique enrichment terms classified by Metascape into 18 functional clusters. Representative enrichment terms and networks illustrating the relationships between enrichment terms across Metascape defined clusters are shown in Figure 3.9. Redundancy in both groups was addressed in order to select protein subsets that might differentiate between experimental groups. Enrichment terms were collapsed together into the 101 and 49 largest unique sets of genes for the positive and negative groups, respectively, and terms of interest were grouped subjectively based on similar annotation; the resulting protein subsets were not strictly associated with Metascape defined clusters. Seven protein subsets were considered: chaperone response, glutathione-related, mitochondrial, muscle (positive), stress response were identified in the positive group, while ECM/structure and muscle (negative) were identified in the negative. Table 3.4 provides the five most significant individual proteins associated with each analysis subset, and the complete enrichment results and collapsed lists are provided in Supplementary Table 1 (available here: https://doi.org/10.1038/s41598-021-03489-0).

Table 3.4**.** Selection of proteins from enrichment analysis**.** The top five proteins identified in the vocal fold tissue of rabbits exposed to low and moderate humidity arranged by ascending p-value within each of the protein subsets tested. The UniProt ID displayed is the first of multiple when multiple mappings were provided. Name is a non-unique identifier obtained from the FASTA header for the protein. Uncorrected p-values (P) were obtained by Welch's t-test. Mean difference (D) of the log2 transformed LFQ values are provided along with the corresponding 95% confidence interval (LCL, UCL). Correlations to PC1 from Analysis 2 (C) are provided. Bolded entries represent statistical significance or meaningful magnitude.

	Name from FASTA Header	**UniprotID**	**P**	**LCL**	**D**	**UCL**	**C**
Chaperone	BCL2 associated athanogene 3	G1T1S7	**0.004**	0.20	0.50	0.79	**0.72**
	Parkinsonism associated deglycase	G1TBS1	**0.008**	0.12	0.39	0.66	**0.92**
	Endoplasmic reticulum protein 44	A0A5F9D0M4	**0.024**	0.19	**1.17**	2.15	**0.79**
	Heat shock protein family B (small) member 1	G1T3V2	**0.025**	0.05	0.29	0.53	**0.76**
	Prolactin regulatory element binding	G1SR63	**0.026**	0.18	**1.23**	2.27	**0.65**

Table 3.4 Continued

ECM/Structure	EH domain containing 4	G1TA48	**0.008**	-3.65	**-2.27**	-0.90	**-0.87**
	N-myc downstream regulated 1	G1TBJ4	**0.029**	-2.01	**-1.09**	-0.17	**-0.82**
	Tubulin beta chain	A0A5F9CMV1	**0.033**	-0.70	-0.37	-0.04	**-0.88**
	Leucine rich repeat containing 59	G1SM52	**0.033**	-1.89	**-0.99**	-0.10	-0.54
	Fibulin 2	A0A5F9CWM4	**0.038**	-2.78	**-1.44**	-0.10	**-0.65**
Glutathione	Carnosine dipeptidase 2	G1SKV7	**0.007**	0.62	**1.49**	2.37	**0.64**
	Parkinsonism associated deglycase	G1TBS1	**0.008**	0.12	0.39	0.66	**0.92**
	Glutathione S-transferase	A0A5F9DDG6	**0.011**	0.11	0.38	0.66	**0.87**
	Sulfite oxidase	G1SEI0	**0.020**	0.38	**1.66**	2.94	**0.84**
	Heat shock protein family B (small) member 1	G1T3V2	**0.025**	0.05	0.29	0.53	**0.76**
Mitochondria	Nucleoside diphosphate kinase	G1U7U3	**0.000**	2.32	**3.34**	4.36	**0.86**
	Pyrophosphatase (inorganic) 2	G1SPZ9	**0.004**	0.14	0.34	0.53	0.60
	BCL2 associated athanogene 3	G1T1S7	**0.004**	0.20	0.50	0.79	**0.72**
	Transmembrane protein 109	G1TA10	**0.006**	1.78	**4.07**	6.36	**0.70**
	Calsequestrin*	G1U507	**0.008**	0.12	0.36	0.60	**0.89**
Muscle.Neg	Calsequestrin*	G1SZM4	**0.039**	-0.49	-0.25	-0.02	-0.69
	Myosin binding protein H	G1T0G2	**0.040**	-1.40	**-0.72**	-0.04	**-0.42**
	Myosin IC	A0A5F9DIY4	0.051	-0.57	-0.29	0.00	**-0.82**
	Desmin (Predicted)	B7NZH1	0.059	-0.34	-0.17	0.01	**-0.72**
	Myosin binding protein C, slow type	G1TKC1	0.085	-2.52	**-1.16**	0.21	**-0.76**
Muscle.Pos	WD repeat domain 1	G1SHS7	**0.000**	0.28	0.41	0.53	**0.80**
	BCL2 associated athanogene 3	G1T1S7	**0.004**	0.20	0.50	0.79	**0.72**
	Tripartite motif-containing protein 72	G1T9F0	**0.006**	0.05	0.14	0.22	0.68
	Calsequestrin	G1U507	**0.008**	0.12	0.36	0.60	**0.89**
	Glutathione S-transferase	A0A5F9DDG6	**0.011**	0.11	0.38	0.66	**0.87**
Stress	WD repeat domain 1	G1SHS7	**0.000**	0.28	0.41	0.53	**0.80**
	BCL2 associated athanogene 3	G1T1S7	**0.004**	0.20	0.50	0.79	**0.72**
	Glucose-6-phosphate isomerase	A0A5F9CZL7	**0.005**	0.14	0.36	0.58	**0.89**
	Transmembrane protein 109	G1TA10	**0.006**	1.78	**4.07**	6.36	**0.70**
	Cathepsin B	A0A5F9C4V2	**0.007**	0.94	**2.32**	3.70	**0.72**

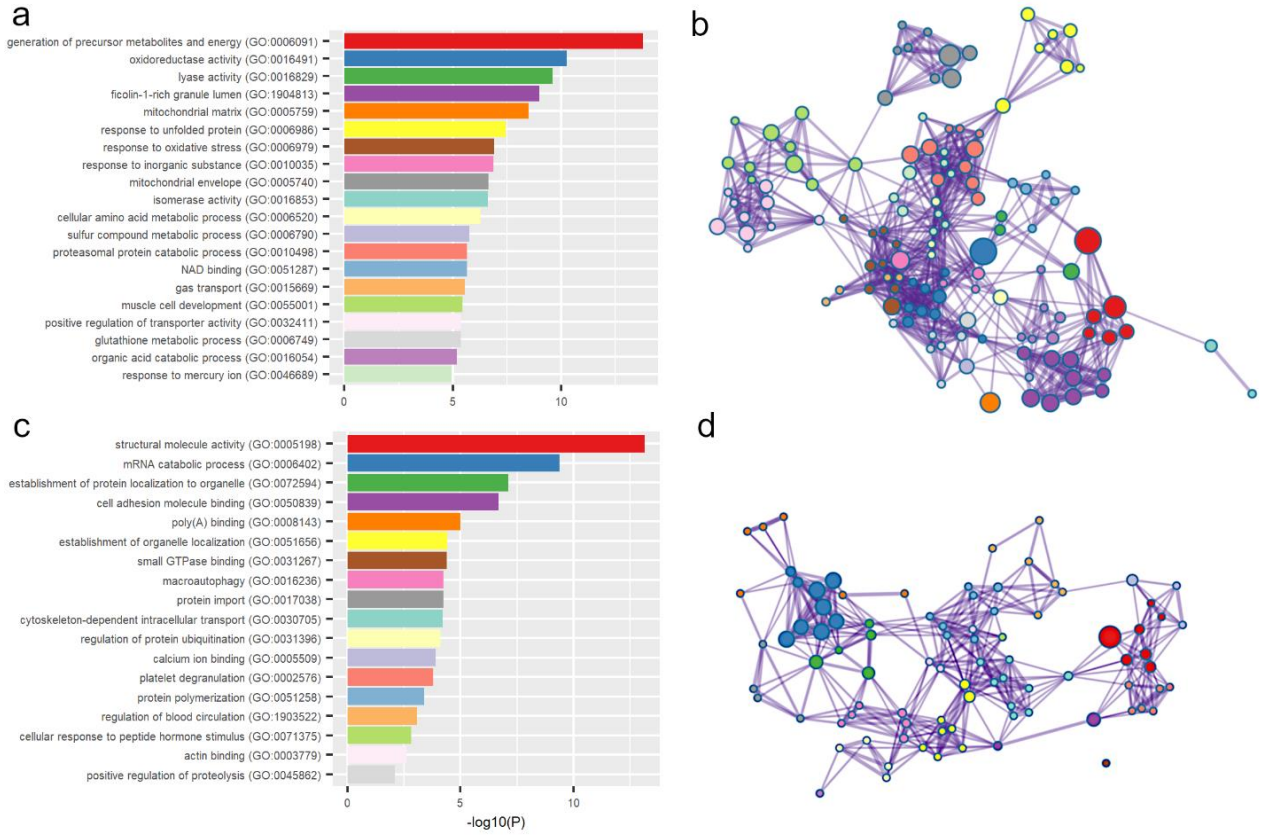

Figure 3.9. Summary of Enrichment Analysis (a) The most significant enrichment term within each of the 20 most significant Metascape defined clusters, each defined by the smallest respective p-values, for the positive group. (b) Network illustrating relatedness of individual enrichment terms, wherein individual nodes represent enrichment terms and nodes of the same color belong to the same Metascape defined cluster. (c,d) The same is shown for the 18 Metascape defined clusters from the negative group. Network maps were derived through modification of data provided by Metascape with the Cytoscape software.

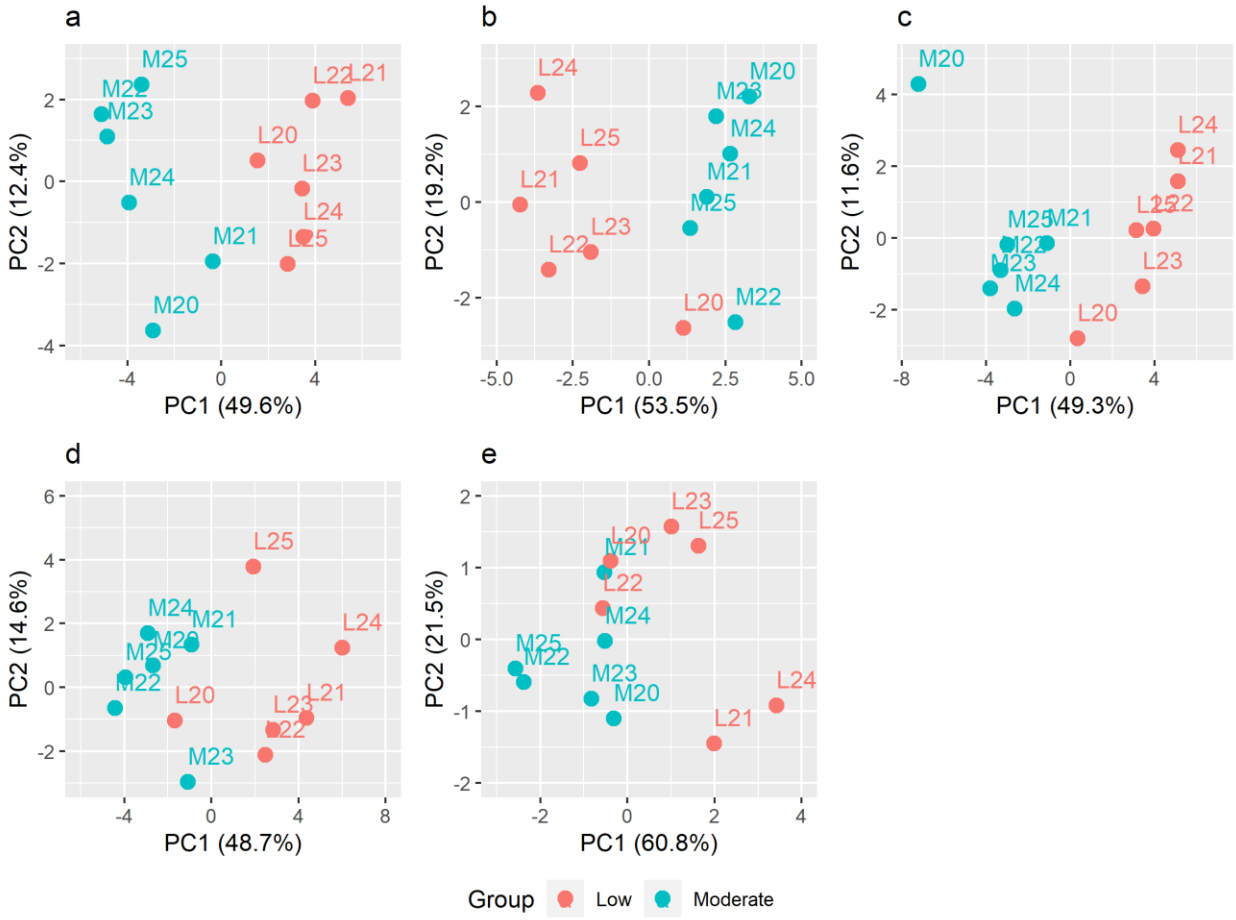

Figure 3.10 Principal component analysis including protein analysis subsets for (a) ECM/structure, (b) mitochondria, (c) muscle (negative), (d) muscle (positive), and (e) stress response

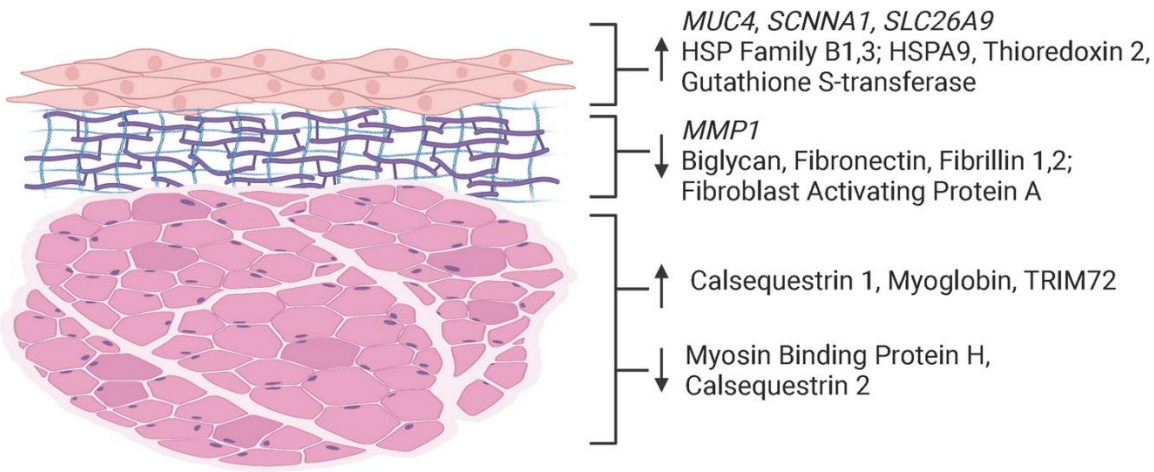

Figure 3.11 Summary of molecular findings in this study. Summary of the genes and proteins discussed. Image is structurally representative but not reflective of true anatomic scale. Created with BioRender.com.

Discrimination between humidity groups was variable across subsets by principal component analysis. Chaperone response (19 proteins, 10 significant, 60.1% overall variance between PC1 and PC2) (Fig 5c), glutathione-related (16 proteins, 10 significant, 65.7% overall variance) (Fig 5d), mitochondrial (30 proteins, 22 significant, 62% overall variance) (Figure 3.10a), muscle-positive set (15 proteins, 9 significant, 72.7% overall variance) (Figure 3.10b), and stress response (34 proteins, 18 significant, 60.9% overall variance) (Figure 3.10c) all provide clear separation of humidity groups. Interestingly, separation by these functional clusters is as pronounced as seen with the full subset of 515 proteins (Figure 5b). Clustering into the correct humidity group for all samples is validated by k-means for chaperone response, glutathione-related, and mitochondrial and for 11 of 12 samples by ECM/structure (24 proteins, 8 significant, 63.3% overall variance) (Figure 3.10d), muscle-positive, and stress response. The muscle-negative (5 proteins, 2 significant, 82.3% overall variance) (Figure 3.10e) exhibited poor separation between humidity groups as expected given its small size. A large carbon metabolism subset is noted but not considered for interpretation in this study.

Enrichment terms for pathways were obtained from the KEGG Pathway and WikiPathways databases via Metascape. KEGG provided 21 and 3 unique enrichment terms for the positive and negative groups, respectively, and WikiPathways provided 11 and 7. Carbon metabolism related pathways are overrepresented. Pathways for glutathione metabolism (hsa00480), drug metabolism (hsanan01, hsa00982), and NRF2 (WP2884) are seen in the positive group. There is some consistency between genes identified in pathways and the analysis subgroup described above. Interestingly, VEGFA-VEGFR2 signaling pathway is represented in both the positive and negative groups. Redundancy and relatively low number of gene hits for the identified enrichment terms preclude a deep pathway analysis.

3.5 Discussion

In this study, we implemented an occupationally relevant exposure to low humidity to evaluate the resulting molecular changes in the vocal folds and surrounding laryngeal tissue from surface dehydration, defined as water loss resulting from evaporation of water from the airway surface fluid. Essential to our conclusions, systemic dehydration was ruled out as a confounding factor by observing no differential changes in PCV between humidity groups. The 15-day recurring nature of exposure was selected to mimic an occupational exposure over multiple

workdays as 20% relative humidity is the lower bound of the Occupational Safety and Health Association (OSHA) recommendation for indoor air quality [156]. Here we find transcriptional and proteomic evidence that surface dehydration perturbed normal vocal fold cellular function. Relevance to the distinct microenvironments of the epithelium, lamina propria, muscle, and extracellular space are discussed below and summarized in Figure 3.11.

3.5.1 Epithelial Gene Expression

We hypothesized that our exposure would perturb transporters, including those for water (aquaporins) and ions (chloride channels, epithelial sodium channel, zinc activated cation channel). The ionic secretory component of airway surface fluid regulation at the apical epithelial membrane is proposed to be regulated predominately by the absorption of sodium ions by the Epithelial Sodium Channel (SCNNA1) and the secretion of chloride ions by the Cystic Fibrosis Transmembrane Conductance Regulator (CFTR) and accessory chloride transporters like Solute Carrier Family 26 Member A9 (SLC26A9) [190,211]. Aquaporins 1, 4, and 5 have been identified within the vocal folds of mice, localizing to the submucosa, the deeper layers of the stratified squamous membrane of the epithelium, and the apical epithelial surface, respectively [76]. Of the seven transporter genes tested, only *SLC26A9* demonstrated a statistically significant up-regulation in expression after exposure to low humidity. Interestingly, the epithelial sodium channel (*SCNNA1*) exhibited a notable increase in mean expression despite not reaching statistical significance. The slight upregulation of *AQP5* seen by RT-qPCR is perhaps suggestive of extracellular water flux. However, the small mean effect and lack of statistical significance across the aquaporin genes suggest that they are not main contributors to the response to recurring surface dehydration, consistent with a study in the murine airway [77]. The increased transcriptional expression of *SCL26A9* may be interpreted as evidence of a homeostatic response to maintain airway surface fluid volume that, along with *SCNNA1*, can preserve baseline membrane polarization. The potential role of paracellular fluid flux was not addressed in this study but should be considered in future experiments.

3.5.2 Epithelial Protein Expression

Airway surface dehydration may present as an epithelial cellular stressor in a variety of other ways besides transporter proteins: diminished luminal clearance due to increased viscosity of the airway surface fluid, osmotic and tonic stresses as a result of water lost to evaporation externally, and internally as intracellular water is lost to homeostatic secretion or absorption. Dehydration is also associated with oxidative stress by enriching reactive oxygen species [212]. We identified two broadly defined enrichment clusters related to various cellular stresses, including misfolded protein response ("chaperone response") and chemical and oxidative stresses. Various cellular stresses can impact the normal production and function of proteins within the cells, eliciting a protein chaperone response. The upregulation of several heat-shock protein family members and accessory proteins, including HSP family B members 1 and 3 and HSP family A member 9, indicates that surface dehydration impacts normal cellular function. Interestingly, having observed a trend toward increased expression of *SCNNA1* by RTq-PCR, HSP70 is implicated in the trafficking of the sodium epithelial channel in MDCK cell lines [213]. Considerable evidence also exists for oxidative stress with two Glutathione S-transferase, Thioredoxin 2 and Thioredoxin-domain containing 12, along with perturbations in multiple Cytochromes and other redox-active proteins. We conclude this represents a homeostatic response to the dehydrated condition though the specific mechanism is unclear. Further analysis targeting the different layers of the vocal folds is planned to establish the potential oxidative contributions of each physiologically distinct tissue layer.

3.5.3 Lamina Propria Gene Expression

The lamina propria of the vocal folds directly affects the biomechanics of phonation [170,214] and may be subject to changes of surface dehydration. Increased expression of *MMP1* has been shown as the result of vocal fold injury in rabbits [188], and Collagen I, a substrate of MMP1, is of principal relevance to the vocal folds as a major constituent of the lamina propria. Therefore, a dramatic decrease in the mean expression of *MMP1* may be indicative of early ECM response to recurring low humidity exposure. Notably, the increased expression of *MMP12* following a single low humidity exposure seen in our previous study [192] was not observed here.

3.5.4 Lamina Propria Protein Expression

The proteomic analysis demonstrates potentially negative changes with decreased expression of various proteins related to the lamina propria and its structural integrity, such as Fibronectin, Fibrillin 1 and 2, and Biglycan. These may be interpreted as destabilizing changes to the lamina propria as Fibronectin [7,188] is itself a major structural component and Fibrillin proteins support fibrillar superstructure. Such changes are likely to influence the biomechanical properties of the vocal folds and would manifest functional impairment in phonation. Interestingly, implications to collagen stability are found in the decreased expression of Fibroblast Activating Protein A, a fibroblast surface associated protease with activity on Collagen I [215]. Comprehensive analysis of the individual structural components underlying normal lamina propria composition is warranted to establish whether the observed changes result from active proteolysis or the diminished production of structural components by epithelial cells and vocal fold fibroblasts.

3.5.5 Muscle Protein Expression

The proteomic analysis demonstrated a fair number of significantly differentially expressed muscle-related proteins. This is expected as muscle is the predominant tissue type of the full thickness vocal fold specimen obtained. The interpretation of changes in expression is challenging, however, with some proteins showing increased expression (e.g., Tripartite motif-containing protein 72 (TRIM72), Myoglobin, SH3 and cysteine-rich domain 3 (STAC3), and the *CASQ1* isoform of Calsequestin) while other proteins exhibited decreased expression (e.g., Myosin binding protein H (MyBPH) and the *CASQ2* isoform of Calsequestrin) with low humidity exposure. TRIM72 is an oxidation sensitivity initial participant in membrane repair in muscle cells [216], and STAC3 is a muscle-specific calcium-channel binding protein involved in excitation-contraction coupling [217]. MyBPH is a thick-filament binding protein whose function is not fully characterized but whose overexpression is associated with amyotrophic lateral sclerosis [218,219], and Calsequestrin is a primary calcium storage protein in the sarcoplasmic reticulum [220]. It is unclear by what mechanisms the molecular composition of muscle would change in response to airway surface dehydration or to anticipate the physiological manifestation of these changes. Water content of the thyroarytenoid muscle was resilsent to *ex vivo* submergence in hypertonic solution [221] suggesting a milder osmotic perturbation from low humidity exposure is unlikely to

affect muscle tissue hydration directly. Evidence exists for mechanisms of epitheial influence on underlying smooth muscle in the airways [79,82,222], but our data substantiate no specific mechanism. Further, extrapolation to human voice production is limited in the absence of spontaneous phonation in rabbits. Analyses with improved coverage of the proteome specifically targeting the muscle are warranted to better understand the expression profile introduced in the present study and the underlying signaling mechanisms involved.

3.5.6 Laryngeal Lumen Components

Lastly, we consider changes to extracellular components supporting the airway surface fluid. In this study, we sought to identify changes in the gene expression of *MUC4* and *MUC5AC*, two well-described airway-related mucins. MUC4 is a transmembrane protein that serves to maintain the airway surface microenvironment. *MUC4* exhibited a remarkable 6.1-fold increase in expression in the low humidity group compared to the moderate humidity control. *MUC5AC*, associated with goblet cell secretion, exhibited a downregulation trend with low variability in the low humidity group compared to the moderate humidity control, but the large variation seen in the moderate humidity group precludes statistical significance. Although increased mucin expression is assumed to be a protective mechanism in the short term, overexpression of *MUC4* is implicated with pathogenic conditions, including pulmonary fibrosis [223]. Notably, the transmembrane mucins can participate in cell signal transductions and intracellular signaling. In the present study, the specific role of increased *MUC4* is not apparent. Therefore, additional studies to elucidate the mechanism of transcriptional upregulation. Interestingly, the proteomic analysis did not identify any mucin among the list of characterized proteins. This may be explained by loss of the protein during sample preparation (*MUC5AC* as a luminal, non-cell associated protein) or relatively low abundance of respiratory epithelium in the full thickness tissue sample collected.

3.5.7 Acknowledgements

We thank Norvin Bruns from the Purdue University Biomedical Engineering Machine Shop for assistance in the design and fabrication of the environmental chambers used in these experiments. We thank Dr. Uma K. Aryal and Dr. Jackeline Franco of the Purdue Proteomics

Facility for their assistance in LC-MS/MS sample preparation, data collection, and data analysis. All the LC-MS/MS data were acquired through the Purdue Proteomics Facility in Purdue's Discovery Park. We thank Dr. Hsin-yi Weng from the Department of Comparative Pathobiology, Purdue University for consultation on statistical analysis of the PCV data. We also thank Chenwei Duan for support during necropsy and sample collection throughout the study.

CHAPTER 4. COMPARATIVE PROTEOMICS SUGGESTS MOLECULAR CHANGES FROM ACUTE SYSTEMIC DEHYDRATION THAT ARE RESISTENT TO SYSTEMIC REHYDRATION

This chapter represents original work intended to be published.

4.1 Abstract

Perturbations in voice are a common health problem, particularly among professional voice users, and may be attributed to many factors. A considerable body of evidence suggests that systemic dehydration can negatively affect voice production; however, there is a dearth of evidence suggestive of the remedial benefits of rehydration. Further, the extant literature is limited largely to physical (e.g., phonation threshold pressure) or subjective measures of vocal effort. In this study, we use a rabbit model of acute (5 days) water restriction-induced systemic dehydration with subsequent rehydration (3 days) to explore the protein-level changes underlying the transition from euhydration to dehydration and following rehydration using LC-MS/MS protein quantification in the vocal folds. We show that a 5-day water restriction led to an average 4.3% decrease in body weight that resolved within 1 day of returning *ad libitum* access to water, with relative increases in anion gap, Cl-, creatinine, Na+, and relative decreases in BUN, iCa2+, K+, and tCO2 compared to control following water restriction. A total of 309 differentially regulated ($p < 0.05$) proteins were identified between the Control and Dehydration group. Unanticipatedly, we observed substantial similarity between the Dehydration and Rehydration groups, both well differentiated from the Control group with 418 differentially regulated ($p < 0.05$) proteins identified between the Control and the pooled average of the Dehydration and Rehydration groups. Gene enrichment and protein-protein interaction enrichment are discussed. Given the relatively minimal difference in vocal fold proteomic profiles between the Dehydration and Rehydration groups, our data call into question the utility of short-term rehydration as a biologically-grounded intervention for the vocal folds in the context of acute systemic dehydration, despite the rapid resolution of clinical measures.

4.2 Introduction

Voice disorders are a common health concern, affecting millions of people annually, worldwide. Dysphonia negatively impacts quality of life [116] and can translate into substantial economic burden [125], especially among professional voice users. Thus, minimally invasive therapeutic or prophylactic measures such as maintaining proper vocal hygiene are valuable. Proper hydration is a commonly recommended vocal hygiene measure. However, while considerable evidence supports an etiological link between systemic dehydration and dysphonia, evidence for the utility of (re)hydration in an acute context is scarce. Further, human studies of phonation are limited to objective observational measures of voice (acoustic and aerodynamic measurements or visual assessment) or subjective measures of phonatory effort or discomfort. While insightful, these measures exhibit limited sensitivity and fail to describe the biological systems that underlie the observed dysphonic changes associated with dehydration. The present study sought to address this gap in our understanding with a focus on the impact of systemic dehydration and subsequent rehydration on the vocal fold proteome.

Dehydration and rehydration as they relate to voice may manifest from distinct channels: systemically as water into or from systemic circulation or superficially from drying or hydration of the laryngeal lumen. The present study focused specifically on the former. Recent work has examined transcriptional and protein changes in water restricted rats by RT-qPCR and Western Blot [101], rabbits following furosemide-induced diuresis by RNA Sequencing [100], and rabbits deprived of water for 3 days [224]. Pertinent changes suggest potential inflammatory processes, perturbations to cellular junctional integrity, and changes to vocal fold extracellular matrix, all of which could contribute to dysphonia. We identify no molecular study of the vocal folds observing the impact of rehydration following dehydration. Interestingly, a recent study of lung function shows that acute systemic rehydration can improve dehydration-induced dysfunction, in contrast to nebulized rehydration [225], supporting the hypothesis that systemic rehydration may diminish dehydration-induced changes.

The present study has used a New Zealand White rabbit model of water restriction-induced systemic dehydration followed by systemic rehydration to examine protein-level changes associated with the perturbed hydration state. Rabbits are a well described surrogate model of vocal fold histological and molecular physiology [24,50]. Molecular studies in humans are largely precluded or restricted to cadaver or surgically resected tissue given the clear ethical concerns.

Most importantly, the *in vivo* model includes the homeostatic mechanisms associated with dehydration stress tolerance which we hypothesized to be fundamental to the dehydration and rehydration responses.

4.3 Materials and Methods

4.3.1 Rabbit Care and Tissue Collection

Experiments were conducted in accordance with the guidelines and after approval of the Purdue Animal Care and Use Committee (Protocol # 1606001428) and following ARRIVE guidelines. New Zealand White rabbits were obtained from Envigo Global (Indianapolis, IN). Twenty-four rabbits were included in the study. Rabbits were between 20.4-22.6 weeks of age on arrival and measurements were taken between 22.4-26.6 weeks of age. Rabbits were allowed at least 1 week for acclimatization and were treated prophylactically for intestinal coccidiosis with a 5-day course of Amprolium in their drinking water.

Rabbits were randomly assigned to one of three experimental groups: Control (euhydrated), Dehydration, and Rehydration (n = 8/group). No rabbits were excluded from the analysis, but blood chemistry data is missing for one rabbit in the Rehydration group for the second day of blood chemistry measurements due to failure of the instrument to read the sample. Sample sizes were selected based on reasonable assumption of statistical power for the proteomics experiment. Food was provided *ad libitum* for the entire experiment. Rabbits were left in their cages except for body weight measurements and blood collection.

Blood was collected via venipuncture of the lateral ear vein with a 23 gauge needle at the start of the dehydration period, at the end of the dehydration period, and immediately prior to euthanasia. Two hematocrit tubes were collected at each blood draw, and an additional sample for chemistry analysis was obtained from each rabbit at the final blood draw. Packed cell volume (PCV) was measured by visual inspection following centrifugation of the hematocrit tubes. Blood chemistry was analyzed with the i-STAT Chem8+ cartridge that includes creatinine, blood urea nitrogen (BUN), glucose, sodium, chloride, potassium, total CO2, ionized calcium, anion gap, hematocrit (Hct, same as PCV), and hemoglobin using the i-STAT Alinity blood analyzer (Abaxis by Zoetis Inc., Parsippany-Troy Hills, NJ, USA). Euthanasia was completed with a

single IV dose (1 mL) of Beuthanasia-D Special (Shering Plough Animal Health Corp., Union, NJ, USA) through a catheter in the lateral ear vein.

Following euthanasia, the larynx was removed, bisected along the posterior sagittal midline, pinned to wax, and the bilateral full-thickness vocal folds removed by microscopy assisted microdissection. Vocal fold tissue was collected into a cryovial, flash frozen in liquid nitrogen, and stored at -80 °C until processing.

4.3.2 Water Restriction Protocol

Systemic dehydration was induced with a water restriction protocol as shown in Figure 4.1. A full daily supply of water was provided at 500 mL. Water volume was measured with a 500 mL graduate cylinder to an accuracy limit of 2.5 mL. The Control hydration group was provided a full water supply for the entire experiment. The Dehydration and Rehydration groups were water restricted for 5 days at 50% of their average individual water intake as measured over 5 days prior to starting the experiment. The 5 days before the experiment is defined as the baseline water intake period. The Dehydration group was euthanized immediately following the dehydration period. The Rehydration group was provided a full supply of water for 3 days following the dehydration period. Control euhydrated and rehydrated rabbits were euthanized immediately following the rehydration period. Rabbit body weight was measured throughout the protocol.

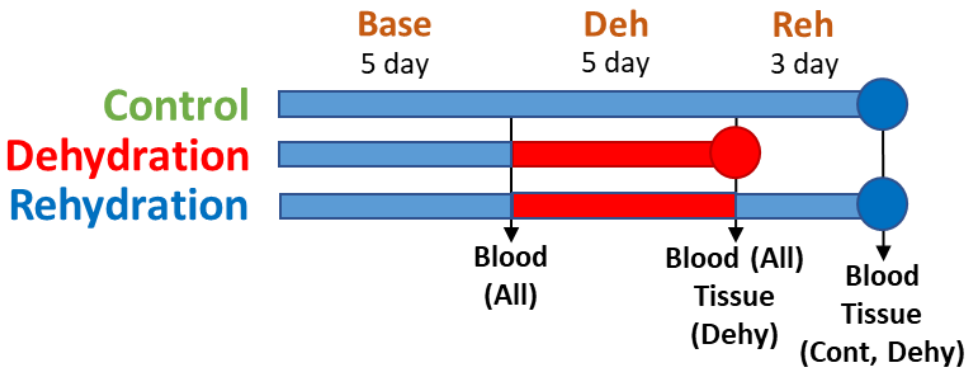

Figure 4.1 Water Restriction Protocol. Base: baseline water intake period (5 days). Deh: dehydration period (5 days). Reh: rehydration period (3 days).

4.3.3 Proteomic Sample Processing and Data Acquisition

Tissue sample preparation and mass spectrometry analysis was as previously described [226] with the following modifications. Soluble and insoluble fractions were digested with Pierce™ Trypsin Protease, MS Grade (Thermo Fisher Scientific, Waltham, MA, USA); LysC was not used for the present study. Peptides were separated with an Aurora UHPLC C18 packed emitter column (25 cm long × 75 µm ID) packed with 1.6 µm 120 Å (Ionopticks, Victoria, Australia). The column temperature was maintained at 50°C. A flow rate of 150 nL/min was used. As in the previous study, soluble and insoluble fractions were run separately during LC-MS acquisition and data merged when searching the database. These fractions are not interpreted by their cellular; rather, the Purdue Proteomics Core has observed this improves overall protein identification. Raw LC-MS/MS data were deposited in MassIVE data repository (massive.ucsd.edu) under ID MSV000089151".

4.3.4 Analysis of Protein Expression

The full resulting set of proteins was filtered for half non-zero LFQ in at least one of the groups (at least n = 4 samples). LFQs were log2 transformed, median centered, and imputation performed sample-wise from a downshifted normal distribution. Group similarities were further assessed with principal component analysis and agglomerative hierarchical clustering with Spearman correlation distance and average linkage. Two differential expression comparisons were considered for further analysis and are discussed. The first comparison was between the Control and Dehydration groups alone ("DEHY") and the second was between the Control and average of the Dehydration and Rehydration groups ("CDR"). Data from two additional comparisons between the Control and Rehydration groups alone ("REHY") and between the Dehydration and Rehydration groups alone ("DR") are included illustratively but are not considered for biological interpretation.

4.3.5 Enrichment and Protein-Protein Interaction Analysis

The UniProt *Retrieve/ID mapping* tool (https://www.uniprot.org/uploadlists/) was used to convert UniProtKB AC/ID from significant protein subsets to available "Gene name" which were used as the input for gene enrichment analysis with Metascape [197]

(https://www.metascape.org). Gene enrichment databases included GO Biological Processes [198,199], KEGG Pathway [201,203], Reactome Gene Sets [227], Transcription factor targets [228], and WikiPathways [200]. Enrichment parameters were set to minimum overlap length of 10, *p*-value cut-off of 0.001, and minimum enrichment factor 5; the GPEC option was selected. Protein-protein interaction enrichment databases included the Metascape Physical Core: STRING [229] (physical interactions), BioGrid [230] (physical interactions), OmniPath [231], and InWeb_IM [232]. Enrichment parameters were set with a network size of between 10 and 500. Results were filtered for minimum overlap length of 6, *p*-value cut-off of 0.001, and minimum enrichment factor 5. Full details of the underlying analysis are available from Metascape. Briefly, an enrichment score and a hypergeometric distribution-based *p*-value are determined for each specific enrichment term based on represented genes. Enrichment terms from GO Biological Processes, KEGG Pathway, and Reactome Gene Sets are further clustered together based on shared member gene identity. These clusters often, but may not strictly, represent a specific functional annotation. The total number of gene sets were further reduced by collapsing them into the largest unique sets of genes to minimize redundancy. Protein-protein interaction in-network clusters are identified with the MCODE algorithm [233]. Associated enrichment terms are mapped onto these clusters independently of the gene-based enrichment. Data presented are modified from the original Metascape output.

4.3.6 Statistical Analysis

All data analyses and visualization were completed using R (v4.1.2) with RStudio™ version 1.4.1717 (RStudio, PBC, Boston, MA, http://www.rstudio.com) except when otherwise specified. General linear models were used for all quantitative comparisons between groups with pertinent contrasts specified with the *emmeans* package. Significance was defined at $\alpha = 0.05$. Pairwise comparisons were corrected by Tukey's adjustment. The Benjamini-Hochberg False Discovery Rate is provided where appropriate with multiple comparisons, although it was not used to filter statistically significant results. *P*-values and Q-values are reported on the log scale where appropriate for ease of interpretation.

4.4 Results

4.4.1 Water Intake

The baseline water intake across individual rabbits was markedly variable with mean of 291 mL and standard deviation of 65 mL (Figure 4.2A). The range for baseline daily water intake within rabbits was between 30 mL and 170 mL. A single anomalous 500 mL volume intake during the baseline period was observed for rabbit D7. There was no difference in mean water intake between groups during the baseline period (all $p > 0.24$). The dehydration period successfully realized an intake of 50% of the average baseline intake for the Dehydration and Rehydration groups (Figure 4.2B). The apparent increase in the mean water intake of the Rehydration group from the Control group during the first day of rehydration is significant ($p < 0.0001$), but the groups show no difference by the second day of rehydration (Figure 4.2B).

4.4.2 Body Weight

Body weight across all rabbits at the last day of the baseline period ranged from 2.61 kg to 3.55 kg with mean of 2.99 kg and standard deviation of 0.26 kg (Figure 4.3A). Given the rapidity with which young rabbits gain body weight and the range of rabbit ages, age in weeks at the time of measurement was included as a covariate. No significant difference between mean body weights between groups was seen at baseline (all $p > 0.27$). Following the first day of water restriction (Deh 1), the Dehydration and Rehydration groups exhibited a significant deviation in body weight from the Control group (body weight loss (BWL) = -3.1%, $p = 0.0005$ and -2.5%, $p = 0.0035$, respectively), which was maintained throughout the water restriction period (Deh 5: BWL = -4.6%, $p < 0.0001$ and -4.0%, $p < 0.0001$, respectively) while the Control group exhibited a 2.9% increase (Figure 4.3B). The Dehydration and Rehydration groups exhibited no difference from each other at any time point (all $p > 0.85$). Differences between the Rehydration and Control groups are non-significant from the first day following rehydration (Reh 1, 2, and 3; p = 0.06, 0.08, 0.14, respectively).

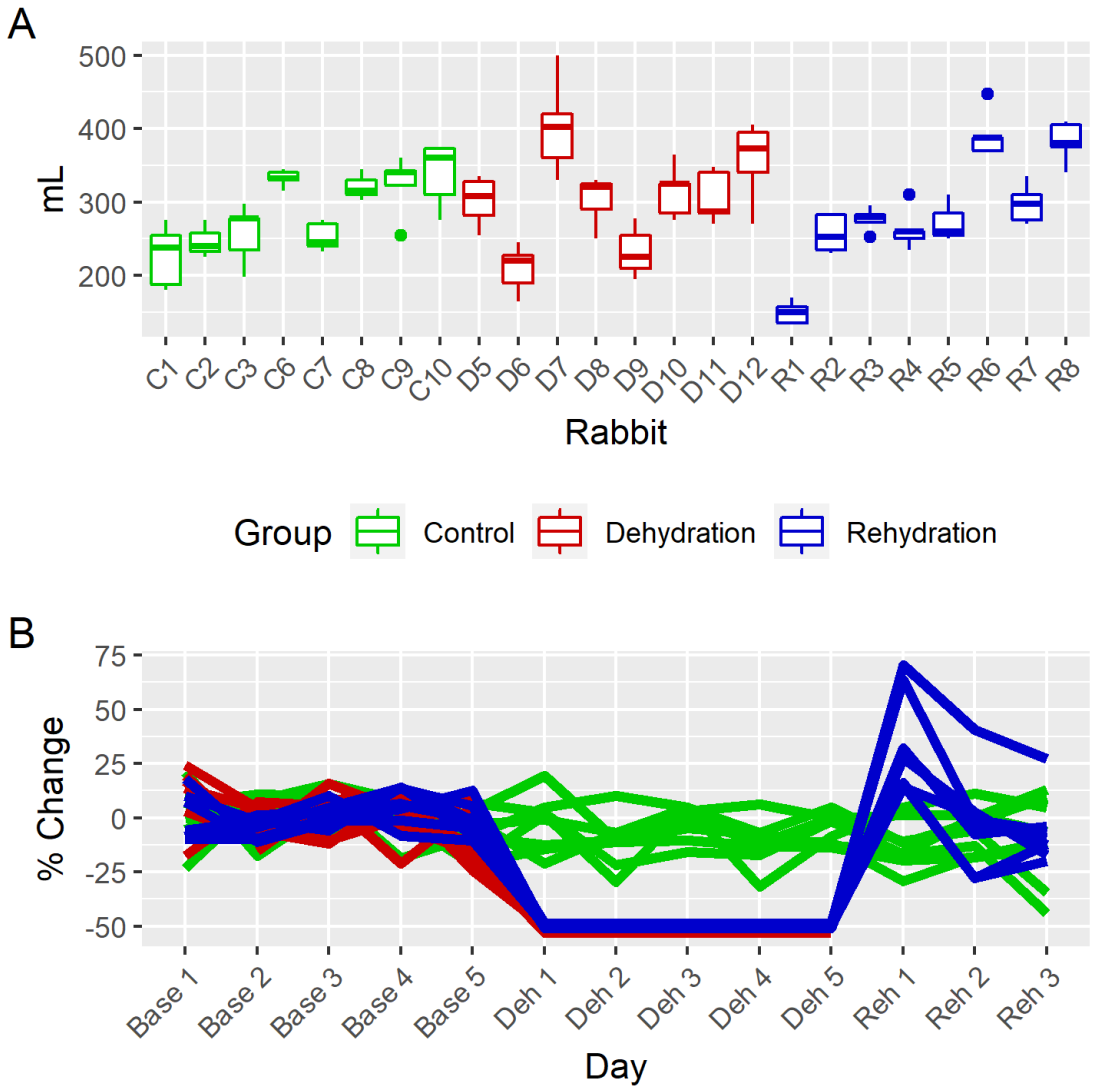

Figure 4.2 (A) Baseline water intake over 5 days for individual rabbits. (B) Water intake for the duration of the experiment standardized to 5 day baseline average. Base: baseline water intake period (5 days). Deh: dehydration period (5 days). Reh: rehydration period (3 days).

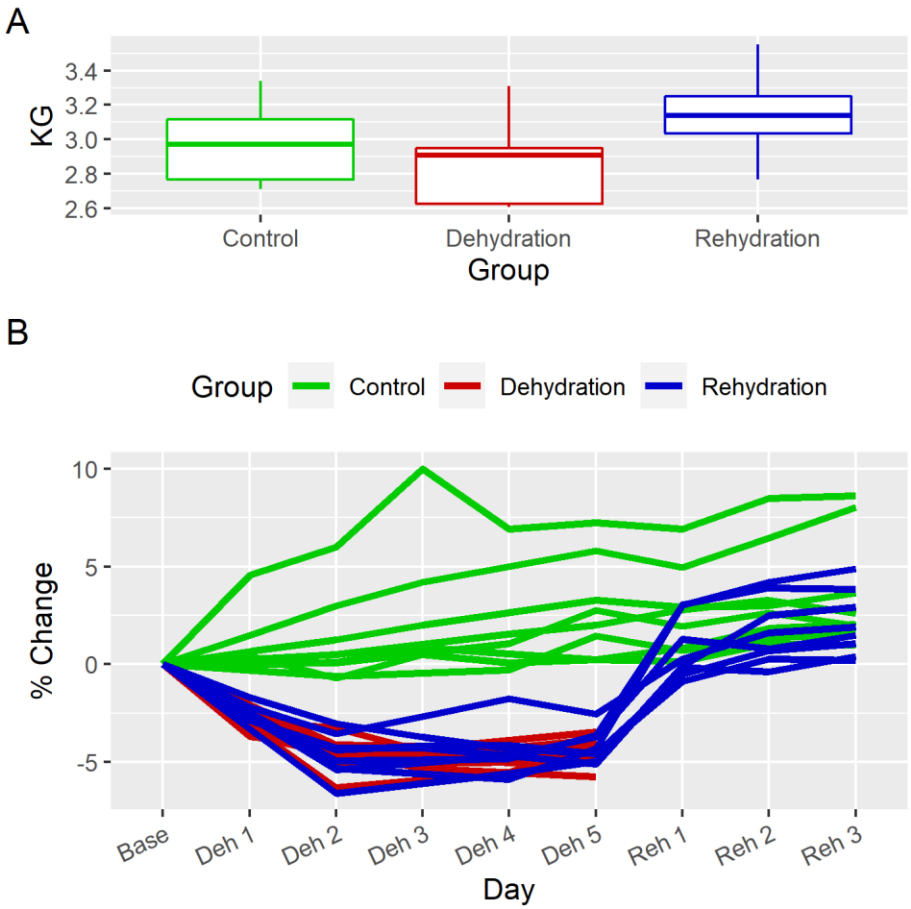

Figure 4.3 Body weight of individual rabbits (A) at last day of baseline period and (B) over the course of the experiment, standardized to the weight at baseline.

4.4.3 Packed Cell Volume and Blood Chemistry

Packed Cell Volume (PCV) at baseline ranged from 37% to 48%. No significant effect of any group was seen at baseline ($F(2, 21) = 0.88$, $p = 0.43$) or following either the dehydration or rehydration periods ($F(7, 56) = 0.9614$, $p = 0.47$). BUN was the only analyte with a significant mutual difference between all three groups following dehydration (all $p < 0.025$), while more analytes showed differences only within the Dehydration group. No additional analytes showed differences between the Control and Rehydration groups. Following this observation and considering the identical treatment state of both Dehydration and Rehydration groups at this time point (Deh 5), a comparison between the Control group and the combined mean of the Dehydration and Rehydration groups was performed representing Control versus "water restricted" status. PCV remained non-significant ($F(3,44) = 0.97$, $p = 0.41$). In contrast, blood chemistry demonstrated significant changes that are shown in Table 4.1 and Figure 4.4B-I. . No significant differences were found between the Control and Rehydration groups during the rehydration period.

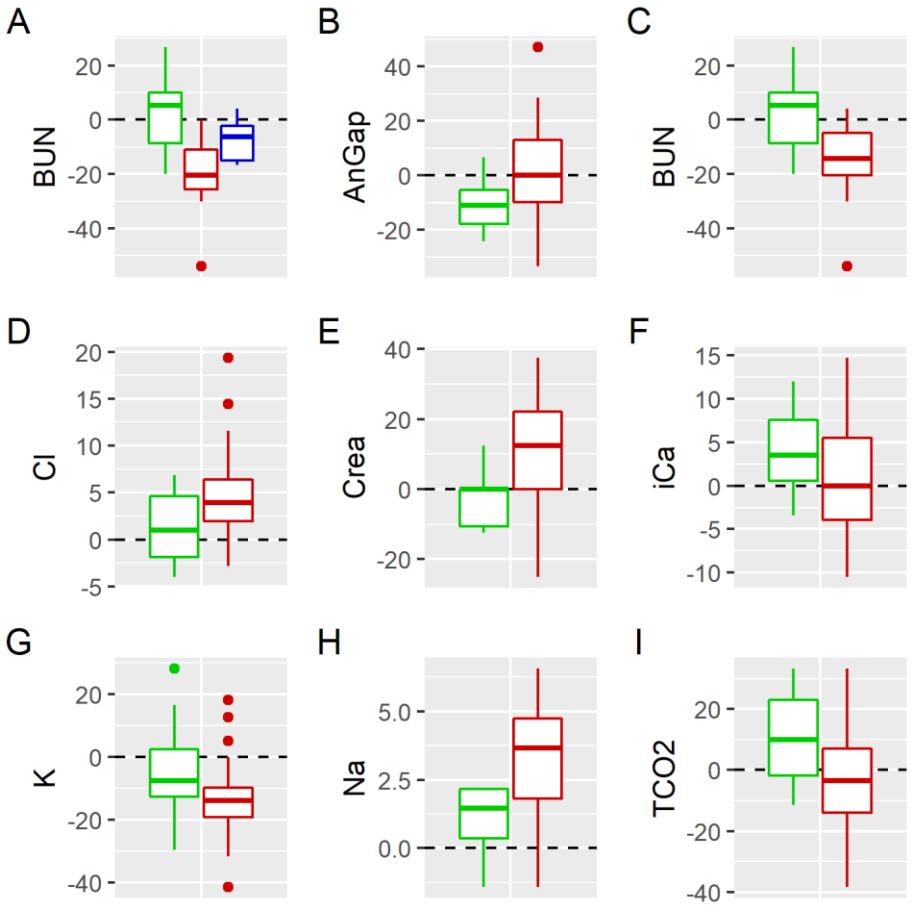

Figure 4.4 Significant findings of blood chemistry (A) between Control, Dehydration and Rehydration groups and (B-I) from the Control compared to pooled Dehydration and Rehydration groups. Y-axis represents %-change from baseline measure. Dashed line lies along the x-axis: value above represent increase and values below represent a decrease from baseline measure. Green bars: (A-I) Control group. Blue bar: (A) Rehydration group. Red bars: (A) Dehydration group and (B-I) pooled Dehydration and Rehydration groups; "water restricted" status.

Table 4.1 Summary statistics of significant findings of blood chemistry from the Control compared to pooled Dehydration and Rehydration groups. Mean is the model estimated mean for the respective group. Contrast estimate is the difference between pooled mean of Dehydration and Rehydration and the mean of Control with the associated p-value.

	Group	**Mean**	**Contrast Estimate**	***P-value***
AnGap	Control	0.889	0.125	0.031
	Dehydration	1.053		
	Rehydration	0.976		
BUN	Control	1.027	-0.167	<0.0001
	Dehydration	0.800		
	Rehydration	0.919		
Cl	Control	1.014	0.032	0.014
	Dehydration	1.059		
	Rehydration	1.034		
Crea	Control	0.981	0.128	0.004
	Dehydration	1.087		
	Rehydration	1.131		
iCa	Control	1.041	-0.037	0.022
	Dehydration	1.003		
	Rehydration	1.006		
K	Control	0.961	-0.095	0.009
	Dehydration	0.828		
	Rehydration	0.904		
Na	Control	1.010	0.023	<0.0001
	Dehydration	1.038		
	Rehydration	1.028		
TCO2	Control	1.109	-0.141	0.005
	Dehydration	0.913		
	Rehydration	1.023		

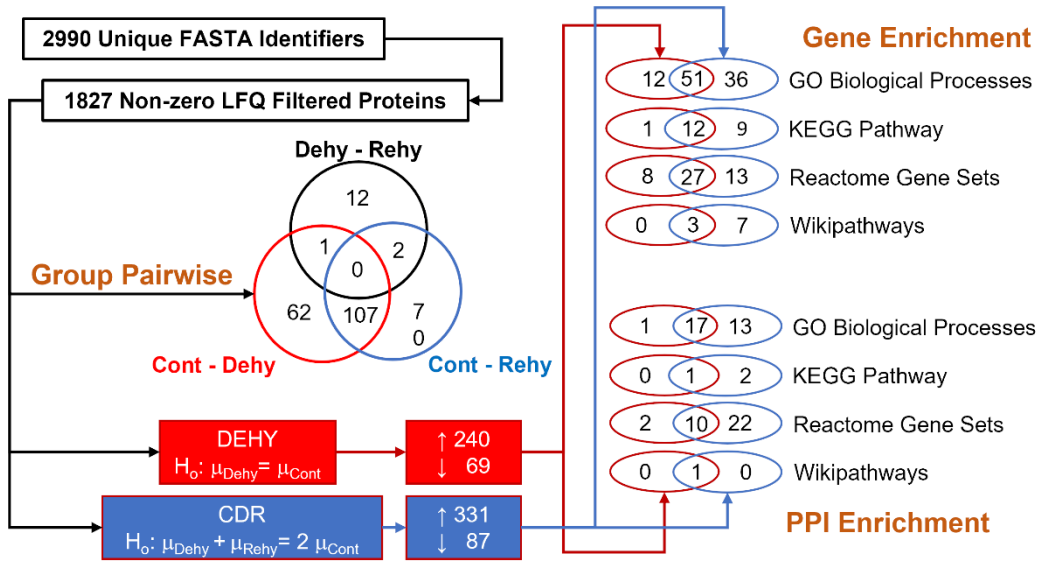

Figure 4.5 Summary of Proteomic Analysis. The full list of 2990 was filtered for a minimum of 4 non-zero LFQ values in at least one group. The resulting list of 1827 was used for all downstream analysis. Differentially regulated proteins between groups were initially tested pairwise with Tukey's adjustment. Venn diagram presents proteins identified within each comparison. A high level of similarity was observed between the Dehydration and Rehydration groups informing the downstream analysis. Two parallel analyses were considered, one for a main effect of Dehydration and the other for an effect of pooled Dehydration and Rehydration groups. Enrichment analysis proceeded with both gene ontology and protein-protein interaction.

4.4.4 Protein Expression

Effects of Dehydration

The analytical approach to differential protein regulation analysis is summarized in Figure 4.5. A total of 2990 unique FASTA identifiers were determined leaving 1827 unique proteins when filtered for non-zero value LFQ criteria. Comparison between Control and Dehydration groups identified 309 significant differentially regulated proteins ($p < 0.05$), with 240 upregulated and 69 downregulated relative to the Control group (Figure 4.6A). Summary details for the top 15 most significant proteins by *p*-value and by group mean difference are provided in Table 4.2. Principal component analysis indicates an apparent difference between the two groups with the full protein set (Figure 4.6B). A more pronounced difference is seen with the significant subset (Figure 4.6C), with the first principal component explaining 43.4.5% of the overall variation. An intermediate similarity between samples D6 and D10 with C2, C3, and C10

is appreciated. Hierarchical clustering, including the full set of proteins, identifies a similar trend of differentiation between the groups (Figure 4.6 D).

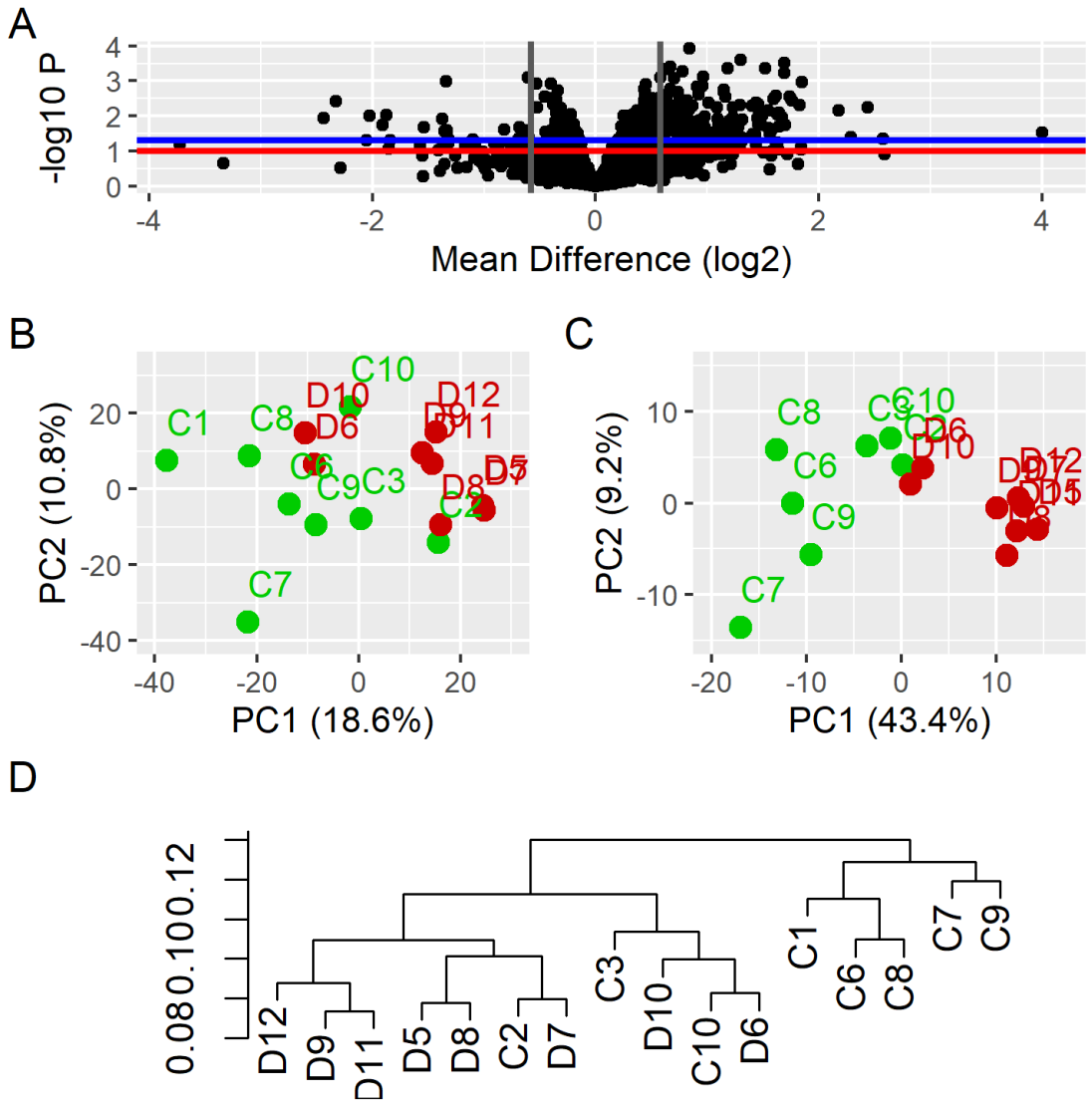

Figure 4.6 Comparisons for DEHY Subset. (A) Volcano plot of protein expression comparisons between Control and Dehydration groups with mean difference (log2 scale) between groups on the x-axis and statistical significance (-log(p)) on the y-axis. There are 309 proteins with $p < 0.05$ (blue line). A p-value of 0.1 is indicated by the red horizontal line. There are 171 proteins with a log2-fold change of at least ±1.5, indicated by the gray vertical lines. (B) Principal component analysis using the full protein set (n=1827) and (C) the subset of 309 statistically significant proteins. (D) Hierarchical clustering from the full protein set ignoring Rehydration group.

Table 4.2 Top 15 Differentially Regulated Proteins by P-value or Group Mean Difference in the DEHY Comparison. LogP: log10(p) for the particular protein. LogQ: log10(FDR). D: mean difference. C: Correlation to principal component 1.

	Uniprot ID	NAME	LogP	LogQ	D	C
***P*-Value**	A0A5F9D693	NEDD8-activating enzyme E1 catalytic subunit	-5.96	-2.70	1.53	0.70
	A0A5F9DCQ8	Clathrin heavy chain	-3.92	-0.98	0.84	0.79
	G1SM52	Leucine rich repeat containing 59	-3.60	-0.98	1.30	0.56
	G1SD44	Metaxin 1	-3.50	-0.98	1.69	0.64
	G1U754	Histidine-rich glycoprotein	-3.40	-0.98	0.67	0.79
	A0A5F9C6C7	Coatomer subunit beta	-3.36	-0.98	1.52	0.83
	G1TZA1	C1q domain-containing protein	-3.35	-0.98	1.19	0.74
	Q9N0Z6	Sodium/potassium-transporting ATPase subunit alpha-1	-3.34	-0.98	0.64	0.83
	G1SGL0	Sarcoglycan delta	-3.27	-0.96	0.78	0.77
	G1TDJ3	Extended synaptotagmin 1	-3.22	-0.96	1.69	0.69
	G1TM88	Serpin family A member 3	-3.12	-0.95	0.96	0.88
	P07293	Voltage-dependent L-type calcium channel subunit alpha-1S	-3.10	-0.95	0.58	0.71
	G1TIZ1	Ubiquitin carboxyl-terminal hydrolase	-3.09	-0.95	-0.60	-0.68
	A0A5F9DIY4	Myosin IC	-3.07	-0.95	0.70	0.90
	G1SES8	Mitochondrial ribosomal protein S22	-2.99	-0.92	-1.34	-0.41
Mean Difference	A0A5F9DT67	SERPIN domain-containing protein	-1.53	-0.62	4.01	0.43
	A0A5F9DDP4	Beta-microseminoprotein	-1.35	-0.55	2.58	0.43
	G1SEN8	Sacchrp_dh_NADP domain-containing protein	-2.24	-0.84	2.44	0.74
	G1U442	Mitochondrial pyruvate carrier	-1.38	-0.56	2.29	0.52

Table 4.2 continued

Mean Difference	A0A5F9C4W7	SERPIN domain-containing protein	-2.16	-0.79	2.18	0.66
	G1SZP0	Target of myb1 membrane trafficking protein	-2.96	-0.92	1.85	0.75
	G1SMI2	Acyl-CoA thioesterase 9	-2.30	-0.84	1.83	0.54
	G1T5A5	Reticulon 4 interacting protein 1	-2.45	-0.87	1.76	0.70
	G1U8F0	AP-2 complex subunit alpha	-2.56	-0.87	1.74	0.89
	G1T338	Peptidyl-prolyl cis-trans isomerase	-1.73	-0.68	1.70	0.52
	G1TDJ3	Extended synaptotagmin 1	-3.22	-0.96	1.69	0.69
	G1SD44	Metaxin 1	-3.50	-0.98	1.69	0.64
	G1SWS5	Phospholysine phosphohistidine inorganic pyrophosphate phosphatase	-1.95	-0.76	1.67	0.58
	G1TDC2	Solute carrier family 37 member 4	-2.08	-0.78	1.64	0.72
	G1SKE6	Gamma-sarcoglycan	-1.69	-0.68	1.64	0.56

Effects of Rehydration following Dehydration

A total of 418 proteins were found with a significant difference between the Control group and the joint mean of Dehydration and Rehydration groups (CDR comparison), 331 upregulated and 87 downregulated relative to the Control group. Summary details for the top 15 most significant proteins by *p*-value and by group mean difference are provided in Table 4.3. Principal component analysis provides evidence of differences between the Control and Rehydration groups with or without inclusion of the Dehydration group (Figure 4.7A-B). The similarity among the Dehydration and Rehydration groups is apparent by principal component analysis of the entire protein set with no clear divergence from each other when restricted to either the significant CDR or REHY (Control vs. Rehydration group alone) subsets (Figure 4.7C-D). The Control and Rehydration groups cluster moderately well alone (Figure 4.8A) or when considering all three groups from the full protein set (Figure 4.8B) and the significant CDR subset (Figure 4.8C).

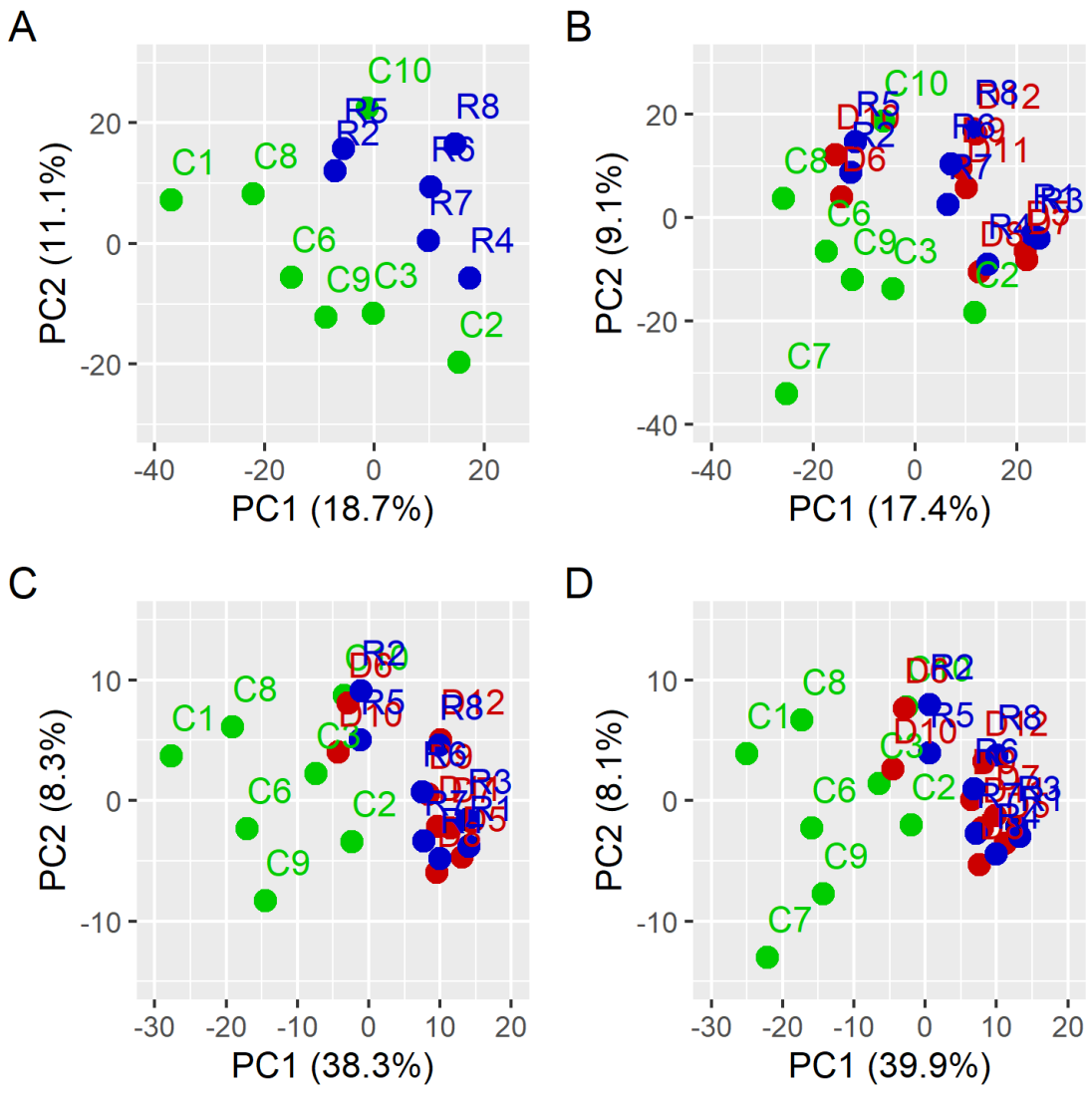

Figure 4.7 Principal component analysis showing (A) the Control and Rehydration groups and (B) all three groups from the full protein set (n= 1827). The same patterns are seen from (C) the significant CDR subset (n= 418) and (D) the significant REHY subset (n= 332).

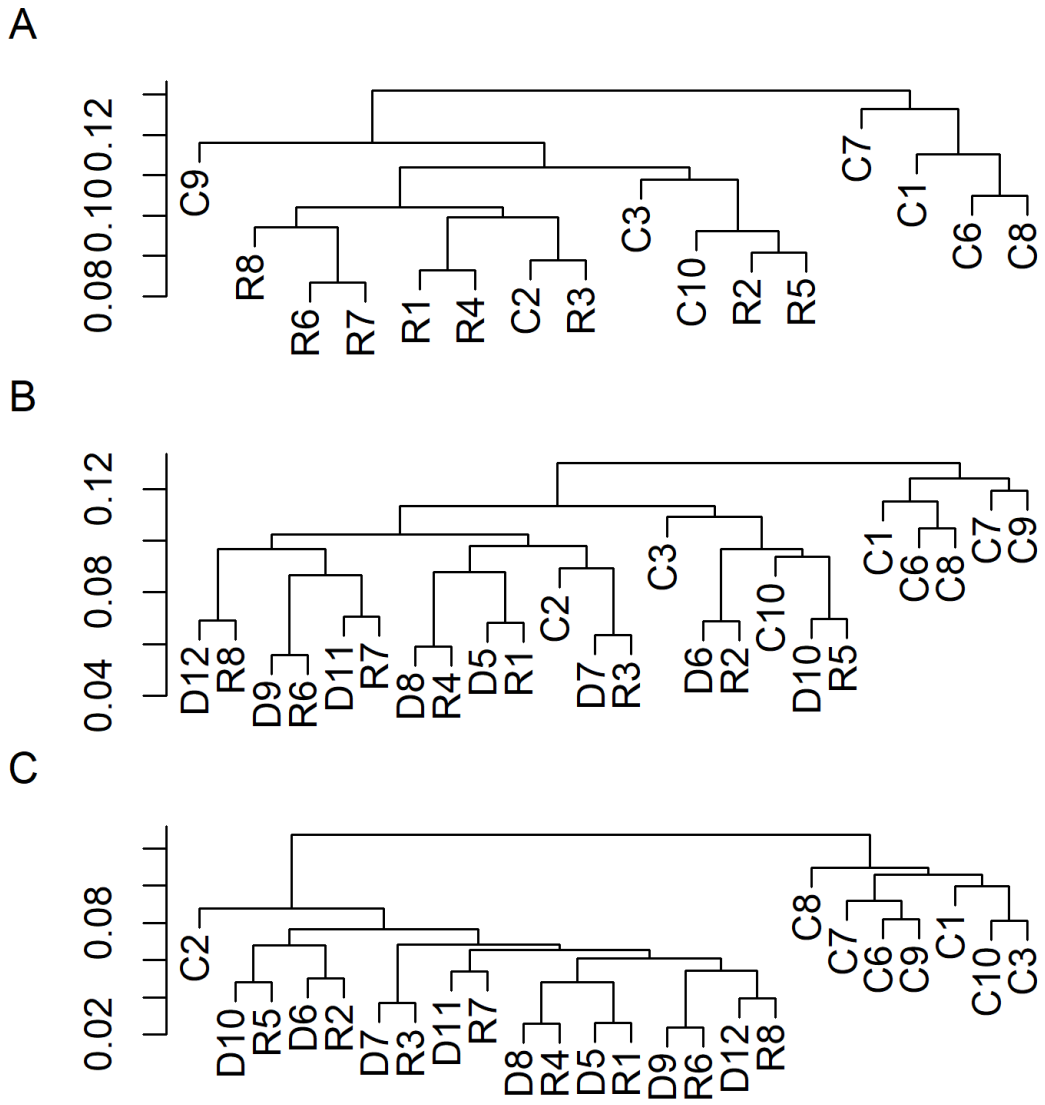

Figure 4.8 Hierarchical Clustering. (A) Clustering using full protein set (n=1824), ignoring dehydration group, (B) the full protein set (n=1827), and (C) the significant CDR subset (n= 418).

Table 4.3 Top 15 Differentially Regulated Proteins by P-value or Group Mean Difference in the CDR Comparison.

	Uniprot ID	NAME	LogP	LogQ	D	C
***P*-Value**	A0A5F9D693	NEDD8-activating enzyme E1 catalytic subunit	-6.51	-3.25	2.88	0.58
	A0A5F9DCQ8	Clathrin heavy chain	-4.64	-1.68	1.68	0.78
	Q9N0Z6	Sodium/potassium-transporting ATPase subunit alpha-1	-4.33	-1.55	1.36	0.82
	G1U754	Histidine-rich glycoprotein	-4.05	-1.54	1.34	0.76
	A0A5F9DPU2	Cullin 3	-4.01	-1.54	2.16	0.82
	G1T6E9	CDGSH iron sulfur domain 2	-3.89	-1.54	3.90	0.64
	G1SM52	Leucine rich repeat containing 59	-3.83	-1.54	2.36	0.59
	G1TIZ1	Ubiquitin carboxyl-terminal hydrolase	-3.80	-1.54	-1.23	-0.71
	G1U1V6	CSD domain-containing protein	-3.79	-1.54	-5.70	-0.58
	A0A5F9CSX3	Amine oxidase	-3.72	-1.54	2.56	0.77
	P07293	Voltage-dependent L-type calcium channel subunit alpha-1S	-3.69	-1.54	1.15	0.66
	G1T2Z8	S-methyl-5-thioadenosine phosphorylase	-3.68	-1.54	3.48	0.52
	G1TZA1	C1q domain-containing protein	-3.67	-1.54	2.21	0.69
	G1SK52	X-prolyl aminopeptidase 1	-3.65	-1.54	-0.79	-0.59
	G1SGL0	Sarcoglycan delta	-3.51	-1.43	1.43	0.73
Mean Difference	A0A5F9DT67	SERPIN domain-containing protein	-2.50	-1.21	9.92	0.50
	A0A5F9DDP4	Beta-microseminoprotein	-1.62	-0.83	5.07	0.41
	G1U442	Mitochondrial pyruvate carrier	-1.79	-0.90	4.76	0.52
	G1SEN8	Sacchrp_dh_NADP domain-containing protein	-2.59	-1.21	4.69	0.66
	A0A5F9DV00	Platelet activating factor acetylhydrolase 1b catalytic subunit 2	-2.76	-1.24	4.25	0.45
	G1T6E9	CDGSH iron sulfur domain 2	-3.89	-1.54	3.90	0.64
	A0A5F9C4W7	SERPIN domain-containing protein	-2.23	-1.10	3.85	0.64
	G1T7Q5	Carboxylic ester hydrolase	-1.42	-0.73	3.52	0.45
	G1T2Z8	S-methyl-5-thioadenosine phosphorylase	-3.68	-1.54	3.48	0.52
	G1T338	Peptidyl-prolyl cis-trans isomerase	-2.13	-1.05	3.41	0.54
	G1TDC2	Solute carrier family 37 member 4	-2.62	-1.21	3.37	0.71
	G1TBL1	Solute carrier family 25 member 20	-2.85	-1.30	3.30	0.68
	A0A5F9CVH3	Chloride intracellular channel protein	-1.94	-0.96	3.26	0.48
	G1SMI2	Acyl-CoA thioesterase 9	-2.36	-1.14	3.23	0.35
	G1SLF8	Ecm29 proteasome adaptor and scaffold	-3.05	-1.37	3.19	0.78

LogP: log10(p) for the particular protein. LogQ: log10(FDR). D: mean difference. C: Correlation to principal component 1.

The Dehydration and Rehydration groups were directly compared further, ignoring the Control group (DR comparison). The Dehydration and Rehydration groups exhibit exceedingly few differentially regulated proteins from each other (n = 34, uncorrected $p < 0.05$; n = 15, Tukey's adjusted $p < 0.05$; data not shown). Principal component analysis with the full protein set suggests a high level of similarity between the two groups, with only 30.4% of the overall variance explained (Figure 4.9A) with a marginal improvement to 34.8% when considering only the significant CDR and REHY subsets (Figure 4.9B-C). Among the significant proteins in the REHY subset, the majority of proteins exhibit very similar magnitudes of mean difference from the Control group and statistical significance in both Dehydration and Rehydration groups (Figure 4.9D).

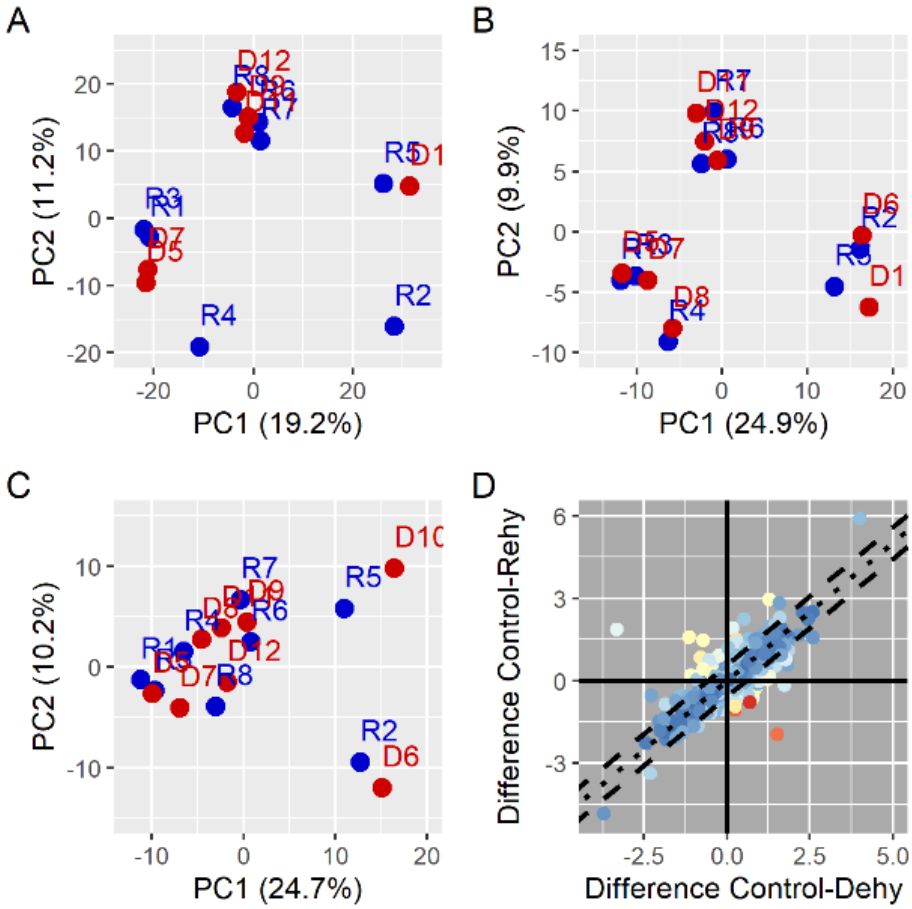

Figure 4.9 Comparison of Dehydration and Rehydration Groups. Principal component analysis of Dehydration and Rehydration groups from (A) the full protein set (n=1827), (B) the significant CDR subset (n= 418), and (C) the significant REHY subset (n= 332). (D) Illustrative plot of differential expression between the Dehydration and Rehydration groups relative to Control. Dehydration-Control difference (log2 scale) is shown along the x-axis and Rehydration-Control difference (log2 scale) along the y-axis. Point color represents magnitude of the ratio of -log10P for the respective Dehydration to Rehydration comparison, with red indicating higher significance. There are 34 proteins with $p < 0.05$ and 62 with $p < 0.1$. The dashed lines indicate a band corresponding to ±1.5 fold change expression with the dotted representing equality.

4.4.5 Enrichment Analysis and Protein-Protein Interaction

A total of 116 enrichment terms were identified for the DEHY subset and 159 for the CDR subset. There is considerable overlap between the two sets. The top enrichment terms following gene set reduction, up to 3, from the first 5 Metascape-defined clusters from each comparison are provided in Table 4.4. Protein-protein interaction networks are shown in Figure 4.10. A total of 8 MCODE clusters were identified for the DEHY subset and 13 for the CDR

subset; after filtering criteria similar to that used for the enrichment analysis were applied, 3 and 5 MCODE clusters were represented, respectively. The top enrichment terms, up to 3, for the filtered MCODE clusters are shown in Table 4.5. The protein interactions described within each cluster are shown in Figure 4.10. The Transcription Factor Targets analysis provided two results for the DEHY comparison (M40825, NR1H4; M14141, NRF2) and a single, shared result for the CDR comparison (M40825, NR1H4).

Table 4.4 Gene Enrichment from Differentially Regulated Proteins

Metascape Cluster	**Enrichment ID**	**Description**	**LogP**	**LogQ**	**E**	**Prots**
DEHY1	GO:1990542	mitochondrial transmembrane transport	-19.4	-15.3	103.9	11
	GO:0006839	mitochondrial transport	-6.2	-4.1	7.9	10
DEHY2	R-HSA-109582	Hemostasis	-18.3	-14.9	6.8	35
	hsa04610	Complement and coagulation cascades	-18.0	-14.6	111.1	10
	GO:0050878	regulation of body fluid levels	-14.8	-11.8	31.0	12
DEHY3	R-HSA-174824	Plasma lipoprotein assembly, remodeling, and clearance	-18.9	-15.3	134.9	10
DEHY4	R-HSA-9711123	Cellular response to chemical stress	-10.3	-7.6	10.9	14
	R-HSA-162906	HIV Infection	-7.2	-5.0	6.9	13
	R-HSA-195721	Signaling by WNT	-7.0	-4.9	5.6	15
DEHY5	R-HSA-5653656	Vesicle-mediated transport	-13.5	-10.6	5.6	30
	GO:0048193	Golgi vesicle transport	-6.3	-4.3	5.8	13
	R-HSA-446203	Asparagine N-linked glycosylation	-5.9	-3.9	5.3	13
CDR1	R-HSA-109582	Hemostasis	-23.8	-19.5	16.0	26
	hsa04610	Complement and coagulation cascades	-19.2	-15.8	58.5	13
CDR1	R-HSA-76002	Platelet activation, signaling and aggregation	-17.9	-14.8	9.5	27

Table 4.4 continued

CDR2	GO:0003013	circulatory system process	-22.0	-18.2	17.9	23
	GO:1903522	regulation of blood circulation	-18.8	-15.5	25.4	17
	GO:0090257	regulation of muscle system process	-15.9	-13.2	22.9	15
CDR3	R-HSA-6798695	Neutrophil degranulation	-19.7	-16.1	7.2	36
CDR4	R-HSA-9711123	Cellular response to chemical stress	-18.8	-15.5	35.9	15
	WP183	Proteasome degradation	-16.9	-14.0	65.7	11
	hsa05020	Prion disease	-15.3	-12.7	21.0	15
CDR5	hsa04961	Endocrine and other factor-regulated calcium reabsorption	-17.9	-14.8	79.4	11
	R-HSA-174824	Plasma lipoprotein assembly, remodeling, and clearance	-16.4	-13.6	60.1	11
	R-HSA-9679506	SARS-CoV Infections	-7.9	-6.1	7.9	13

LogP: log10(p) for the enrichment term. LogQ: log10(FDR). E: Enrichment factor of the enrichment term. Prots: The number of proteins represented by the enrichment term from the collapsed gene set.

Table 4.5 Protein-protein Interaction Enrichment Terms

MCODE Cluster	**Enrichment ID**	**Description**	**LogP**	**Log Q**	**E**	**Prots**
DEHY 1	R-HSA-1280218	Adaptive Immune System	-6.4	-4.6	14	7
DEHY 2	R-HSA-1280218	Adaptive Immune System	-11	-8.3	21	10
	R-HSA-9006934	Signaling by Receptor Tyrosine Kinases	-6.2	-4.5	18	6
	R-HSA-199991	Membrane Trafficking	-5.7	-4.1	15	6
DEHY 4	R-HSA-114608	Platelet degranulation	-25	-21	180	12

Table 4.5 continued

DEHY 4 cont.	R-HSA-76005	Response to elevated platelet cytosolic Ca2+	-25	-21	170	12
	R-HSA-8957275	Post-translational protein phosphorylation	-24	-20	190	11
CDR 1	GO:0043604	amide biosynthetic process	-5.7	-4.3	15	6
	R-HSA-382551	Transport of small molecules	-4.6	-3.5	9.9	6
	GO:0043603	cellular amide metabolic process	-4.6	-3.4	9.7	6
CDR 2	R-HSA-446203	Asparagine N-linked glycosylation	-6.9	-5.4	25	6
	R-HSA-199991	Membrane Trafficking	-5.1	-3.8	12	6
	R-HSA-5653656	Vesicle-mediated transport	-4.9	-3.7	11	6
CDR 3	R-HSA-8957275	Post-translational protein phosphorylation	-28	-23	190	13
	R-HSA-381426	Regulation of Insulin-like Growth Factor (IGF)*	-27	-23	170	13
	R-HSA-114608	Platelet degranulation	-27	-23	160	13
CDR 4	R-HSA-162909	Host Interactions of HIV factors	-15	-12	110	8
	R-HSA-4086400	PCP/CE pathway	-13	-11	140	7
	R-HSA-162906	HIV Infection	-13	-9.9	61	8
CDR 5	R-HSA-9711123	Cellular response to chemical stress	-9.6	-7.5	67	6
	hsa05022	Pathways of neurodegeneration - multiple diseases	-6.8	-5.3	22	6
	R-HSA-2262752	Cellular responses to stress	-5.6	-4.3	14	6

LogP: log10(p) for the enrichment term. LogQ: log10(FDR). E: Enrichment factor the enrichment term. Prots: The number of proteins represented by the enrichment term from the collapsed gene set.

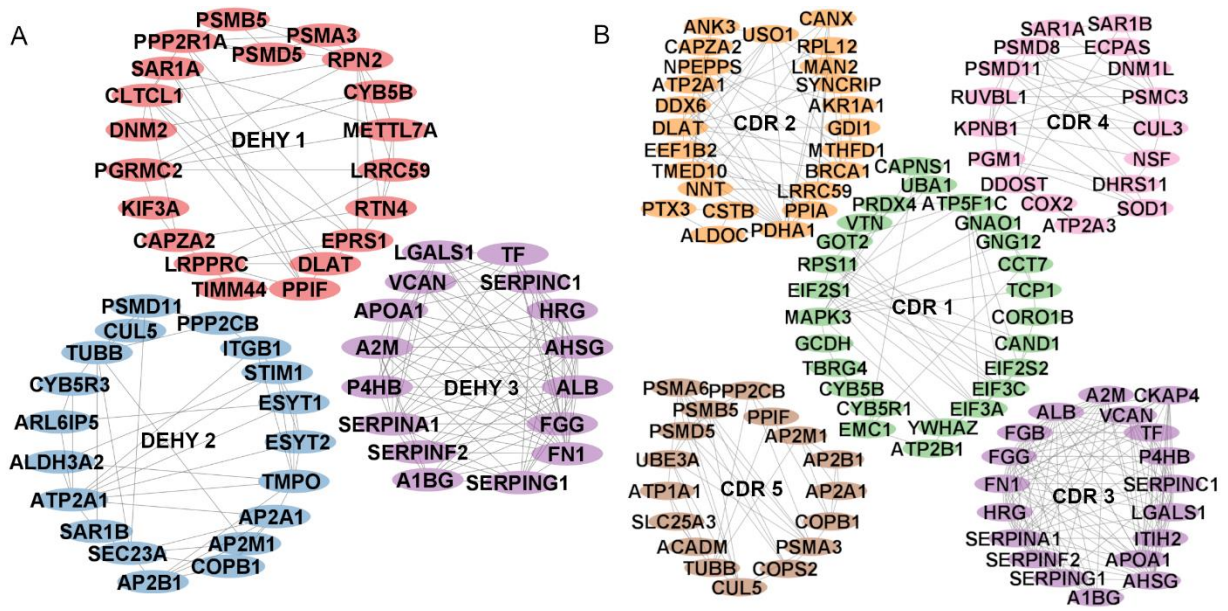

Figure 4.10 PPI Clusters Identified by MCODE. Nodes represent proteins, and edges represent interaction between those proteins. Full clusters are shown, beyond the number of the specific enrichment terms in Table 4.5. The 3 clusters on the left represent the DEHY subset MCODE clusters, and the 5 on the right, the CDR subset.

4.5 Discussion

4.5.1 Water Intake, Restriction, and Dehydration

Dehydration is a common physiological state that may arrive through many different mechanisms. As it relates to our current study and desired inference to voice in humans, water restriction-induced dehydration is a physiologically relevant and realistic context. We base this on the assumption that baseline water intake of rabbits, when not precluded by time or volume restrictions, maintains a state of euhydration and thus represents an “optimal” water intake. Interestingly, we observed a dramatic range of daily water intake between rabbits. Restricting volume to half the average intake conceptually mimics the circumstance of a human individual with full access to water who consumes a practically sustainable but suboptimal amount. While other restrictive means such as total water deprivation may arrive more quickly to a more pronounced state of dehydration, this is less applicable to the assumed lived experience of professional voice users. Our choice of 5 days of water restriction and 3 days of rehydration further reinforces the clinical relevance. In the absence of the confounding thermal dysregulation

and exercise-induced oxidative stress often associated with dehydration studies, we conclude confidently that the changes we observed are due to dehydration induced by water restriction. While the definition of dehydration is straightforward in describing suboptimal water content, means by which dehydration is measured are more nuanced and present additional challenges.

4.5.2 PCV, Blood Chemistry, and Body Weight

We make the fundamental assumption that rabbits are euhydrated at baseline; however, the ability to test this empirically is limited. Common clinical measures of dehydration include packed cell volume or hematocrit, blood analytes including BUN and creatinine, and physical measurements such as body weight and skin turgor. However, individual measurements may have limited diagnostic power; this is evidenced by the rabbits' baseline PCV that ranged from 37-48%, with a comparable spread at the other observed time points. Despite our repeated within-rabbit measures, PCV failed to indicate a shift from euhydrated to dehydrated state. Conversely, a number of blood analytes measured with the i-STAT Chem8+ panel were significantly different following water restriction. As expected, we observed increases in Na+, Cl-, and creatinine. Interestingly, BUN decreased following dehydration and was the only measure to exhibit significant mutual difference among all three groups following water restriction, with the Rehydration group falling below the Control and above the Dehydration group. Body weight is our strongest indicator of water restriction-induced dehydration, with a clear decrease following restriction and a rapid increase following the rehydration protocol. Taken together, our 5-day water restriction and 3-day rehydration protocol induced clinically observable changes consistent with dehydration and resolution, respectively.

4.5.3 Group Comparisons

Our study was motivated by the documented observation that systemic dehydration negatively impacts voice outcomes [63,234]. Recent work from our group has begun to describe associated transcriptional changes in the vocal folds [100,192,226], but our novel approach here was a shift to focus on the functional level of the proteome. Our results were consistent with the anticipated changes in protein regulation following the 5 days of water restriction. Our second aim was to identify the effects of rehydration following the water restriction. We hypothesized

reversal of changes induced by water restriction either back to a Control state or an intermediate of Control and Dehydration. The remarkable similarity of the Dehydration and Rehydration groups was unexpected. The Rehydration status has no context without having first been dehydrated, so while we consider this group distinct from a protein regulation perspective, we cannot interpret Rehydration directly as its own treatment. The decision to conduct a second analysis with the pooled Dehydration and Rehydration groups followed this observation, and we interpret these results as changes from dehydration that persist despite the rehydration protocol. While we emphasize the proteomic similarity between these two groups, we recognize that these are disparate physiological states.

At the level of individual proteins, both the Dehydration (DEHY) and pooled Dehydration-Rehydration (CDR) comparisons demonstrated upregulation of a substantial number of pertinent structural proteins, including collagens (1A2, 4A1, 4A2, and 6A3), fibrillin 2, fibulin 3, multiple serpins (A1, A3, F2, G1, and H1), and versican. These findings suggest perturbation of structural maintenance of the vocal fold lamina propria with considerable implications. Collagen is one of the fundamental structural components of the vocal folds [235] that, along with elastin and other extracellular matrix components like hyaluronic acid, contribute to the viscoelastic nature of the vocal folds that underlie phonatory capacity. The serpins (serine protease inhibitors) are a large family of protease inhibitors with pleiotropic effects. The three identified here could play a role in vocal pathology induced by dehydration: A1 is an inhibitor of a variety of proteases including elastase, which may degrade elastin or collagen fibers [236] and stimulate fibroblasts [237], A3 may indirectly influence collagen stability by protection of the fibular accessory protein decorin [238], and H1 is a collagen-specific chaperone important for the successful maturation of collagen fibers [239]. Interestingly, serpin H1 has recently been shown as a potential therapeutic target against fibrosis in the vocal folds [240]. Versican and fibulin 3 influence collagen superstructure among many other extracellular matrix modifying activities [241-243], while fibrillin 2 is associated with elastic fibers. Although we have not tested it empirically, there is a considerable capacity for changes in these proteins to negatively impact voice by influencing the underlying vocal fold biomechanics.

The annotated enrichment through Metascape suggests a diverse set of physiological changes associated with dehydration. Of particular interest are changes related to hemostasis and mitochondrial function and response to cellular stress. Dehydration is expected to increase both

serum and interstitial osmolarity, and thus it is reasonable to expect a response of endothelial cells. This is substantiated by a recent study demonstrating the diversity among and transcriptional changes of renal endothelial cells in response to dehydration [244], recognizing the difference in expected magnitudes of osmotic changes between the vocal folds and the kidneys. Interestingly, dehydration has been suggested as a potential modifying factor for risk of developing deep venous thromboembolism [245]. Taken together, the vocal fold endothelium and implications to the submucosal interstitium are attractive targets for further analysis. Oxidative changes secondary to dehydration is an anticipated stress and are evidenced by enrichments for mitochondrial function, cellular stress response, and targets of the transcription factor NRF2. NRF2 is a transcription factor that regulates response to oxidative and other stresses [246]. Oxidative stress has long been associated with dehydration. Recently, rapid bodyweight loss by water restriction has been shown to increase markers of oxidative stress in a study of young-adult male wrestlers [247], and chronic water restriction in a lizard species manifested oxidative changes that varied between sexes [248]. Evaluation of the *in vivo* effects of oxidative stress in the vocal folds is limited, but reactive oxygen species production is associated with early wound healing [249], and oxidative stress is associated with age-related changes [250]. More generally, chronic oxidative stress could damage the vocal fold microenvironment leading to dysphonia.

The most striking observation of this study was the overwhelming similarity of the proteomic profiles of the Dehydration and Rehydration groups. Dehydration is commonly identified in the clinical setting, and fluid restoration is a ubiquitous intervention that is often intended to rapidly restore a euhydrated state. We demonstrate herein that our clinical markers of dehydration fully resolve within 1 to 2 days following an oral rehydration protocol. However, the persistence of protein-level changes has profound implications on how we should conceptualize the clinical intervention of systemic hydration within the vocal folds. Our results suggest that euhydration is necessary but not enough to present a baseline molecular state and that an unremarkable superficial clinical evaluation may be uncoupled from the underlying molecular pathology. We assume the observed changes from dehydration are transient, but we conclude that the 3-day rehydration period is insufficient time.

4.5.4 Limitations and Future Directions

Our study is limited to a between-group design as each rabbit possesses only two vocal folds, and a unilateral vocal fold resection at an experimental midpoint is precluded by the acute nature of the experiment and risk of complications. We chose water restriction as a practically relevant dehydration protocol, but due to the dramatic variation in baseline water intake among rabbits, we were limited to define dehydration protocol in terms of water restriction relative to the individual. We chose to standardize the time of water restriction over a targeted decrease in body weight, so while we demonstrate significant body weight loss, there is likely inherent variability in our measure of dehydration. We have assumed that rabbits began at a relative euhydrated state supported by their daily water intake. We chose proteomic analysis to focus on describing functional changes in the tissues following dehydration and rehydration. While the presence of differentially regulated proteins associated with enrichment terms implies upregulation of the associated genes at some point before sample collection, we recognize the limitation of proteomics to infer real-time transcriptional processes. Future longitudinal studies that assess a more granular time interval approach and couple transcriptomic and proteomic analyses will be informative. Further, we used full-thickness tissue samples in this study which confound the distinct contributions of individual tissues layers. Our data suggest that parallel interrogation of epithelial, mesenchymal, and immune cells would improve our molecular understanding.

4.6 Acknowledgements

We thank Chenwei Duan and Anumitha Venkatraman for their assistance with sample collection. We thank Dr. Uma K. Aryal and Dr. Jackeline Franco of the Purdue Proteomics Facility. All the LC-MS/MS sample preparation was performed and data acquired through the Purdue Proteomics Facility in Purdue's Discovery Park.

CHAPTER 5. CONCLUSIONS AND IMPLICATIONS TO FUTURE WORK

The purpose of this project was to describe molecular changes in the vocal folds associated with dehydration in hopes of providing a basis for the dehydration-related dysphonic changes that are otherwise well described. We have considered dehydration under two distinct physiological paradigms: mucosal surface dehydration via exposure to low humidity and systemic dehydration via water restriction. We have shown evidence of differential transcriptional and protein regulation in response to both a single acute exposure and recurring exposures to low humidity, as well as a short-term water restriction protocol. Our results strongly support a potential role for molecular perturbations to contribute to dehydration-induced dysphonia.

A secondary goal of the third study in this project was to identify the effects of a post-dehydration oral rehydration protocol. Hydration therapy follows the logical assumption that if a lack of water is negative, replacing water should be recuperative. We found that indeed the clinical manifestations of systemic dehydration resolve rapidly once *ad libitum* access to water is returned, but unexpectedly, the proteomic signatures identified following water restriction persist even after 3 days of *ad libitum* consumption. This curious observation points toward a likely multifaceted impact of dehydration on the vocal folds. Evidence suggests a reasonable assertion that perturbations in tissue hydration modulate tissue dynamics that should result in dysphonic changes; however, our results highlight the importance of considering concurrent molecular perturbations which may be induced or resolved on different timelines. To this end, further characterization of the interaction between dehydration and other dysphonia inducing processes would add valuable insight to our understanding.

Although we have identified no clear mechanistic pathways within our data, a couple interesting themes that warrant further exploration are identified. Both surface dehydration studies identified a number of differentially regulated muscle-related genes and proteins. This is a curious finding considering that the muscle is the deepest layer of the vocal fold with respect to the mucosal surface, and it highlights a need to consider the vocal folds holistically in the context of even surface dehydration. Response to oxidative stress is identified in all three studies. One primary limitation of our studies is the whole-tissue sample processing that does not allow the

parallel analysis of different tissue layers. Oxidative stress could originate from a variety of sources, including the epithelium, endothelium, and muscle with different implications to the underlying cause and effective intervention. Further target analysis of the different tissue compartments would provide valuable insight. Lastly, the abundance of differentially regulated structural proteins in the final study is interesting. While it is unreasonable to infer gross fibrotic changes over such an acute period, this does suggest that the mesenchymal cell population is active, which could have significant implications in a chronic context. Further, the persistence of the dehydration-induced changes following the rehydration period highlights a need to co-interpret clinical presentation and underlying pathology with care as they may be uncoupled in time.

REFERENCES

1 Sato, K. *Functional Histoanatomy of the Human Larynx*. (Singapore : Springer Singapore : Imprint: Springer, 2018).

2 Alipour, F. & Jaiswal, S. Phonatory characteristics of excised pig, sheep, and cow larynges. *The Journal of the Acoustical Society of America* **123**, 4572-4581, doi:10.1121/1.2908289 (2008).

3 Riede, T., Lingle, S., Hunter, E. J. & Titze, I. R. Cervids with different vocal behavior demonstrate different viscoelastic properties of their vocal folds. *Journal of morphology (1931)* **271**, 1-11, doi:10.1002/jmor.10774 (2010).

4 Kazarine, A. *et al.* Multimodal virtual histology of rabbit vocal folds by nonlinear microscopy and nano computed tomography. *Biomedical optics express* **10**, 1151-1164, doi:10.1364/BOE.10.001151 (2019).

5 Benboujja, F. & Hartnick, C. Quantitative evaluation of the human vocal fold extracellular matrix using multiphoton microscopy and optical coherence tomography. *Sci Rep* **11**, 2440-2440, doi:10.1038/s41598-021-82157-9 (2021).

6 Ward, P. D., Thibeault, S. L. & Gray, S. D. Hyaluronic Acid: Its Role in Voice. *Journal of Voice* **16**, 303-309, doi:10.1016/S0892-1997(02)00101-7 (2002).

7 Hirschi, S. D., Gray, S. D. & Thibeault, S. L. Fibronectin. *Journal of Voice* **16**, 310-316, doi:10.1016/s0892-1997(02)00102-9 (2002).

8 Klemuk, S. A., Riede, T., Walsh, E. J. & Titze, I. R. Adapted to Roar: Functional Morphology of Tiger and Lion Vocal Folds.(Research Article). *PLoS ONE* **6**, e27029, doi:10.1371/journal.pone.0027029 (2011).

9 Lang, A., Koch, R., Rohn, K. & Gasse, H. Histomorphometric Analysis of Collagen and Elastic Fibres in the Cranial and Caudal Fold of the Porcine Glottis.(Report). **44**, 186, doi:10.1111/ahe.12125 (2015).

10 Toya, Y. *et al.* Interspecies comparison of stellate cell-containing macula flavae and vitamin A storage in vocal fold mucosa. *Journal of Anatomy* **225**, 298-305, doi:10.1111/joa.12211 (2014).

11 Widdicombe, J. *et al.* Distribution of tracheal and laryngeal mucous glands in some rodents and the rabbit. *J. Anat.* **198**, 207-221 (2001).

12 Choi, H., Finkbeiner, W. & Widdicombe, J. A comparative study of mammalian tracheal mucous glands. *J. Anat.* **197**, 361-372 (2000).

13 Hoffman, M. R., Braden, M. N. & Mcmurray, J. S. in *Multidisciplinary Management of Pediatric Voice and Swallowing Disorders* 49-61 (Springer International Publishing, 2020).

14 Hirano, M. Morphological Structure of the Vocal Cord as a Vibrator and its Variations. *Folia Phoniatrica et Logopaedica* **26**, 89-94, doi:10.1159/000263771 (1974).

15 Scholp, A. *et al.* Study of spatiotemporal liquid dynamics in a vibrating vocal fold by using a self-oscillating poroelastic model. *J Acoust Soc Am* **148**, 2161-2172, doi:10.1121/10.0002163 (2020).

16 Vahabzadeh-Hagh, A. M., Zhang, Z. & Chhetri, D. K. Hirano's cover–body model and its unique laryngeal postures revisited. *The Laryngoscope* **128**, 1412-1418, doi:10.1002/lary.27000 (2018).

17 Sato, K., Hirano, M. & Nakashima, T. Comparative Histology of the Maculae Flavae of the Vocal Folds. *Annals of Otology, Rhinology & Laryngology* **109**, 136-140, doi:10.1177/000348940010900205 (2000).

18 Kim, D., Lee, S., Lim, J. Y. & Kwon, S. Characteristics and Responses of Human Vocal Fold Cells in a Vibrational Culture Model. *Laryngoscope* **128**, E258-E264, doi:10.1002/lary.27113 (2018).

19 Gracioso Martins, A. M., Biehl, A., Sze, D. & Freytes, D. O. Bioreactors for Vocal Fold Tissue Engineering. *Tissue engineering. Part B, Reviews* **28**, 182-205, doi:10.1089/ten.TEB.2020.0285 (2022).

20 Gaston, J., Quinchia Rios, B., Bartlett, R., Berchtold, C. & Thibeault, S. L. The response of vocal fold fibroblasts and mesenchymal stromal cells to vibration. *PloS one* **7**, e30965, doi:10.1371/journal.pone.0030965 (2012).

21 Hiwatashi, N. *et al.* Biocompatibility and Efficacy of Collagen/Gelatin Sponge Scaffold With Sustained Release of Basic Fibroblast Growth Factor on Vocal Fold Fibroblasts in 3-Dimensional Culture. *Annals of Otology, Rhinology & Laryngology* **124**, 116-125, doi:10.1177/0003489414546396 (2015).

22 Fukahori, M. *et al.* Regeneration of Vocal Fold Mucosa Using Tissue-Engineered Structures with Oral Mucosal Cells. *PLoS ONE* **11**, doi:10.1371/journal.pone.0146151 (2016).

23 Kim, D., Lim, J.-Y. & Kwon, S. Development of Vibrational Culture Model Mimicking Vocal Fold Tissues. *The Journal of the Biomedical Engineering Society* **44**, 3136-3143, doi:10.1007/s10439-016-1587-5 (2016).

24 Mizuta, M., Kurita, T., Kimball, E. E. & Rousseau, B. Structurally and functionally characterized in vitro model of rabbit vocal fold epithelium. *Tissue & cell* **49**, 427, doi:10.1016/j.tice.2017.03.006 (2017).

25 Walimbe, T., Panitch, A. & Sivasankar, M. P. An In vitro Scaffold-Free Epithelial-Fibroblast Coculture Model for the Larynx. *Laryngoscope* **127**, E185-E192, doi:10.1002/lary.26388 (2017).

26 Bartlett, R., Gaston, J., Ye, S., Kendziorski, C. & Thibeault, S. Mechanotransduction of vocal fold fibroblasts and mesenchymal stromal cells in the context of the vocal fold mechanome. *Journal of Biomechanics* **83**, 227, doi:10.1016/j.jbiomech.2018.11.050 (2019).

27 Kirsch, A. *et al.* Development and validation of a novel phonomimetic bioreactor. *PLoS One* **14**, e0213788, doi:10.1371/journal.pone.0213788 (2019).

28 Kim, D. & Kwon, S. Vibrational stress affects extracellular signal-regulated kinases activation and cytoskeleton structure in human keratinocytes. *PLoS One* **15**, e0231174, doi:10.1371/journal.pone.0231174 (2020).

29 Murray, P. R. & Thomson, S. L. Synthetic, multi-layer, self-oscillating vocal fold model fabrication. *Journal of visualized experiments : JoVE*, doi:10.3791/3498 (2011).

30 Murray, P. R. & Thomson, S. L. Vibratory responses of synthetic, self-oscillating vocal fold models. *The Journal of the Acoustical Society of America* **132**, 3428-3438, doi:10.1121/1.4754551 (2012).

31 Knaneh-Monem, H. *et al.* Differential epithelial growth in tissue-engineered larynx and trachea generated from postnatal and fetal progenitor cells. *Biochemical and Biophysical Research Communications* **510**, 205-210, doi:10.1016/j.bbrc.2019.01.060 (2019).

32 Erickson-DiRenzo, E., Leydon, C. & Thibeault, S. L. Methodology for the establishment of primary porcine vocal fold epithelial cell cultures. *The Laryngoscope* **129**, E355-E364, doi:10.1002/lary.27909 (2019).

33 Mo, T.-T. *et al.* Optimized Generation of Primary Human Epithelial Cells from Larynx and Hypopharynx: A Site-Specific Epithelial Model for Reflux Research. *Cell Transplantation* **28**, 630-637, doi:10.1177/0963689719838478 (2019).

34 Lungova, V., Chen, X., Wang, Z., Kendziorski, C. & Thibeault, S. L. Human induced pluripotent stem cell-derived vocal fold mucosa mimics development and responses to smoke exposure. *Nature communications* **10**, 4161, doi:10.1038/s41467-019-12069-w (2019).

35 Chen, X. *et al.* Novel immortalized human vocal fold epithelial cell line: In vitro tool for mucosal biology. *The FASEB journal* **35**, e21243-n/a, doi:10.1096/fj.202001423R (2021).

36 Rhee, H. S. & Hoh, J. F. Y. Immunohistochemical Analysis of Myosin Heavy Chain Expression in Laryngeal Muscles of the Rabbit, Cat, and Baboon. *Journal of Histochemistry & Cytochemistry* **56**, 929-950, doi:10.1369/jhc.2008.951756 (2008).

37 Phillips, R., Zhang, Y., Keuler, M., Tao, C. & Jiang, J. Measurement of liquid and solid component parameters in canine vocal fold lamina propria. *J. Acoust. Soc. Am.* **125**, 2282-2287, doi:10.1121/1.3086276 (2009).

38 Rousseau, B. *et al.* Characterization of chronic vocal fold scarring in a rabbit model. *Journal of Voice* **18**, 116-124, doi:10.1016/j.jvoice.2003.06.001 (2004).

39 Garrett, C. G., Coleman, J. R. & Reinisch, L. Comparative Histology and Vibration of the Vocal Folds: Implications for Experimental Studies in Microlaryngeal Surgery. *Laryngoscope* **110**, 814-824, doi:10.1097/00005537-200005000-00011 (2000).

40 Thomas, L., Stemple, J., Andreatta, R. & Andrade, F. Establishing a New Animal Model for the Study of Laryngeal Biology and Disease: An Anatomic Study of the Mouse Larynx. *Journal of Speech, Language, and Hearing Research* **52**, 802-811, doi:10.1044/1092-4388(2008/08-0087) (2009).

41 Lang, A., Koch, R., Rohn, K. & Gasse, H. The histological components of the phoniatrical body-cover model in minipigs of different ages. *PLoS One* **10**, e0128085-e0128085, doi:10.1371/journal.pone.0128085 (2015).

42 Riede, T., York, A., Furst, S., Müller, R. & Seelecke, S. Elasticity and stress relaxation of a very small vocal fold. *Journal of biomechanics* **44**, 1936, doi:10.1016/j.jbiomech.2011.04.024 (2011).

43 Welham, N. V., Yamashita, M., Choi, S. H., Ling, C. & Cotterill, S. Cross-Sample Validation Provides Enhanced Proteome Coverage in Rat Vocal Fold Mucosa. *PLoS ONE* **6**, doi:10.1371/journal.pone.0017754 (2011).

44 Loewen, M. S. & Walner, D. L. Dimensions of rabbit subglottis and trachea. *Laboratory animals* **35**, 253, doi:10.1258/0023677011911714 (2001).

45 Ryan, S., McNicholas, W. T., O' Regan, R. G. & Nolan, P. Intralaryngeal neuroanatomy of the recurrent laryngeal nerve of the rabbit. *Journal of Anatomy* **202**, 421-430, doi:10.1046/j.1469-7580.2003.00177.x (2003).

46 Ajlan, A. M. *et al.* Helical computed tomography scanning of the larynx and upper trachea in rabbits. *Acta Veterinaria Scandinavica* **57**, doi:10.1186/s13028-015-0157-4 (2015).

47 Lodewyck, D., Menco, B. & Fisher, K. Immunolocalization of Aquaporins in Vocal Fold Epithelia. *Archives of Otolaryngology–Head & Neck Surgery* **133**, 557-563, doi:10.1001/archotol.133.6.557 (2007).

48 Sivasankar, M. & Fisher, K. Vocal Fold Epithelial Response to Luminal Osmotic Perturbation. *Journal of Speech, Language, and Hearing Research* **50**, 886-898, doi:10.1044/1092-4388(2007/063) (2007).

49 Luo, R., Kong, W., Wei, X., Lamb, J. & Jiang, J. J. Development of Excised Larynx. *Journal of Voice* **34**, 38-43, doi:10.1016/j.jvoice.2018.07.023 (2020).

50 Gartling, G. J., Sayce, L., Kimball, E. E., Sueyoshi, S. & Rousseau, B. A Comparison of the Localization of Integral Membrane Proteins in Human and Rabbit Vocal Folds. *The Laryngoscope* **131**, doi:10.1002/lary.29243 (2021).

51 Kolosova, K. *et al.* Characterizing Vocal Fold Injury Recovery in a Rabbit Model With Three-Dimensional Virtual Histology. *The Laryngoscope* **131**, 1578-1587, doi:10.1002/lary.29028 (2021).

52 Kojima, T. *et al.* Effects of phonation time and magnitude dose on vocal fold epithelial genes, barrier integrity, and function. *Laryngoscope* **124**, 2770-2778, doi:10.1002/lary.24827 (2014).

53 Ge, P. J., French, L. C., Ohno, T., Zealear, D. L. & Rousseau, B. Model of Evoked Rabbit Phonation. *Annals of otology, rhinology & laryngology* **118**, 51-55, doi:10.1177/000348940911800109 (2009).

54 Novaleski, C. K. *et al.* Nonstimulated rabbit phonation model: Cricothyroid approximation. *The Laryngoscope* **126**, 1589-1594, doi:10.1002/lary.25559 (2016).

55 Maytag, A. L. *et al.* Use of the Rabbit Larynx in an Excised Larynx Setup. *Journal of voice* **27**, 24-28, doi:10.1016/j.jvoice.2012.08.004 (2013).

56 Döllinger, M. *et al.* Investigation of phonatory characteristics using ex vivo rabbit larynges. *The Journal of the Acoustical Society of America* **144**, 142-152, doi:10.1121/1.5043384 (2018).

57 Hemler, R. J. B., Wieneke, G. H., Lebacq, J. & Dejonckere, P. H. Laryngeal mucosa elasticity and viscosity in high and low relative air humidity. *European Archives of Oto-Rhino-Laryngology* **258**, 125-129, doi:10.1007/s004050100321 (2001).

58 Ayache, S., Ouaknine, M., Dejonkere, P. H., Prindere, P. & Giovanni, A. Experimental study of the effects of surface mucus viscosity on the glottic cycle. *Journal of Voice* **18**, 107-115, doi:10.1016/j.jvoice.2003.07.004 (2004).

59 Jiang, J., Verdolini, K., Jennie, N., Aquino, B. & Hanson, D. Effects of Dehydration on Phonation in Excised Canine Larynges. *Annals of Otology, Rhinology & Laryngology* **109**, 568-575, doi:10.1177/000348940010900607 (2000).

60 Witt, R. E. *et al.* Effect of Dehydration on Phonation Threshold Flow in Excised Canine Larynges. *Annals of Otology, Rhinology & Laryngology* **118**, 154-159, doi:10.1177/000348940911800212 (2009).

61 Witt, R. E., Taylor, L. N., Regner, M. F. & Jiang, J. J. Effects of Surface Dehydration on Mucosal Wave Amplitude and Frequency in Excised Canine Larynges. *Otolaryngology–Head and Neck Surgery* **144**, 108-113, doi:10.1177/0194599810390893 (2011).

62 Leydon, C., Wroblewski, M., Eichorn, N. & Sivasankar, M. A Meta-Analysis of Outcomes of Hydration Intervention on Phonation Threshold Pressure. *Journal of voice* **24**, 637-643, doi:10.1016/j.jvoice.2009.06.001 (2010).

63 Alves, M., Krüger, E., Pillay, B., van Lierde, K. & van Der Linde, J. The Effect of Hydration on Voice Quality in Adults: A Systematic Review. *Journal of Voice* **33**, 125.e113-125.e128, doi:10.1016/j.jvoice.2017.10.001 (2019).

64 Southern, K., Funkhouser, W., Kazachkova, I. & Godfrey, V. Airway surface liquid recovered by lavage with perfluorocarbon liquid in cats. *European Journal of Clinical Investigation* **32**, 956, doi:10.1046/j.1365-2362.2002.01100.x (2002).

65 Freed, A. N. & Davis, M. S. Hyperventilation with dry air increases airway surface fluid osmolality in canine peripheral airways. *American journal of respiratory and critical care medicine* **159**, 1101, doi:10.1164/ajrccm.159.4.9802072 (1999).

66 Chen, B. T. & Yeates, D. B. Differentiation of ion-associated and osmotically driven water transport in canine airways. *American journal of respiratory and critical care medicine* **162**, 1715, doi:10.1164/ajrccm.162.5.9912120 (2000).

67 Robinson, N. P., Kyle, H., Webber, S. E. & Widdicombe, J. G. Electrolyte and other chemical concentrations in tracheal airway surface liquid and mucus. *Journal of Applied Physiology* **66**, 2129-2135, doi:10.1152/jappl.1989.66.5.2129 (1989).

68 Joris, L., Dab, I. & Quinton, P. M. Elemental composition of human airway surface fluid in healthy and diseased airways. *The American review of respiratory disease* **148**, 1633, doi:10.1164/ajrccm/148.6_Pt_1.1633 (1993).

69 Jayaraman, S., Song, Y., Vetrivel, L., Shankar, L. & Verkman, A. S. Noninvasive in vivo fluorescence measurement of airway-surface liquid depth, salt concentration, and pH. *The Journal of clinical investigation* **107**, 317, doi:10.1172/JCI11154 (2001).

70 Sivasankar, M. P., Carroll, T. L., Kosinski, A. M. & Rosen, C. A. Quantifying the effects of altering ambient humidity on ionic composition of vocal fold surface fluid. *Laryngoscope* **123**, 1725-1728, doi:10.1002/lary.23924 (2013).

71 Cowley, E., Govindaraju, K., Guilbault, C., Radzioch, D. & Eidelman, D. Airway surface liquid composition in mice. *Am. J. Physiol.-Lung Cell. Mol. Physiol.* **278**, L1213-L1220 (2000).

72 Jayaraman, S., Song, Y. & Verkman, A. Airway surface liquid osmolality measured using fluorophore-encapsulated liposomes. *J. Gen. Physiol.* **117**, 423-430 (2001).

73 Cowley, E., Govindaraju, K., Lloyd, D. & Eidelman, D. Airway surface fluid composition in the rat determined by capillary electrophoresis. *Am. J. Physiol.-Lung Cell. Mol. Physiol.* **273**, L895-L899 (1997).

74 Chan, R. W. & Titze, I. R. Viscoelastic shear properties of human vocal fold mucosa: theoretical characterization based on constitutive modeling. *The Journal of the Acoustical Society of America* **107**, 565, doi:10.1121/1.428354 (2000).

75 Webster, M. & Tarran, R. in *Cell Volume Regulation* Vol. 81 (Elsevier Science & Technology Academic Press, 2018).

76 Ahmed, M. *et al.* Localization and regulation of aquaporins in the murine larynx. *Acta Oto-Laryngol.* **132**, 439-446, doi:10.3109/00016489.2011.644253 (2012).

77 Song, Y., Jayaraman, S., Yang, B., Matthay, M. A. & Verkman, A. S. Role of aquaporin water channels in airway fluid transport, humidification, and surface liquid hydration. *The Journal of general physiology* **117**, 573, doi:10.1085/jgp.117.6.573 (2001).

78 Grubb, B., Schiretz, F. & Boucher, R. C. Volume transport across tracheal and bronchial airway epithelia in a tubular culture system. *Am. J. Physiol.-Cell Physiol.* **273**, C21-C29, doi:10.1152/ajpcell.1997.273.1.C21 (1997).

79 Munakata, M., Mitzner, W. & Menkes, H. Osmotic stimuli induce epithelial-dependent relaxation in the guinea pig trachea. *Journal of applied physiology (Bethesda, Md. : 1985)* **64**, 466, doi:10.1152/jappl.1988.64.1.466 (1988).

80 Finney, M. J. B., Anderson, S. D. & Black, J. L. The effect of non-isotonic solutions on human isolated airway smooth muscle. *Respiration Physiology* **69**, 277-286, doi:10.1016/0034-5687(87)90082-X (1987).

81 Matsui, H., Davis, C. W., Tarran, R. & Boucher, R. C. Osmotic water permeabilities of cultured, well-differentiated normal and cystic fibrosis airway epithelia. *J. Clin. Invest.* **105**, 1419-1427, doi:10.1172/JCI4546 (2000).

82 Willumsen, N. J., Davis, C. W. & Boucher, R. C. Selective response of human airway epithelia to luminal but not serosal solution hypertonicity. Possible role for proximal airway epithelia as an osmolality transducer. *The Journal of clinical investigation* **94**, 779, doi:10.1172/JCI117397 (1994).

83 Prazma, J., Coleman, C. C., Shockley, W. W. & Boucher, R. C. Tracheal vascular response to hypertonic and hypotonic solutions. *Journal of applied physiology (Bethesda, Md. : 1985)* **76**, 2275, doi:10.1152/jappl.1994.76.6.2275 (1994).

84 Smith, T. L., Prazma, J., Coleman, C. C., Drake, A. F. & Boucher, R. C. Control of the mucosal microcirculation in the upper respiratory tract. *Otolaryngology--head and neck surgery : official journal of American Academy of Otolaryngology-Head and Neck Surgery* **109**, 646 (1993).

85 Umeno, E., McDonald, D. M. & Nadel, J. A. Hypertonic saline increases vascular permeability in the rat trachea by producing neurogenic inflammation. *The Journal of clinical investigation* **85**, 1905, doi:10.1172/JCI114652 (1990).

86 Woie, J. K., Koller, K. M.-E., Heyeraas, K. K. & Reed, K. R. Neurogenic Inflammation in Rat Trachea Is Accompanied by Increased Negativity of Interstitial Fluid Pressure. *Circulation Research* **73**, 839-845, doi:10.1161/01.RES.73.5.839 (1993).

87 Wells, U. M., Hanafi, Z. & Widdicombe, J. G. Osmolality alters tracheal blood flow and tracer uptake in anesthetized sheep. *Journal of applied physiology (Bethesda, Md. : 1985)* **77**, 2400, doi:10.1152/jappl.1994.77.5.2400 (1994).

88 Gjerde, E.-A. B., Woie, K., Wei, E. T. & Reed, R. K. Corticotropin-releasing hormone inhibits lowering of interstitial pressure in rat trachea after neurogenic inflammation. *European Journal of Pharmacology* **352**, 99-102, doi:10.1016/S0014-2999(98)00403-8 (1998).

89 Gottlieb, H. B., Ji, L. L. & Cunningham, J. T. Role of superior laryngeal nerve and Fos staining following dehydration and rehydration in the rat. *Physiol Behav* **104**, 1053-1058, doi:10.1016/j.physbeh.2011.07.008 (2011).

90 Munakata, M. *et al.* Pharmacological differentiation of epithelium-derived relaxing factor from nitric oxide. *Journal of Applied Physiology* **69**, 665-670, doi:10.1152/jappl.1990.69.2.665 (1990).

91 Wu, T. *et al.* Identification of BPIFA1/SPLUNC1 as an epithelium-derived smooth muscle relaxing factor. *Nature Communications* **8**, 14118, doi:10.1038/ncomms14118 (2017).

92 Xu, J. *et al.* Epithelial expression and role of secreted STC1 on asthma airway hyperresponsiveness through calcium channel modulation. *Allergy* **76**, 2475-2487, doi:10.1111/all.14727 (2021).

93 Fedan, J. S., Thompson, J. A., Ismailoglu, U. B. & Jing, Y. Tracheal epithelium cell volume responses to hyperosmolar, isosmolar and hypoosmolar solutions: relation to epithelium-derived relaxing factor (EpDRF) effects. *Frontiers in physiology* **4**, 287-287, doi:10.3389/fphys.2013.00287 (2013).

94 Kumai, Y. Pathophysiology of Fibrosis in the Vocal Fold: Current Research, Future Treatment Strategies, and Obstacles to Restoring Vocal Fold Pliability. *International Journal of Molecular Sciences* **20**, doi:10.3390/ijms20102551 (2019).

95 Miri, A. K., Barthelat, F. & Mongeau, L. Effects of Dehydration on the Viscoelastic Properties of Vocal Folds in Large Deformations. *Journal of Voice* **26**, 688-697, doi:10.1016/j.jvoice.2011.09.003 (2012).

96 Yang, S., Zhang, Y., Mills, R. D. & Jiang, J. J. Quantitative Study of the Effects of Dehydration on the Viscoelastic Parameters in the Vocal Fold Mucosa. *Journal of Voice* **31**, 269-274, doi:10.1016/j.jvoice.2016.05.002 (2017).

97 Duan, C. *et al.* Hydration State and Hyaluronidase Treatment Significantly Affect Porcine Vocal Fold Biomechanics. *J Voice*, doi:10.1016/j.jvoice.2021.01.014 (2021).

98 Oleson, S., Cox, A., Liu, Z., Sivasankar, M. P. & Lu, K. H. In Vivo Magnetic Resonance Imaging of the Rat Vocal Folds After Systemic Dehydration and Rehydration. *Journal of speech, language, and hearing research : JSLHR* **63**, 135-142, doi:10.1044/2019_JSLHR-19-00062 (2019).

99 Oleson, S., Lu, K. H., Liu, Z., Durkes, A. C. & Sivasankar, M. P. Proton density–weighted laryngeal magnetic resonance imaging in systemically dehydrated rats. *Laryngoscope* **128**, E222-E227, doi:10.1002/lary.26978 (2018).

100 Cannes do Nascimento, N., dos Santos, A. P., Sivasankar, M. P., Cox, A. & Jette, M. Unraveling the molecular pathobiology of vocal fold systemic dehydration using an in vivo rabbit model. *PloS one* **15**, e0236348-e0236348, doi:10.1371/journal.pone.0236348 (2020).

101 Duan, C., Nascimento, N. C., Calve, S., Cox, A. & Sivasankar, M. P. Restricted Water Intake Adversely Affects Rat Vocal Fold Biology. *The Laryngoscope*, doi:10.1002/lary.28881 (2020).

102 Chan, R. W. & Titze, I. R. Dependence of Phonation Threshold Pressure on Vocal Tract Acoustics and Vocal Fold Tissue Mechanics. *The Journal of the Acoustical Society of America* **119**, 2351-2362, doi:10.1121/1.2173516 (2006).

103 Tabka, Z., Jebria, A. B. & Guénard, H. Effect of breathing dry warm air on respiratory water loss at rest and during exercise. *Respiration Physiology* **67**, 115-125, doi:10.1016/0034-5687(87)90034-X (1987).

104 Zou, Z.-f., Chen, W., Li, W. & Yuan, K. Impact of Vocal Fold Dehydration on Vocal Function and Its Treatment. *Curr Med Sci* **39**, 310-316, doi:10.1007/s11596-019-2036-0 (2019).

105 Vermeulen, R., van der Linde, J., Abdoola, S., van Lierde, K. & Graham, M. A. The Effect of Superficial Hydration, With or Without Systemic Hydration, on Voice Quality in Future Female Professional Singers. *Journal of voice* **35**, 728, doi:10.1016/j.jvoice.2020.01.008 (2020).

106 Souza, B. O., Santos, M. A. R., Plec, E. M. R. L., Diniz, M. L. & Gama, A. C. C. Nebulized Saline Solution: A Multidimensional Voice Analysis. *Journal of voice*, doi:10.1016/j.jvoice.2021.02.024 (2021).

107 Borragan, M. *et al.* Nasal Breathing Through a Damp Gauze Enhances Surface Hydration of the Vocal Folds and Optimizes Vocal Function. *Journal of voice*, doi:10.1016/j.jvoice.2021.06.023 (2021).

108 Pereira, M. C. B. *et al.* Immediate effect of surface laryngeal hydration associated with tongue trill technique in amateur singers. *CoDAS (São Paulo)* **33**, e20200009-e20200009, doi:10.1590/2317-1782/20202020009 (2021).

109 Verdolini-Marston, K., Sandage, M. & Titze, I. R. Effect of hydration treatments on laryngeal nodules and polyps and related voice measures. *Journal of Voice* **8**, 30-47, doi:10.1016/S0892-1997(05)80317-0 (1994).

110 Dane, R. L. *Effects of short-term dehydration and rehydration on acoustic measures of voice*, Texas Tech University, (1998).

111 Franca, M. C. & Simpson, K. O. Effects of Hydration on Voice Acoustics. *Contemporary issues in communication science and disorders* **36**, 142-148, doi:10.1044/cicsd_36_F_142 (2009).

112 Fourie, K., Richardson, M., van Der Linde, J., Abdoola, S. & Mosca, R. The Reported Incidence and Nature of Voice Disorders in the Private Healthcare Context of Gauteng. *Journal of voice : official journal of the Voice Foundation* **31**, 774.e723, doi:10.1016/j.jvoice.2017.02.013 (2017).

113 Lai, Y.-T. *et al.* The Epidemiology of Benign Voice Disorders in Taiwan: A Nationwide Population-Based Study. *Annals of Otology, Rhinology & Laryngology* **128**, 406-412, doi:10.1177/0003489419826136 (2019).

114 Mohammadzadeh, A. & Sandoughdar, N. Prevalence of Voice Disorders in Iranian Primary School Students. *Journal of voice : official journal of the Voice Foundation* **31**, 263.e213, doi:10.1016/j.jvoice.2016.04.004 (2017).

115 National Institute on Deafness and Other Communication Disorders, i. b. *Taking care of your voice*. Updating April 2014. edn, (Bethesda, Maryland : U.S. Department of Health and Human Services, National Institutes of Health, National Institute on Deafness and Other Communication Disorders, 2014).

116 Naunheim, M. R., Goldberg, L., Dai, J. B., Rubinstein, B. J. & Courey, M. S. Measuring the impact of dysphonia on quality of life using health state preferences. *The Laryngoscope*, doi:10.1002/lary.28148 (2019).

117 Pernambuco, L., Espelt, A., Góis, A. C. B. & de Lima, K. C. Voice Disorders in Older Adults Living in Nursing Homes: Prevalence and Associated Factors. *Journal of voice : official journal of the Voice Foundation* **31**, 510.e515, doi:10.1016/j.jvoice.2016.11.015 (2017).

118 Roy, N. *et al.* Prevalence of voice disorders in teachers and the general population. *Journal of speech, language, and hearing research : JSLHR* **47**, 281, doi:10.1044/1092-4388(2004/023) (2004).

119 Bhattacharyya, N. The prevalence of voice problems among adults in the United States. *Laryngoscope* **124**, 2359-2362, doi:10.1002/lary.24740 (2014).

120 Bainbridge, K. E., Roy, N., Losonczy, K. G., Hoffman, H. J. & Cohen, S. M. Voice disorders and associated risk markers among young adults in the United States.(Clinical report). *The Laryngoscope* **127**, 2093, doi:10.1002/lary.26465 (2017).

121 Byeon, H. Occupational risks for voice disorders: Evidence from a Korea national cross-sectional survey. *Logopedics, phoniatrics, vocology* **42**, 39, doi:10.1080/14015439.2016.1178326 (2017).

122 Da Rocha, L. M., de Lima Bach, S., Do Amaral, P. L., Behlau, M. & de Mattos Souza, L. D. Risk Factors for the Incidence of Perceived Voice Disorders in Elementary and Middle School Teachers. *Journal of voice : official journal of the Voice Foundation* **31**, 258.e257, doi:10.1016/j.jvoice.2016.05.018 (2017).

123 Mori, M. C., Francis, D. O. & Song, P. C. Identifying Occupations at Risk for Laryngeal Disorders Requiring Specialty Voice Care. *Otolaryngology--head and neck surgery : official journal of American Academy of Otolaryngology-Head and Neck Surgery* **157**, 670, doi:10.1177/0194599817726528 (2017).

124 Trinite, B. Epidemiology of Voice Disorders in Latvian School Teachers. *Journal of Voice* **31**, 508.e501-508.e509, doi:10.1016/j.jvoice.2016.10.014 (2017).

125 Cohen, S. M., Kim, J., Roy, N., Asche, C. & Courey, M. Direct health care costs of laryngeal diseases and disorders. *Laryngoscope* **122**, 1582-1588, doi:10.1002/lary.23189 (2012).

126 de Souza, C. M., Granjeiro, R. C., de Castro, M. P., Ibiapina, R. d. C. & Oliveira, G. M. G. F. Outcomes of teachers away from work for voice disorders, State Secretariat for Education, Federal District, 2009-2010/ Desfecho dos professores afastados da Secretaria de Estado de Educacao do Distrito Federal por disturbios vocais entre 2009-2010.(ARTIGO ORIGINAL). *Revista Brasileira de Medicina do Trabalho* **15**, 324, doi:10.5327/Z1679443520170044 (2017).

127 Sataloff, R. T. Vol. 2017 (Plural Publishing, Inc, Beaverton, 2017).

128 Behlau, M. & Oliveira, G. Vocal hygiene for the voice professional. *Current Opinion in Otolaryngology & Head and Neck Surgery* **17**, 149-154, doi:10.1097/MOO.0b013e32832af105 (2009).

129 Benninger, M. S., Murry, T. & Johns, M. M. *The performer's voice*. Second edition. edn, (San Diego, California : Plural Publishing, 2016).

130 Brozmanova, A., Jochem, J., Javorka, K., Zila, I. & Zwirska-Korczala, K. Diuretic-induced dehydration/hypovolemia inhibits thermal panting in rabbits. *Respiratory Physiology & Neurobiology* **150**, 99-102, doi:10.1016/j.resp.2005.10.008 (2006).

131 Fisher, K. V., Ligon, J., Sobecks, J. L. & Roxe, D. M. Phonatory effects of body fluid removal. *Journal of speech, language, and hearing research : JSLHR* **44**, 354, doi:10.1044/1092-4388(2001/029) (2001).

132 Verdolini, K. *et al.* Biological mechanisms underlying voice changes due to dehydration.(Statistical Data Included). *Journal of Speech, Language, and Hearing Research* **45**, 268, doi:10.1044/1092-4388(2002/021) (2002).

133 Fujiki, R., Chapleau, A., Sundarrajan, A., McKenna, V. & Sivasankar, M. P. The Interaction of Surface Hydration and Vocal Loading on Voice Measures. *J. Voice* **31**, 211-217, doi:10.1016/j.jvoice.2016.07.005 (2017).

134 Li, L., Zhang, Y., Maytag, A. L. & Jiang, J. J. Quantitative Study for the Surface Dehydration of Vocal Folds Based on High-Speed Imaging. *Journal of Voice* **29**, 403-409, doi:10.1016/j.jvoice.2014.09.025 (2015).

135 Mahalingam, S. & Boominathan, P. Effects of Steam Inhalation on Voice Quality-Related Acoustic Measures. *Laryngoscope* **126**, 2305-2309, doi:10.1002/lary.25933 (2016).

136 Patel, R. R., Walker, R. & Sivasankar, P. M. Spatiotemporal Quantification of Vocal Fold Vibration After Exposure to Superficial Laryngeal Dehydration: A Preliminary Study. *Journal of Voice* **30**, 427-433, doi:10.1016/j.jvoice.2015.07.009 (2016).

137 liHemler, R. J. B., Wieneke, G. H., Lebacq, J. & Dejonckere, P. H. Laryngeal mucosa elasticity and viscosity in high and low relative air humidity. *European Archives of Oto-Rhino-Laryngology* **258**, 125-129, doi:10.1007/s004050100321 (2001).

138 Warren, N., Crampin, E. & Tawhai, M. The Role of Airway Epithelium in Replenishment of Evaporated Airway Surface Liquid From the Human Conducting Airways. *Annals of Biomedical Engineering* **38**, 3535-3549, doi:10.1007/s10439-010-0111-6 (2010).

139 Anderson, S. D. & Holzer, K. Vol. 106 419-428 (2000).

140 Levendoski, E. E. & Sivasankar, M. P. Vocal Fold Ion Transport and Mucin Expression Following Acrolein Exposure. *The Journal of Membrane Biology* **247**, doi:10.1007/s00232-014-9651-2 (2014).

141 Sivasankar, M., Erickson, E., Rosenblatt, M. & Branski, R. C. Hypertonic Challenge to Porcine Vocal Folds: Effects on Epithelial Barrier Function. *Otolaryngology–Head and Neck Surgery* **142**, 79-84, doi:10.1016/j.otohns.2009.09.011 (2010).

142 Sato, K., Chitose, S. I. & Umeno, H. Dimensions and morphological characteristics of human newborn glottis. *Laryngoscope* **125**, E186-E189, doi:10.1002/lary.25142 (2015).

143 Branski, R. C., Rosen, C. A., Verdolini, K. & Hebda, P. A. Biochemical markers associated with acute vocal fold wound healing: a rabbit model. *Journal of Voice* **19**, 283, doi:10.1016/j.jvoice.2004.04.003 (2005).

144 Hansen, J. K., Thibeault, S. L., Walsh, J. F., Shu, X. Z. & Prestwich, G. D. In Vivo Engineering of the Vocal Fold Extracellular Matrix with Injectable Hyaluronic Acid Hydrogels: Early Effects on Tissue Repair and Biomechanics in a Rabbit Model. *Annals of Otology, Rhinology & Laryngology* **114**, 662-670, doi:10.1177/000348940511400902 (2005).

145 Jin, H.-J. *et al.* Morphological and Histological Changes of Rabbit Vocal Fold after Steroid Injection. *Otolaryngology–Head and Neck Surgery* **149**, 277-283, doi:10.1177/0194599813489657 (2013).

146 Kojima, T., Garrett, C., Novaleski, C. & Rousseau, B. Quantification of Acute Vocal Fold Epithelial Surface Damage with Increasing Time and Magnitude Doses of Vibration Exposure. *PLoS One* **9**, e91615, doi:10.1371/journal.pone.0091615 (2014).

147 Kojima, T., Mitchell, J. R., Garrett, C. G. & Rousseau, B. Recovery of vibratory function after vocal fold microflap in a rabbit model. *Laryngoscope* **124**, 481-486, doi:10.1002/lary.24324 (2014).

148 Mitchell, J. R., Kojima, T., Wu, H., Garrett, C. G. & Rousseau, B. Biochemical basis of vocal fold mobilization after microflap surgery in a rabbit model. *Laryngoscope* **124**, 487-493, doi:10.1002/lary.24263 (2014).

149 Okhovat, S., Milner, T. D., Clement, W. A., Wynne, D. M. & Kunanandam, T. Validation of Animal Models for Simulation Training in Pediatric Laryngotracheal Reconstruction. *Annals of Otology, Rhinology & Laryngology* **129**, 46-54, doi:10.1177/0003489419870820 (2020).

150 Cole, T. *et al.* Transcript assembly and quantification by RNA-Seq reveals unannotated transcripts and isoform switching during cell differentiation. *Nature Biotechnology* **28**, 511, doi:10.1038/nbt.1621 (2010).

151 Dobin, A. *et al.* STAR: ultrafast universal RNA-seq aligner. *Bioinformatics* **29**, 15-21, doi:10.1093/bioinformatics/bts635 (2013).

152 Huang, D. W., Sherman, B. T. & Lempicki, R. A. Bioinformatics enrichment tools: paths toward the comprehensive functional analysis of large gene lists. *Nucleic acids research* **37**, 1, doi:10.1093/nar/gkn923 (2009).

153 Livak, K. J. & Schmittgen, T. D. Analysis of Relative Gene Expression Data Using Real-Time Quantitative PCR and the $2^{-\Delta\Delta CT}$ Method. *Methods* **25**, 402-408, doi:10.1006/meth.2001.1262 (2001).

154 Wickham, H. *et al.* Welcome to the Tidyverse. *Journal of Open Source Software* **4**, doi:10.21105/joss.01686 (2019).

155 Komsta, L. *outliers v0.14*, <https://www.rdocumentation.org/packages/outliers> (2011).

156 OSHA. Reiteration of Existing OSHA Policy on Indoor Air Quality: Office Temperature/Humidity and Environmental Tobacco Smoke. (2003).

157 NRC. *Guide for the care and use of laboratory animals*. 8th ed. edn, (National Academy Press, 2011).

158 Nakamura, K., Ito, I., Kobayashi, M., Herndon, D. N. & Suzuki, F. Orosomucoid 1 drives opportunistic infections through the polarization of monocytes to the M2b phenotype. *Cytokine* **73**, 8-15, doi:10.1016/j.cyto.2015.01.017 (2015).

159 Zhang, S. & Mark, K. S. α1-Acid glycoprotein induced effects in rat brain microvessel endothelial cells. *Microvascular Research* **84**, 161-168, doi:10.1016/j.mvr.2012.05.003 (2012).

160 Yu, N. *et al.* Serum amyloid A, an acute phase protein, stimulates proliferative and proinflammatory responses of keratinocytes. *Cell Proliferation* **50**, n/a-n/a, doi:10.1111/cpr.12320 (2017).

161 Tsai, S.-Y. *et al.* DAMP molecule S100A9 acts as a molecular pattern to enhance inflammation during influenza A virus infection: role of DDX21-TRIF-TLR4-MyD88 pathway. *PLoS pathogens* **10**, e1003848-e1003848, doi:10.1371/journal.ppat.1003848 (2014).

162 Kallinich, T., Wittkowski, H., Keitzer, R., Roth, J. & Foell, D. Neutrophil-derived S100A12 as novel biomarker of inflammation in familial Mediterranean fever. *Annals of the Rheumatic Diseases* **69**, 677, doi:10.1136/ard.2009.114363 (2010).

163 Bijangi-Vishehsaraei, K., Blum, K., Zhang, H., Safa, A. R. & Halum, S. L. Microarray Analysis Gene Expression Profiles in Laryngeal Muscle After Recurrent Laryngeal Nerve Injury. *Annals of Otology, Rhinology & Laryngology* **125**, 247-256, doi:10.1177/0003489415608866 (2016).

164 Hedbrant, A. *et al.* Quartz Dust Exposure Affects NLRP3 Inflammasome Activation and Plasma Levels of IL-18 and IL-1Ra in Iron Foundry Workers. *Mediators of Inflammation* **2020**, doi:10.1155/2020/8490908 (2020).

165 Gronski, T. J. *et al.* Hydrolysis of a broad spectrum of extracellular matrix proteins by human macrophage elastase. *The Journal of biological chemistry* **272**, 12189, doi:10.1074/jbc.272.18.12189 (1997).

166 Adams, G. M., Xu, C. C. & Chan, R. W. Senescence of human vocal fold fibroblasts in primary culture.(Report). *Journal of Biomedical Science and Engineering (JBiSE)* **3**, 148 (2010).

167 Lavigne, M. C. *et al.* Human bronchial epithelial cells express and secrete MMP-12. *Biochemical and Biophysical Research Communications* **324**, 534-546, doi:10.1016/j.bbrc.2004.09.080 (2004).

168 Tewari, A., Grys, K., Kollet, J., Sarkany, R. & Young, A. R. Upregulation of MMP12 and Its Activity by UVA1 in Human Skin: Potential Implications for Photoaging. *Journal of Investigative Dermatology* **134**, 2598-2609, doi:10.1038/jid.2014.173 (2014).

169 Chan, R., Fu, M., Young, L. & Tirunagari, N. Relative Contributions of Collagen and Elastin to Elasticity of the Vocal Fold Under Tension. *The Journal of the Biomedical Engineering Society* **35**, 1471-1483, doi:10.1007/s10439-007-9314-x (2007).

170 Rohlfs, A.-K. *et al.* The anisotropic nature of the human vocal fold: an ex vivo study. *European archives of oto-rhino-laryngology : official journal of the European Federation of Oto-Rhino-Laryngological Societies (EUFOS) : affiliated with the German Society for Oto-Rhino-Laryngology - Head and Neck Surgery* **270**, 1885, doi:10.1007/s00405-013-2428-x (2013).

171 Le Quément, C., Guénon, I., Gillon, J.-Y., Lagente, V. & Boichot, E. MMP-12 induces IL-8/CXCL8 secretion through EGFR and ERK1/2 activation in epithelial cells. *American journal of physiology. Lung cellular and molecular physiology* **294**, L1076, doi:10.1152/ajplung.00489.2007 (2008).

172 Wolf, M. *et al.* Effects of MMP12 on cell motility and inflammation during corneal epithelial repair. *Experimental Eye Research* **160**, 11-20, doi:10.1016/j.exer.2017.04.007 (2017).

173 Zhu, Q. Z. *et al.* Isolation and structure of corticostatin peptides from rabbit fetal and adult lung. *Proceedings of the National Academy of Sciences of the United States of America* **85**, 592, doi:10.1073/pnas.85.2.592 (1988).

174 Erickson, E. & Sivasankar, M. Simulated reflux decreases vocal fold epithelial barrier resistance. *Laryngoscope* **120**, 1569-1575, doi:10.1002/lary.20983 (2010).

175 Rousseau, B., Suehiro, A., Echemendia, N. & Sivasankar, M. Raised intensity phonation compromises vocal fold epithelial barrier integrity. *The Laryngoscope* **121**, 346, doi:10.1002/lary.21364 (2011).

176 Davies, P., Wang, W., Hales, T. & Kirkness, E. A Novel Class of Ligand-gated Ion Channel Is Activated by Zn super(2+). *Journal of Biological Chemistry* **278**, 712-717, doi:10.1074/jbc.M208814200 (2003).

177 Samuels, T. L. *et al.* Mucin Gene Expression in Human Laryngeal Epithelia: Effect of Laryngopharyngeal Reflux. *Annals of Otology, Rhinology & Laryngology* **117**, 688-695, doi:10.1177/000348940811700911 (2008).

178 Yi, Y. *et al.* Mucin 21/epiglycanin modulates cell adhesion. *The Journal of biological chemistry* **285**, 21233, doi:10.1074/jbc.M109.082875 (2010).

179 Yoshimoto, T. *et al.* Mucin 21 is a key molecule involved in the incohesive growth pattern in lung adenocarcinoma. *Cancer Science* **110**, 3006-3011, doi:10.1111/cas.14129 (2019).

180 Lungova, V., Verheyden, J. M., Herriges, J., Sun, X. & Thibeault, S. L. Ontogeny of the mouse vocal fold epithelium. *Developmental biology* **399**, 263, doi:10.1016/j.ydbio.2014.12.037 (2015).

181 Park, G. T., Lim, S. E., Jang, S.-I. & Morasso, M. I. Suprabasin, a novel epidermal differentiation marker and potential cornified envelope precursor. *The Journal of biological chemistry* **277**, 45195, doi:10.1074/jbc.M205380200 (2002).

182 Aoshima, M. *et al.* Decreased expression of suprabasin induces aberrant differentiation and apoptosis of epidermal keratinocytes: Possible role for atopic dermatitis. *Journal of dermatological science* **95**, 107, doi:10.1016/j.jdermsci.2019.07.009 (2019).

183 Nakazawa, S. *et al.* 650 Suprabasin-deficient mice show limited but discernible defective barrier in both skin and upper digestive tract. *Journal of Investigative Dermatology* **138**, S111-S111, doi:10.1016/j.jid.2018.03.659 (2018).

184 Pinette, J. A. *et al.* Brush border protocadherin CDHR2 promotes the elongation and maximized packing of microvilli in vivo. *Molecular biology of the cell* **30**, 108, doi:10.1091/mbc.E18-09-0558 (2019).

185 Lutter, R. & Ravanetti, L. Cadherin-related family member 3 (CDHR3) drives differentiation of ciliated bronchial epithelial cells and facilitates rhinovirus C infection, although with a little help. *The Journal of Allergy and Clinical Immunology* **144**, 926-927, doi:10.1016/j.jaci.2019.07.021 (2019).

186 Lundström, A., Serre, G., Haftek, M. & Egelrud, T. Evidence for a role of corneodesmosin, a protein which may serve to modify desmosomes during cornification, in stratum corneum cell cohesion and desquamation. *Archives of dermatological research* **286**, 369, doi:10.1007/BF00371795 (1994).

187 Oji, V. *et al.* Loss of Corneodesmosin Leads to Severe Skin Barrier Defect, Pruritus, and Atopy: Unraveling the Peeling Skin Disease. *American Journal of Human Genetics* **87**, 274-281, doi:10.1016/j.ajhg.2010.07.005 (2010).

188 Rousseau, B., Ge, P. J., Ohno, T., French, L. C. & Thibeault, S. L. Extracellular Matrix Gene Expression after Vocal Fold Injury in a Rabbit Model. *Annals of Otology, Rhinology & Laryngology* **117**, 598-603, doi:10.1177/000348940811700809 (2008).

189 Hengen, J., Peterson, M. & McAllister, A. Patient characteristics and intervention effect as measured by Voice Handicap Index. *Logopedics Phoniatrics Vocology* **42**, 93-98, doi:10.1080/14015439.2016.1219387 (2017).

190 Tarran, R. Regulation of airway surface liquid volume and mucus transport by active ion transport. *Proceedings of the American Thoracic Society* **1**, 42, doi:10.1513/pats.2306014 (2004).

191 Tarran, R., Grubb, B., Gatzy, J., Davis, C. & Boucher, R. The relative roles of passive surface forces and active ion transport in the modulation of airway surface liquid volume and composition. *The Journal of General Physiology* **118**, 223-236, doi:10.1085/jgp.118.2.223 (2001).

192 Bailey, T. W. *et al.* RNA sequencing identifies transcriptional changes in the rabbit larynx in response to low humidity challenge. *BMC Genomics* **21**, 888-888, doi:10.1186/s12864-020-07301-7 (2020).

193 Boyd, J. W. The Relationships between Blood Haemoglobin Concentration, Packed Cell Volume and Plasma Protein Concentration in Dehydration. *Br Vet J* **137**, 166-172, doi:10.1016/S0007-1935(17)31734-7 (1981).

194 Foote, A. G., Wang, Z., Kendziorski, C. & Thibeault, S. L. Tissue specific human fibroblast differential expression based on RNAsequencing analysis. *BMC Genomics* **20**, 308-308, doi:10.1186/s12864-019-5682-5 (2019).

195 Fahy, J. V. & Dickey, B. F. Airway Mucus Function and Dysfunction. *The New England Journal of Medicine* **363**, 2233-2247, doi:10.1056/NEJMra0910061 (2010).

196 Cox, J. & Mann, M. MaxQuant enables high peptide identification rates, individualized p.p.b.-range mass accuracies and proteome-wide protein quantification. *Nat Biotechnol* **26**, 1367-1372, doi:10.1038/nbt.1511 (2008).

197 Zhou, Y. *et al.* Metascape provides a biologist-oriented resource for the analysis of systems-level datasets. *Nat Commun* **10**, 1523-1523, doi:10.1038/s41467-019-09234-6 (2019).

198 Ashburner, M. *et al.* Gene Ontology: tool for the unification of biology. *Nature Genetics* **25**, 25-29, doi:10.1038/75556 (2000).

199 Carbon, S. *et al.* The Gene Ontology resource: enriching a GOld mine. *Nucleic Acids Research* **49**, D325-D334, doi:10.1093/nar/gkaa1113 (2021).

200 Martens, M. *et al.* WikiPathways: connecting communities. *Nucleic Acids Research* **49**, D613-D621, doi:10.1093/nar/gkaa1024 (2021).

201 Kanehisa, M. KEGG: Kyoto Encyclopedia of Genes and Genomes. *Nucleic Acids Research* **28**, 27-30, doi:10.1093/nar/28.1.27 (2000).

202 Kanehisa, M. Toward understanding the origin and evolution of cellular organisms. *Protein science* **28**, 1947-1951, doi:10.1002/pro.3715 (2019).

203 Kanehisa, M., Furumichi, M., Sato, Y., Ishiguro-Watanabe, M. & Tanabe, M. KEGG: integrating viruses and cellular organisms. *Nucleic acids research* **49**, D545-D551, doi:10.1093/nar/gkaa970 (2021).

204 Otasek, D., Morris, J. H., Bouças, J., Pico, A. R. & Demchak, B. Cytoscape Automation: empowering workflow-based network analysis. *Genome Biology* **20**, doi:10.1186/s13059-019-1758-4 (2019).

205 Kassambara, A. *ggpubr: 'ggplot2' Based Publication Ready Plots. R package version 0.4.0.*, <https://CRAN.R-project.org/package=ggpubr> (2020).

206 Ahlmann-Eltze, C. & Patil, I. ggsignif: R Package for Displaying Significance Brackets for 'ggplot2'. *PsyArxiv*, doi:doi:10.31234/osf.io/7awm6 (2021).

207 Douglas, B., Martin, M., Ben, B. & Steve, W. Fitting Linear Mixed-Effects Models Using lme4. *Journal of statistical software* **67**, 1-48, doi:10.18637/jss.v067.i01 (2015).

208 Komsta, L. *outliers: Tests for outliers. R package version 0.14*, <https://CRAN.R-project.org/package=outliers> (2011).

209 Lemon, J. Plotrix: a package in the red light district of R. *R-News* **6**, 8-12 (2006).

210 Wickham, H. *stringr: Simple, Consistent Wrappers for Common String Operations. R package version 1.4.0*, <https://CRAN.R-project.org/package=stringr> (2019).

211 Balázs, A. & Mall, M. A. Role of the SLC26A9 Chloride Channel as Disease Modifier and Potential Therapeutic Target in Cystic Fibrosis. *Front Pharmacol* **9**, 1112-1112, doi:10.3389/fphar.2018.01112 (2018).

212 França, M. B., Panek, A. D. & Eleutherio, E. C. A. Oxidative stress and its effects during dehydration. *Comp Biochem Physiol A Mol Integr Physiol* **146**, 621-631, doi:10.1016/j.cbpa.2006.02.030 (2007).

213 Chanoux, R. A. *et al.* Hsp70 promotes epithelial sodium channel functional expression by increasing its association with coat complex II and its exit from endoplasmic reticulum. *The Journal of biological chemistry* **287**, 35540-35540, doi:10.1074/jbc.A112.357756 (2012).

214 Rohlfs, A.-K. *et al.* Quantification of change in vocal fold tissue stiffness relative to depth of artificial damage. *Logopedics Phoniatrics Vocology* **42**, 108-117, doi:10.1080/14015439.2016.1221445 (2017).

215 Park, J. E. *et al.* Fibroblast Activation Protein, a Dual Specificity Serine Protease Expressed in Reactive Human Tumor Stromal Fibroblasts. *Journal of Biological Chemistry* **274**, 36505-36512, doi:10.1074/jbc.274.51.36505 (1999).

216 Cai, C. *et al.* MG53 nucleates assembly of cell membrane repair machinery. *Nature cell biology* **11**, 56-64, doi:10.1038/ncb1812 (2008).

217 Nelson, B. R. *et al.* Skeletal muscle-specific T-tubule protein STAC3 mediates voltage-induced Ca2+ release and contractility. *Proceedings of the National Academy of Sciences* **110**, 11881-11886, doi:10.1073/pnas.1310571110 (2013).

218 Gilbert, R., Cohen, J. A., Pardo, S., Basu, A. & Fischman, D. A. Identification of the A-band localization domain of myosin binding proteins C and H (MyBP-C, MyBP-H) in skeletal muscle. *J Cell Sci* **112 (Pt 1)**, 69 (1999).

219 Conti, A. *et al.* Increased expression of Myosin binding protein H in the skeletal muscle of amyotrophic lateral sclerosis patients. *Biochimica et biophysica acta. Molecular basis of disease* **1842**, 99-106, doi:10.1016/j.bbadis.2013.10.013 (2014).

220 Wang, Q. & Michalak, M. Calsequestrin. Structure, function, and evolution. *Cell Calcium* **90**, 102242, doi:10.1016/j.ceca.2020.102242 (2020).

221 King, R. E., Steed, K., Rivera, A. E., Wisco, J. J. & Thibeault, S. L. Magnetic resonance imaging quantification of dehydration and rehydration in vocal fold tissue layers. *PloS one* **13**, e0208763-e0208763, doi:10.1371/journal.pone.0208763 (2018).

222 Fedan, J. S., Dowdy, J. A., Van Scott, M. R., Wu, D. X.-Y. & Johnston, R. A. Hyperosmolar Solution Effects in Guinea Pig Airways. III. Studies on the Identity of Epithelium-Derived Relaxing Factor in Isolated Perfused Trachea Using Pharmacological Agents. *Journal of Pharmacology and Experimental Therapeutics* **308**, 30-36, doi:10.1124/jpet.103.051664 (2004).

223 Milara, J. *et al.* MUC4 is overexpressed in idiopathic pulmonary fibrosis and collaborates with transforming growth factor β inducing fibrotic responses. *Mucosal immunology*, doi:10.1038/s41385-020-00343-w (2020).

224 Kimball, E. E. *Assessing Structural and Physiologic Laryngeal Changes in Response to Systemic Dehydration in a Rabbit Model*, (2020).

225 Marshall, H. *et al.* Systemic but not local rehydration restores dehydration-induced changes in pulmonary function in healthy adults. *Journal of applied physiology (1985)* **130**, 517-527, doi:10.1152/japplphysiol.00311.2020 (2021).

226 Bailey, T. W. *et al.* Recurring exposure to low humidity induces transcriptional and protein level changes in the vocal folds of rabbits. *Scientific reports* **11**, 24180-24180, doi:10.1038/s41598-021-03489-0 (2021).

227 Jassal, B. *et al.* The reactome pathway knowledgebase. *Nucleic Acids Research*, doi:10.1093/nar/gkz1031 (2019).

228 Subramanian, A. *et al.* Gene Set Enrichment Analysis: A Knowledge-Based Approach for Interpreting Genome-Wide Expression Profiles. *Proceedings of the National Academy of Sciences - PNAS* **102**, 15545-15550, doi:10.1073/pnas.0506580102 (2005).

229 Szklarczyk, D. *et al.* STRING v11: protein–protein association networks with increased coverage, supporting functional discovery in genome-wide experimental datasets. *Nucleic acids research* **47**, D607-D613, doi:10.1093/nar/gky1131 (2019).

230 Stark, C. *et al.* BioGRID: a general repository for interaction datasets. *Nucleic acids research* **34**, D535-D539, doi:10.1093/nar/gkj109 (2006).

231 Turei, D., Korcsmaros, T. & Saez-Rodriguez, J. OmniPath: guidelines and gateway for literature-curated signaling pathway resources. *Nature methods* **13**, 965-967, doi:10.1038/nmeth.4077 (2016).

232 Li, T. *et al.* A scored human protein-protein interaction network to catalyze genomic interpretation. *Nature methods* **14**, 61-64, doi:10.1038/nmeth.4083 (2017).

233 Bader, G. D. & Hogue, C. W. An automated method for finding molecular complexes in large protein interaction networks. *BMC bioinformatics* **4**, 2-2, doi:10.1186/1471-2105-4-2 (2003).

234 Hartley, N. A. & Thibeault, S. L. Systemic Hydration: Relating Science to Clinical Practice in Vocal Health. *Journal of Voice* **28**, 652.e651-652.e620, doi:10.1016/j.jvoice.2014.01.007 (2014).

235 Tang, S. S., Mohad, V., Gowda, M. & Thibeault, S. L. Insights Into the Role of Collagen in Vocal Fold Health and Disease. *Journal of Voice* **31**, 520-527, doi:10.1016/j.jvoice.2017.01.008 (2017).

236 Gooptu, B., Ekeowa, U. I. & Lomas, D. A. Mechanisms of emphysema in 1-antitrypsin deficiency: molecular and cellular insights. *European Respiratory Journal* **34**, 475-488, doi:10.1183/09031936.00096508 (2009).

237 Dabbagh, K. *et al.* Alpha-1-antitrypsin stimulates fibroblast proliferation and procollagen production and activates classical MAP kinase signalling pathways. *Journal of cellular physiology* **186**, 73-81, doi:10.1002/1097-4652(200101)186:1<73::AID-JCP1002>3.0.CO;2-Q (2001).

238 Ang, L. S. *et al.* Serpina3n attenuates granzyme B-mediated decorin cleavage and rupture in a murine model of aortic aneurysm. *Cell death & disease* **2**, e209-e209, doi:10.1038/cddis.2011.88 (2011).

239 Ito, S. & Nagata, K. Biology of Hsp47 (Serpin H1), a collagen-specific molecular chaperone. *Seminars in cell & developmental biology* **62**, 142-151, doi:10.1016/j.semcdb.2016.11.005 (2017).

240 Kishimoto, Y. *et al.* Reversal of Vocal Fold Mucosal Fibrosis Using siRNA against the Collagen-Specific Chaperone Serpinh1. *Molecular Therapy - Nucleic Acids* **16**, 616-625, doi:10.1016/j.omtn.2019.04.014 (2019).

241 Chen, D. *et al.* Distinct effects of different matrix proteoglycans on collagen fibrillogenesis and cell-mediated collagen reorganization. *Scientific reports* **10**, 19065-19065, doi:10.1038/s41598-020-76107-0 (2020).

242 Wight, T. N. *et al.* Versican-A Critical Extracellular Matrix Regulator of Immunity and Inflammation. *Frontiers in immunology* **11**, 512-512, doi:10.3389/fimmu.2020.00512 (2020).

243 Livingstone, I., Uversky, V. N., Furniss, D. & Wiberg, A. The Pathophysiological Significance of Fibulin-3. *Biomolecules (Basel, Switzerland)* **10**, 1294, doi:10.3390/biom10091294 (2020).

244 Dumas, S. J. *et al.* Single-Cell RNA Sequencing Reveals Renal Endothelium Heterogeneity and Metabolic Adaptation to Water Deprivation. *Journal of the American Society of Nephrology* **31**, 118-138, doi:10.1681/ASN.2019080832 (2020).

245 Elias, S., Hoffman, R., Saharov, G., Brenner, B. & Nadir, Y. Dehydration as a Possible Cause of Monthly Variation in the Incidence of Venous Thromboembolism. *Clinical and applied thrombosis/hemostasis* **22**, 569-574, doi:10.1177/1076029616649435 (2016).

246 He, F., Ru, X. & Wen, T. NRF2, a Transcription Factor for Stress Response and Beyond. *International journal of molecular sciences* **21**, 4777, doi:10.3390/ijms21134777 (2020).

247 Nishimaki, M. *et al.* Effects of different periods of rapid weight loss on dehydration and oxidative stress. *Archives of budo* **14**, 319 (2018).

248 Dupoué, A. *et al.* Chronic water restriction triggers sex-specific oxidative stress and telomere shortening in lizards. *Biology letters (2005)* **16**, 20190889, doi:10.1098/rsbl.2019.0889 (2020).

249 Mizuta, M. *et al.* Expression of Reactive Oxygen Species during Wound Healing of Vocal Folds in a Rat Model. *Annals of otology, rhinology & laryngology* **121**, 804-810, doi:10.1177/000348941212101206 (2012).

250 Mizuta, M. *et al.* Effect of AST on age-associated changes of vocal folds in a rat model. *The Laryngoscope* **124**, E411-E417, doi:10.1002/lary.24733 (2014).